DOCTORAATSPROEFSCHRIFT

2007 | Faculteit Wetenschappen

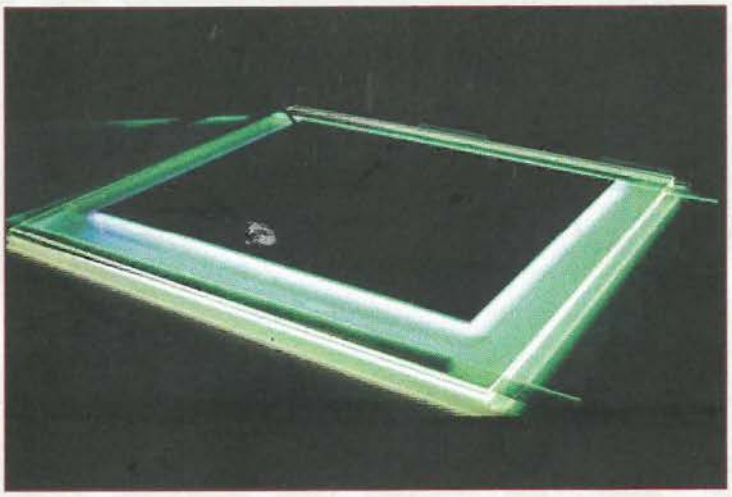

Plasma deposition of conjugated polymers at atmospheric pressure

Proefschrift voorgelegd tot het behalen van de graad van
Doctor in de Wetenschappen, richting scheikunde, te verdedigen door:

Roel DAMS

Promotor: prof. dr. Dirk Vanderzande
Copromotor: dr. Dirk Vangeneugden

universiteit hasselt

DOCTORAATSPROEFSCHRIFT

2007 | Faculteit Wetenschappen

Plasma deposition of conjugated polymers at atmospheric pressure

Proefschrift voorgelegd tot het behalen van de graad van
Doctor in de Wetenschappen, richting scheikunde, te verdedigen door:

Roel DAMS

Promotor: prof. dr. Dirk Vanderzande
Copromotor: dr. Dirk Vangeneugden

D/2007/2451/28

VITO

universiteit
hasselt

Voorwoord

Na drie jaar onderzoek eindigt mijn doctoraat met het schrijven van dit proefschrift. Dit werk zou echter nooit tot stand gekomen zijn zonder de hulp van anderen. Vandaar zou ik graag starten met een dankwoordje aan al diegenen die mij hierbij hebben bijgestaan.

In de eerste plaats zou ik mijn promotor, Prof. Dr. Dirk Vanderzande en co-promotor Dr. Dirk Vangeneugden willen bedanken omdat ze mijn de kans hebben gegeven aan doctoraatsonderzoek te doen in hun labo. Verder was hun begeleiding en wetenschappelijk advies van onschatbare waarde.

Ook van de overige mensen uit de plasmagroep heb ik veel hulp gehad. Laten we starten met mijn collega-doctoraatstudenten. Bedankt Pieter voor het helpen ontwerpen van een nieuwe reactor en voor de gezellige etentjes tijdens de middag. DJ Alexander voor het draaien van mijn verzoeknummers. En Sanaa voor het presenteren van mijn onderzoeksresultaten op ICMCTF. Ook Myriam en Olivier die ondertussen al andere oorden hebben opgezocht hebben mij op weg geholpen.

Naast de doctoraatsstudenten telde de plasmagroep ook nog een vast team met diverse specialiteiten waarbij je voor alles wel bij iemand terecht kon. Vooreerst wil ik hierbij Robby bedanken, mijn (ex)bureaugenoot die ik reeds kende van op't LUC. Ik ben nog niet vergeten dat je mij aan het VITO gelinkt hebt. Verder hebben we veel discussies kunnen voeren over plasma en chemie die zelfs doorgingen tot aan den toog. In het labo werd ik vaak bijgestaan door Danny en Jan. Jan bood me spontaan hulp wanneer ik weer eens de verkeerde vijs vast had, terwijl Danny overweg kan met zowat elk toestel in het gebouw. Bedankt Bert voor onze vruchtbare samenwerking in het TRASU project. Je zal wel blij zijn dat ik je even niet lastig val met die vervelende corrosie vraagstukken. Bedankt Annick, jouw lach zorgde steeds voor een aangename sfeer. Bedankt Ria voor de kwaliteitsvolle zorgen. En français of in't Nederlands, bij Marjorie kon je altijd terecht. En ook Sabine stond me bij met

raad en daad, tussen twee zwangerschappen in. Dank aan Ludo voor de talrijke herstellingen aan de elektronica. En Erwin was degene door wie de PC ook deed wat je er van verlangde. Vic zorgde voor een lichtpunt in de duisternis met zijn LEDjes. En bij Erik kon ik terecht met al mijn frustraties over de voetbal. Ik hoop dat Dessel in tweede blijft, maar niet ten koste van Geel! Karel is ondertussen al een tijdje weg, maar de filosofische discussies met hem zal ik nooit vergeten. Ook Ine was maar korte tijd bij ons. Toch heeft haar recente thesis ervaring bijgedragen tot het vlot schrijven van dit werk.

Naast de collega's uit de plasma groep zijn er ook nog verschillende andere Vito-mensen die het mij makkelijker maakten. Zo zijn er de mensen van CMA². In het bijzonder Myrjam voor de hulp bij infrarood metingen en UV/VIS. Hong en Bert voor XPS metingen en analyses. Raymond voor de prachtige SEM foto's en Michel voor de microscoop beeldjes. Ook de mensen van 't atelier, Paul en Louis, bedankt voor het knutselwerk. Bedankt Wim voor het zaagwerk. Bedankt mensen van het secretariaat, Greet, Marie-José, voor de hulp bij de administratie.

Je voudrais par la même occasion remercier les personnes du Centre de Recherche Publique Henri Tudor. En particulier Julien, Jérôme et Hugues pour leur aide à l'exécution des expériences et à la caractérisation des échantillons.

Verder wil ik nog een dankwoord richten aan mijn vroegere collega's van de Universiteit Hasselt. Ik ben er maar een jaartje geweest maar dat was wel een zeer leerrijk jaar, dat zeker ook een belangrijke invloed heeft gehad op mijn evolutie bij Vito.

Vito zelf wil ik bedanken voor de financiële steun en de kans die ik zo gekregen heb om mij verder te ontwikkelen als wetenschapper.

Ten slotte wil ik ook nog de mensen bedanken die niet rechtstreeks met het wetenschappelijk werk te maken hebben maar zonder wie het ook nooit zou gelukt zijn. In de eerste plaats denk ik dan aan mijn ouders die me de kans

hebben gegeven om te studeren en me bovendien steeds hebben gesteund. Ook dank aan mijn zusje Joke om steeds in mij te geloven.

Ook dank aan mijn vriendin Lies. We kennen mekaar nog niet zo lang en je hebt me zeker niet leren kennen in een ideale periode, waarin ik het vaak druk had. Toch ben je geduldig gebleven en heb je me steeds gesteund. Ik hoop dat we nog lang zullen samenblijven.

De boog kan niet altijd gespannen staan. Gelukkig had ik mijn vrienden die mij de nodige ontspanning bezorgden. Bedankt om er steeds te zijn.

Roel

Table of Contents

Chapter 1

General Introduction

1.1 Plasma's

History and definition

On earth, we are familiar with three states of matter, namely solid, liquid and gas. However, in 1879, the English physicist, Sir William Crooks identified a fourth state, which was called plasma (after the medical term) in 1929 by Irving Langmuir. Such plasma is defined as an assemblage of charged particles, called electrons and ions, that react collectively to forces exerted by electric and magnetic fields.

The differences between the four states of matter, can be explained by the energy and interactions of molecules (figure 1-1). Between molecules, a strong attraction force exists. To overcome these forces, a certain amount of energy is necessary. Because the energy of the molecules is too low to cause free movement in solids, molecules are ordered in regular patterns. When enough energy is added, it becomes liquid. Now, molecules posses the energy to break the rigid pattern, but they can not move out of the attraction field of each other. Addition of even more energy causes matter to turn into a gas. Molecules then no longer have intermolecular interactions and can move freely. In these three conditions, molecules don't posses a charge because the positive charge of the nucleus of an atom is always compensated by the charge of the surrounding electron cloud. When enough energy is added to a gas, electrons are able to escape from the electric field, created by the nucleus. At this point, molecules can break and the gas gets ionized, resulting in a plasma. Such plasma is highly energetic and reactive and consists of ions, electrons and neutrals, that

remained intact. The temperature and energy ranges of the different states of matter are compared in table 1-1.

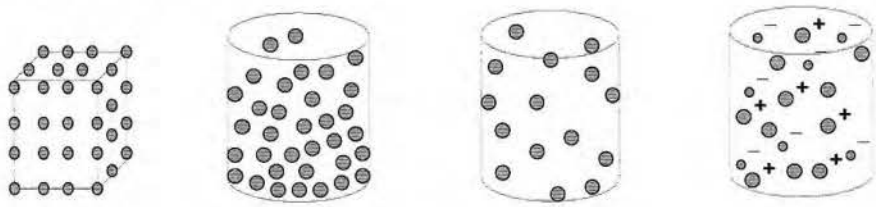

Figure 1-1: Schematic presentation of the four states of matter.

State of matter	Temperature (K)	Particle energy (eV)
Solid	100-5000	0,01-0,4
Liquid	100-6000	0,01-0,5
Gas	100-20.000	0,01-2
Plasma	10.000-100.000	1-10

Table 1-1: Temperature and energy for the different states of matter[1].

Cold plasmas

Examples of plasmas in nature are lightning, the northern light, the sun and the stars (figure 1-2). As can be seen in table 1-1, these plasmas are very hot, and therefore difficult to handle in the laboratory. The first man-made plasma was the arc discharge, created by Petrov and Humphry around 1800. The application of a high voltage on two carbon electrodes resulted in a very hot arc plasma.

Figure 1-2: Examples of plasma in nature: lightning, northern light and the sun.

Around 1900, Wilson and Townsend found that electrons are the main charge carriers in artificial plasmas. Electrons are accelerated by an external electric field and transfer this energy by means of collisions. The ions lose their energy by means of radiation or heat transfer. Since the electrons are much smaller, they lose less energy than the ions and neutrals. The temperature of electrons can therefore lie in a completely different range than the ions and neutrals. It is the temperature of the ions and neutrals, that is responsible for the actual measured gas temperature. Generally, plasmas are distinguished in three categories[2]:

- Complete thermodynamical equilibrium: All plasma temperatures are equal. These plasma conditions only occur in stars during strong explosions and do not exist on a laboratory scale.
- Local thermal equilibrium: All plasma temperatures, except the radiation temperature, are equal in small volumes of the plasma. These plasmas are very hot and are also called thermal plasmas.
- No local thermal equilibrium plasmas: In these plasmas, electron temperature is much higher than the temperature of ions and neutrals, which present the actual gas temperature. These plasmas are therefore also called non-thermal plasmas or cold plasmas.

The fact that cold plasmas can operate at low temperatures makes them useful for a lot of new industrial applications such as polymer surface treatment or thin film deposition[3, 4]. The first non-thermal plasmas operated at low pressure, because only moderate voltages are necessary. However, for industrial applications, working at atmospheric pressure is more interesting because the possibility for in-line processing and the absence of expensive vacuum equipment.

1.2 Atmospheric pressure plasma

Types of plasma discharges

In contrast with low pressure plasmas, the density of species is high at atmospheric pressure, which increases the probability for collisions between these species. Since the higher number of collisions make energy transfer more efficient, atmospheric pressure plasma's have the tendency to occur at local thermal equilibrium in which ion and electron temperatures are equal in small volumes of the plasma (hot plasma's). However, the energy transfer efficiency not only depends on the gas pressure but also on the discharge length, which is equal to the distance between the electrodes. When this distance is kept small, it is still possible to obtain a cold plasma, since the shorter path length of the electron through the plasma gas decreases it's probability to collide. When pressure (p) is increased, the discharge length (d) should be decreased in a way to keep the product p.d constant.

Although a gas is a perfect insulator in it's normal state, it becomes conductive in the plasma state because of electrical breakdown in ions and electrons. Traditionally, plasma discharges are classified by their current-voltage characteristics. Figure 1-3 shows the subdivision of the most common types of gas discharges, as has been derived by Druyvesteyn and Penning[5]. Although, their research was performed on low pressure discharges, it is still useful to use this classification, because many fundamental aspects also apply at atmospheric pressure.

When a very low voltage is applied, extremely low currents are observed, due to multiplication of electrons by collisions with gas molecules, resulting in ionization. The original electrons arise from cosmic radiation. If the cathode (negatively charged electrode) is illuminated by UV light are x-ray radiation, additional electrons are produced and cause a current increase. However, when the external source is removed, the current drops again. This phenomenon is called the "non self sustained discharge" (region A-B).

If the potential is further increased, the current rises rapidly and the external radiation source is no longer necessary. Each electron that leaves the cathode

produces ions and excited molecules by collision when it is accelerated towards the anode. These ions are accelerated towards the cathode and can produce new electrons by collision (secondary electron emission). New electrons can also be produced by radiation, caused by excited molecules that return to their ground state. If at least one electron is formed at the cathode for each electron that moves from the cathode to the anode, the process repeats itself making the discharge self sustaining (region B-C). Such self sustained discharge is also called a "Townsend discharge" or "dark discharge". The current in this type of discharge is so small (10^{-15} - 10^{-6} A/cm²) that almost no light is emitted, which explains the name "dark discharge". To sustain the current, a relatively high voltage is necessary.

When the current is allowed to increase beyond 10^{-5} - 10^{-6} A/cm², the discharge becomes visible and the potential across the electrodes drops a few hundreds of volts until it reaches a constant value. At this point, space charges start playing a role because they distort the applied electric field. The discharge conditions are now more favorable, making ionization easier and reducing losses of ions and electrons, so that a lower potential is sufficient to sustain the discharge, which is called the "glow discharge" (region D-H). The glow discharge can be subdivided in three different types. When it develops from the townsend discharge and the voltage drops, it is in the "subnormal discharge" regime (region D-E). If the voltage remains constant when the current is further decreased, the discharge is in the "normal glow" regime (region E-F). Here, the current covers only a part of the cathode area, while this area increases proportional with a current increase. When the whole cathode area is covered, the potential will rise with increasing current. The glow discharge is now in the "abnormal glow" regime (region F-H).

An even further increase of the current causes a drop of the potential to very low values. The ionic current towards the cathode is then so high that arcs are formed. This type of discharge is called an "arc discharge" (region K-…), which is a thermal plasma.

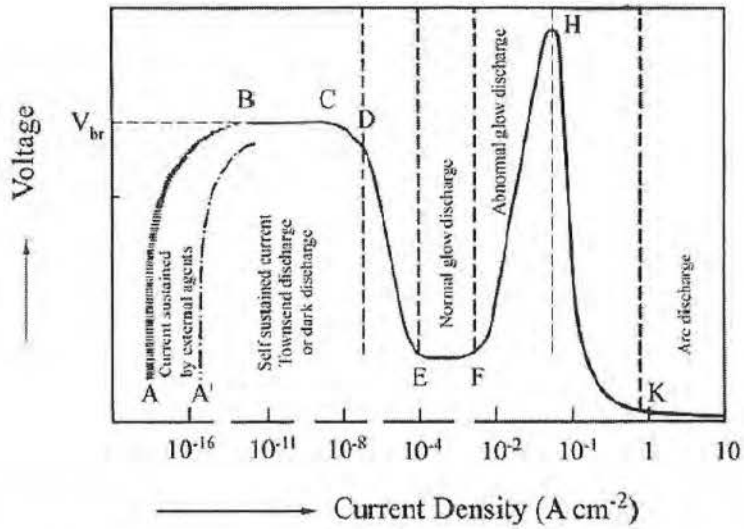

Figure 1-3: Discharge characterization for air at atmospheric pressure, based on the Druyvesteyn and Penning diagram.

Dielectric barrier discharge

Various types of atmospheric pressure plasma discharges can be distinguished: direct current (DC) discharges, pulsed DC discharges, RF discharges and microwave discharges[6]. The discharge type, that will be the subject of this thesis is the dielectric barrier discharge.

The first dielectric barrier discharge (DBD) reactor was developed by Werner von Siemensen for the generation of ozone. Typical for this kind of reactor is the presence of at least one dielectric barrier between the two electrodes. As dielectric material, usually glass, quartz or ceramics are used, which have dielectric constants from 1,5 up to 3000. This dielectric can cover one, both are lie in between the two electrodes (figure 1-4). Besides the system with two parallel plates, also a cylindrical system exists.

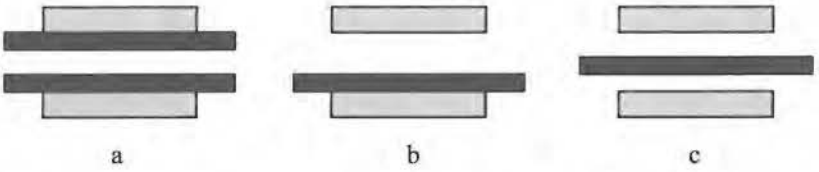

Figure 1-4: Schematic presentation of different setups for DBD reactors: a) both electrodes ■ covered with a dielectric ■ b) one electrode covered, c) dielectric in the middle.

To maintain the discharge in a DBD reactor, an alternating current (AC) voltage is required, because the charge would extinguish when a DC voltage was applied. A high ignition voltage is used to initiate breakdown of the gas in the inter-electrode gap. The dielectric at the high voltage electrode will charge positive, while the one at the grounded electrode becomes negatively charged. This decreases the electric field in the inter-electrode gap and would normally extinguish the discharge. However, when the polarity of the applied voltage is changed, the discharge will ignite again. This time, the electric field over the gap is the sum of the charges on the dielectric, created in the first discharge cycle (memory voltage) and the applied voltage. For this reason the voltage necessary to sustain the discharge is lower than the ignition voltage[7].

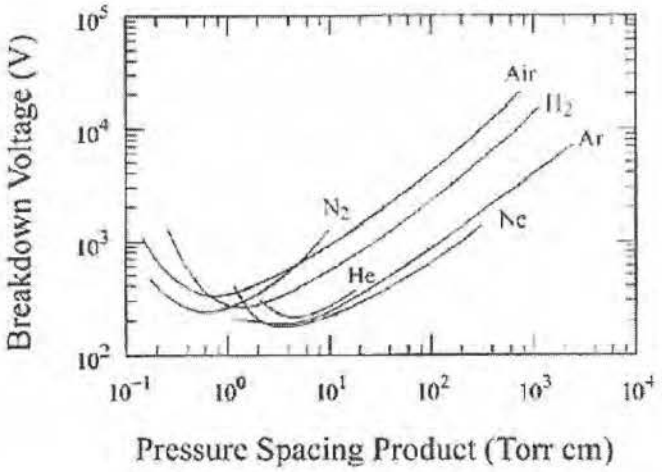

Figure 1-5: Paschen breakdown curves for some common plasma gases[8].

The applied voltage in a DBD reactor ranges from a few hundred volts to tens of kilovolts. The AC frequency can vary from hertz up to microwave frequencies. The pressure ranges from 10 mbar to atmospheric pressure (or higher). The inter electrode gap has a value in between 0.1 mm and a few cm. The breakdown voltage for a certain gas depends on the product of the pressure and the discharge length, as is shown in the Paschen breakdown curves (figure 1-5). So, the maximum inter-electrode distance at which a DBD reactor can work, depends on the pressure and the gas used. The maximum length of this gap is therefore smaller when the DBD is operated at atmospheric pressure. Nevertheless, it is more interesting to work at atmospheric pressure because the advantage of in-line processing. In this thesis, the DBD operating at low pressure is not discussed.

Filaments or glows?

When the electrical field applied on a DBD reactor is high enough to cause breakdown at atmospheric pressure, the formation of a large number of micro discharges is observed for most gases. In this filamentary mode, the plasma is only conductive in the micro discharges. The gas in between is not ionized and serves as a background reservoir to absorb the energy dissipated in the micro channels[9].

At atmospheric pressure, electrical breakdown in a large number of micro discharges is the normal situation for DBD configurations. Although, apparently diffuse and glow discharges can also be obtained under certain conditions. This is easily realized in pure helium, but also in other gases when special electrode configurations and operating conditions are used. At low pressure, typically below 100 Pa, diffuse discharges can always be obtained.

Two types of breakdown mechanisms can be distinguished: the streamer[10] and the townsend mechanism. The first mechanism occurs when a single electron multiplication (electron avalanche) produces such high space charge that a self propagating micro channel, called a streamer, is formed. A streamer mechanism is thus always filamentary. When the number of electrons in a single electron avalanche is below a critical value, breakdown occurs in a

townsend mechanism. A Townsend discharge can either be filamentary or diffuse. It is assumed that a townsend breakdown first results in a homogeneous glow discharge (first glow), later into a filamentary discharge (second glow) and finally into an arc, as is presented in the Kekez curve[11, 12] (figure 1-6). The transition between these discharge types is dependent on the type of discharge gas, the pressure, the voltage and the inter-electrode gap. Noble gases have long transition times (high ionization energy), which explains why it is relatively easy to obtain a stable glow discharge at atmospheric pressure in these gases.

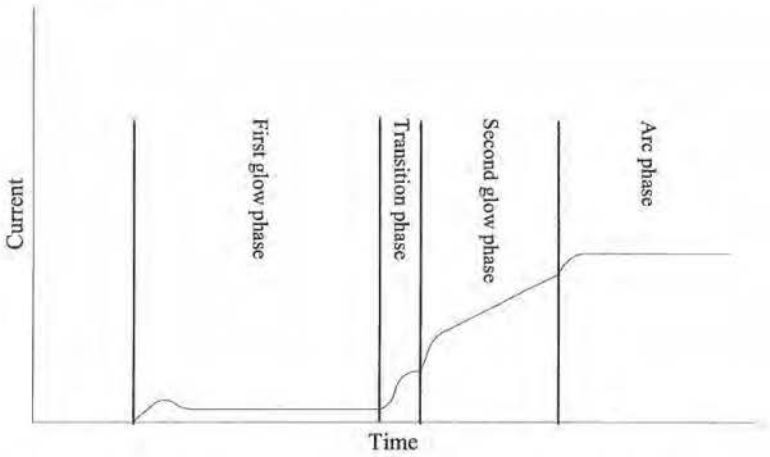

Figure 1-6: The Kekez curve, showing the transition from a glow to an arc discharge at atmospheric pressure[11].

1.3 Conjugated polymers

History and definition

Polymers or plastics are widely used in our society. Generally, they are known to be insulators. As such they are for instance used for insulation of electrical wires. However, this vision changed when a student of the Japanese chemist, Hideki Shirakawa, mistakenly added a thousand times too much catalyst, while synthesizing polyacetylene, in the early 1970's. This resulted in a gleaming

silvery film. At the same time chemist Alan MacDiarmid and physicist Alan Heeger were experimenting with a metallic looking film of the inorganic polymer sulfur nitride. When MacDiarmid and Shirakawa accidentally met at a seminar in Tokyo, they decided to measure the electrical properties of this strange looking polyacetylene coating. It turned out that the conductivity could be increased ten million times by treating the film with molecular iodine[13]. A new class of polymers, the conducting polymers, was born.

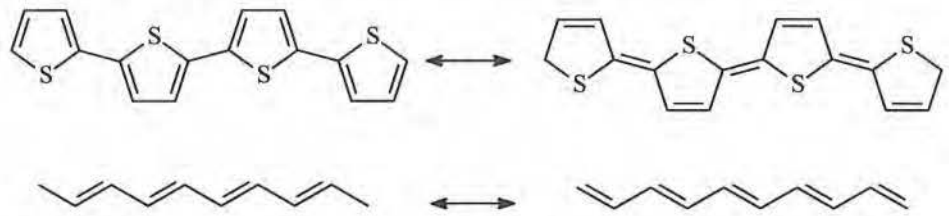

Figure 1-7: Resonance structures in polythiophene and polacetylene, respectively.

Typical for these conducting polymers is the conjugated structure in which double and single bonds are alternated. Due to the delocalized nature of the π-bonds as exemplified by their resonance structures (figure 1-7), conjugated polymers are able to transport charges along their polymer backbone. Some examples of conjugated polymers are presented in figure 1-8.

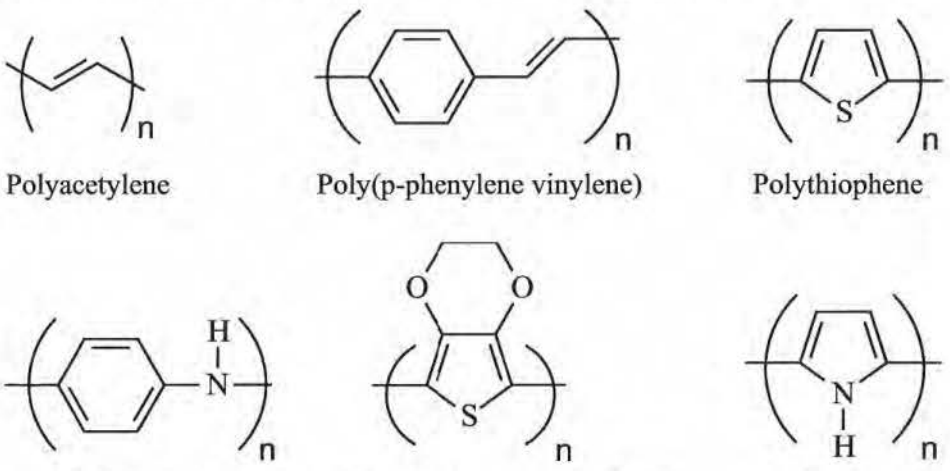

Figure 1-8: Examples of conjugated polymers

Electrical properties

Although conjugated polymers possess an extended conjugated π-system, they still behave as insulators. In contrast with metals, there is a large gap between the top of the valence band (VB), which is the highest occupied molecular orbital (HOMO) and the bottom of the conduction band (CB), which is the lowest unoccupied molecular orbital (LUMO) (figure 1-9)[14]. In order to make the polymer (semi-) conductive, charge carriers have to be injected, which is done by doping. This is presented in figures 1-9b and 1-9c as an insertion of respectively filled or empty energy levels in the energy gap. Filled energy bands are created by the injection of electrons in the polymer chain (reduction). This is called n-doping. When electrons are withdrawn (oxidation) from the polymer chain, holes are created, which results in empty energy bands in the band gap. This is called p-doping and is the most common type of doping.

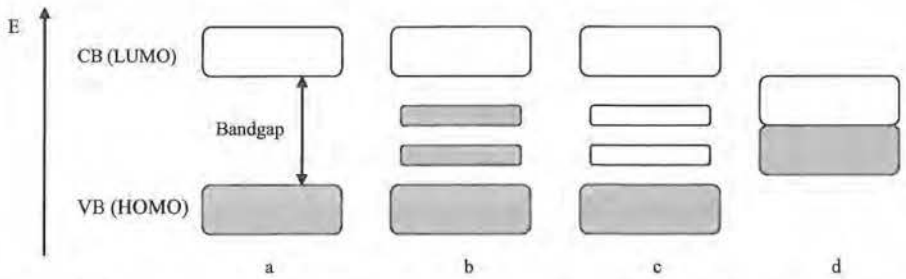

Figure 1-9: Band model of: a) a conjugated polymer, b) an n-doped conjugated polymer, c) a p-doped conjugated polymer and d) a metal.

Colored polymers

Another typical property of conjugated polymers is their interaction with light. When the energy of light is high enough it might excite the polymer. This happens when the electron is able to absorb enough energy to jump from the HOMO to the LUMO (figure 1-10a). The wavelength at which this happens is thus an indication for the energy gap (E). After all:

$$E = h\nu = hc/\lambda$$

With h Planck's constant, ν the frequency of the light, λ the wavelength of the light and c the light speed. When the conjugated polymer is doped, energy levels are inserted into the band gap, which is accompanied by a color change (towards longer wavelengths) (figure 1-10b). Conjugated polymers usually have a band gap between 0.5 and 4 eV, which is consistent with an absorption of light in the visible or near infrared range.

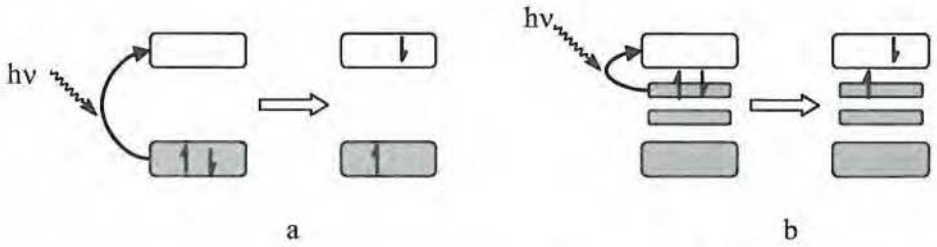

Figure 1-10: Light absorption by: a) a conjugated polymer, b) a doped conjugated polymer.

Applications of conjugated polymers

The use of organic polymers as semi-conductors offers a lot of advantages. Organic materials are light weight and can be produced at low cost. Furthermore, they can be produced on flexible substrates because they don't break when bend. These advantages make them useful for a lot of applications (figure 1-11).

When sandwiched between two electrodes, conjugated polymers can be used as polymer light emitting diodes (polyLEDS)[15, 16](A). Application of an electric field on the conjugated polymer layer will result in the emission of colored light. The color of the emitted light is typical for a certain polymer. The opposite happens in organic solar cells (B), where light is turned into an electrical current[17]. Here, two conducting materials are blended to provide charge separation. Usually a conjugated polymer that is easily oxidized (electron donor) is combined with a fullerene derivative (bucky balls - electron acceptor). When the conjugated polymer blend is sandwiched between two working electrodes, the existing potential difference will separate the electron and hole pair of an excited polymer, creating a current.

Figure 1-11: Examples of conjugated polymers in applications: A) a polyLED tv, B) a flexible polymer solar cell, C) a flexible polymer transistor.

The possibility for charge transportation along the doped conjugated polymer backbone makes them also interesting for application in organic field effect transistors[18] (C), (bio)sensors[19] and antistatic layers. Also remarkable, is the ability of conjugated polymers to protect metals against corrosion[20]. Not only do they provide a barrier against oxygen attack, they also keep on protecting the metal when the coating is scratched, what makes them interesting candidates for the replacement of the toxic chromium conversion coatings. A more detailed discussion about the corrosion protection properties of conjugated polymer coatings is done in chapter 4.

Drawbacks

Conjugated polymers are usually synthesized with chemical and electrochemical methods[21, 22]. Both methods have their drawbacks, however. In general, the typical structure with alternate single and double bonds leads to rigid, insoluble polymers. The situation gets even worse after doping. Processing of the polymers, resulting from chemical polymerization is therefore difficult. If the substrate is conductive, this problem can be solved by using electropolymerization with deposition directly on the substrate. Nevertheless, both chemical and electrochemical synthesis, are usually performed in batch processes, which is the reason why, until today, they are only used for small scale applications with high added values. The most important advantage of polymers, which is high speed in-line processing with

low production cost, does not count here. It is the purpose of this thesis to overcome this problem by studying a new polymerization technique, which could make these polymers more easily available for industrial application.

1.4 Plasmas and polymers

Today, plasma processes are a growing technology in different domains. A lot of technological applications, developed in the latest decennia and now used in industrial processes, could only be made possible with plasma assisted methods. Examples of industrial plasma processes are surface modification, pollution control, sterilization, cleaning and etching. Plasma can also be found in a lot of well known applications, such as lamps and plasma screens[2, 3].
Recently, synthesis of thin polymer films by use of plasma polymerization has emerged as an interesting new approach. Plasma polymerization is a 'dry' technique that doesn't require the use of solvents. From an ecological and economical point of view, the absence of solvents and solvent waste offers a lot of advantages. While plasma polymerization was first used for the formation of thin passive layers, it is now used for many different applications.

Low pressure plasma deposition

Initially, plasma depositions were performed at low pressure, which was especially successful for deposition of wear resistant coatings and dense gas barrier layers. Today, also applications that require retention of specific polymer functions are targeted. In this view, also deposition of conjugated polymers at low pressure has been studied. These reactive vacuum plasmas often result in a significant fragmentation of the monomer structure. In some cases however, a part of the monomer structure could be maintained after plasma treatment. A method for such vacuum plasma deposition of conjugated polymers was patented by Affinito et al. in the European patent EP 1 144 131 and the United States patents US 6 207 239, US 6 228 436 and US 6 274 204. The conjugated polymer is deposited in a glow discharge at low pressure after

flash evaporating an atomized monomer into the reactor chamber. Many different research groups have also documented on the vacuum plasma deposition of conjugated polymers.

Vacuum plasma deposition of polyaniline is studied by Cruz et al.[23]. In plasma, the aromatic rings of aniline had partially degraded and the resulting deposition was cross-linked. The conductivity of the plasma deposited polyaniline was low and dependent on the humidity. Paterno et al.[24] and Zaharias et al.[25] also report degradation of aniline in a low pressure plasma. Aromatic rings were fragmented with formation of aliphatic structures. Mathai et al.[26-28] showed that the aromatic ring of aniline was partially retained after plasma polymerization, resulting in a considerably low dielectric constant. Iodine doping decreased the bandgap. Plasma polyaniline doped in a iodine chamber was compared to in situ doped plasma polyaniline, which was more stable. Also Bhat et al.[29] and Olayo et al.[30, 31] had similar results when they doped plasma polyaniline with iodine. Nastase et al.[32] plasma deposited polyaniline at low pressure with simultaneous injection of the dopant toluene sulphonic acid, which resulted in an increased conductivity. Wang et al.[33] report that low pressure plasma deposited polyaniline is different compared to chemical and electrochemical synthesis methods. Oligomeric depositions with an unconventional benzene substitution pattern were obtained. The conductivity of plasma polyaniline was significantly lower. Gong et al.[34] also deposited a polyaniline like structure with low pressure plasmas.

Low pressure plasma polymerization of thiophene is studied by Silverstein et al.[35]. The molecular structure of the obtained plasma polymer contained opened thiophene rings and oxygen and nitrogen atoms. A conducting iodine percolation network seemed to have formed upon doping with iodine. Kim et al.[36-38] plasma deposited polythiophene like structures with reduced bandgap. Vasquez et al.[39] obtained in situ chlorine doped plasma polythiophene by simultaneous injection of chloroform. The conductivity was dependent on the humidity. Groenewoud et al.[40-43] reported the influence of substitutions on the plasma polymerization of thiophene. Electron donating substituents such as methyl groups suppress fragmentation, whereas the higher electron affinity of electron withdrawing groups such as halogens results in a higer degree of

fragmentation. Fragmentation is always less when the number of substituents is increased. For a specific substituent, substitution on the 2-position results in less fragmentation compared with substitution on the 3-position. Conductivity, after iodine doping was higher for methyl-substituted polythiophene than for nonsubstituted and halogenated polythiophene. Iodine doping resulted in charge transfer complexes and carbon iodine chemical bonds. Since the chemical structure of plasma polythiophene changed after exposure to air before doping, the conductivity decreased. Higher conductivities could be reached when the pressure during plasma polymerization was slightly increased, because this resulted in less fragmentation. Bae et al.[44] reported that plasma deposited polythiophene layers can be used for corrosion protection of metals. Plasma depositions of polythiophene at low pressure were also obtained by other authors[45-50]. Zhou et al. [51]improved the lifetime of chemically produced PEDOT coatings by mild oxygen plasma treatment.

Morales et al.[52] plasma deposited polypyrrole like coatings at low pressure which had a much lower conductivity than conventional polypyrrole. Zhang et al.[53] reports the formation of a dense yellow film when plasma polymerizing pyrrole. Although these plasma polypyrrole coatings still contained a certain amount of intact pyrrole rings, structural degradation by oxygen contamination, was also observed. Martin et al.[54] deposited polypyrrole and polythiophene thin films with a vacuum RF pulsed plasma. The use of a pulsed plasma, which has a lower ionization degree, resulted in slower deposition rates but the chemical structure was better retained and the coating roughness extremely low. Cruz et al.[55] reports vacuum plasma deposition of in situ iodine doped polypyrrole. These polypyrrole films were hygroscopic and absorbed water from ambient air, which increased chain mobility of the polymer. This induced ordering of the polymer chains and increased conductivity. Undoped polypyrrole seemed to have more capacity to store water than doped polypyrrole. Wang et al.[56] compares vacuum RF plasma polymerized with conventionally synthesized polypyrrole and polythiophene. Plasma polymerization results in structures which are substantially different due to fragmentation, trapped free radicals, branching and cross-linking. While the films obtained from vacuum plasma polymerization are smoother and more

homogeneous than those obtained from conventional synthesis methods, their conductivity after iodine doping was significantly lower and less stable. Due to the low conductivity of plasma polymerized polypyrrole, reported by most authors, Kumar et al.[57] even consider to use it as a dielectric material. He succeeded in plasma polymerizing polypyrrole like films with a high dielectric constant. Hosono et al.[58] show that plasma polymerized polypyrrole coatings, doped with 4-ethylbenzenesulfonic acid can be used to sensor volatile organic compounds. Sensitivity of the sensor was dependent on humidity. Plasma polymerization of polypyrrole coatings at low pressure was also studied by John et al.[59] and Eufinger et al.[60]

Plasma copolymerization can easily be done by simultaneously injecting two monomers. This is shown by Morales et al.[61], who report plasma copolymererization at low pressure of pyrrole and aniline. The monomer mass ratio influenced the structural evolution and the physical characteristics of the copolymers. Hirotsu et al.[62] plasma copolymerized pyrrole and silicon containing compounds (hexamethyldisiloxane, hexamethyldisilane and hexamethyldisilazane). Copolymerization had an effect on the physical properties of the film and the hydrophobicity of the surface. Nastase et al.[63] plasma deposited polyaniline-silicon dioxide and polythiophene-silicon dioxide nanocomposites by spraying dispersions of nano sized silica particles in monomer liquids, into the plasma zone. Synthesis of vacuum plasma polymerized bi-layers is done by Morales et al.[64]. Plasma polyaniline/polypyrrole bi-layers were chemically bonded at the interface and had a higher conductivity after doping compared to the separated homopolymers.

In conclusion can be stated that plasma polymerization of conjugated polymers at low pressure leads to fragmentation and unconventional cross-linking, resulting in low conductivity after doping.

Plasma deposition at atmospheric pressure

While first plasma depositions were done at low pressure, recent research is much more oriented towards plasma coating at atmospheric pressure, because it

can be implemented in in-line industrial processes. Furthermore, no expensive vacuum equipment is needed and deposition rates are usually higher.

A typical application of plasma technology at atmospheric pressure is the deposition of siloxanes. For siloxane deposition, structural fragmentation of the precursor is often desired in order to form SiO_2 like structures[65-72]. These coatings can be used for their gas barrier properties, while some also result in hydrophobic layers. For other applications structural retention is required. Some authors show that polymer functionalities can be retained after plasma deposition at atmospheric pressure, which is less aggressive than deposition at low pressure. Klages et al.[73] showed that polymerization of glucidyl methacrylate in a pulsed plasma reactor at atmospheric pressure resulted in retention of 90% of the epoxy groups of glucidyl methacrylate. Furthermore, Ward et al.[74] report that ultrasonic atomization of acrylic acid in an atmospheric pressure helium glow discharge results in deposition of structurally well-defined polymer films. Polymerization proceeded predominantly via the carbon double bond with high retention of the carboxylic acid group.

Despite good results with plasma deposition at atmospheric pressure of other polymers, plasma polymerization of conjugated polymers has never been documented before. Although, patent EP 1 326 718 mentions pyrrole and thiophene as possible precursors for use in their atmospheric pressure plasma reactor. In this thesis, plasma polymerization of conjugated polymers at atmospheric pressure will be described for the first time.

1.5 Objectives

Conjugated polymers posses some unique properties, which make them useful for a lot of applications. However, their rigid structure makes them insoluble and difficult to process. Today, (electro)chemically produced conjugated polymers can be synthesized in batch processes for applications with high added value. In-line processing is still difficult. Therefore, plasma technology at atmospheric pressure is presented in this thesis as an alternative synthesis method. Besides the possibility for in-line deposition directly onto the substrate, there is the advantage of dry processing. No solvents are needed, which is an important environmental benefit.

In this thesis, two objectives were postulated:

- Proof of principle of atmospheric pressure plasma deposition of conjugated polymer coatings, with retention of their typical properties.
- Development of a plasma deposited conjugated polymer coating for corrosion protection of metals, in order to replace toxic chromium conversion coatings.

Chapter 2 reports on plasma deposition experiments, using different precursor molecules. The chemical, mechanical and electrical properties of the resulting coatings are studied. Since polyaniline is known for its good corrosion protection properties, experiments with aniline were done first followed by depositions with pyrrole, thiophene and thiophene derivatives.

In chapter 3, plasma polymerized and in situ doped conjugated polymers are discussed. The possibility for simultaneous injection of another chemical during plasma polymerization is another great advantage of plasma deposition. This way, conjugated polymers can possibly be doped during deposition, which could result in more homogeneous and stable doping.

Chapter 4 describes the corrosion protection properties of the conjugated plasma polymer coatings deposited at atmospheric pressure. It is also studied whether anti-corrosion performance of the plasma coatings can be improved by combining the conjugated polymer coatings with a plasma deposited barrier layer.

1.6 References

1 A. Grill, *IEEE Press* **1994**, 1

2 A. Bogaerts, E. Neyts, R. Gijbels, J. van der Mullen, *Spectrochimica Acta Part B-Atomic Spectroscopy* **2002**, 57, 609

3 R. d'Agostino, P. Favia, C. Oehr, M. R. Wertheimer, *Plasma Processes and Polymers* **2005**, 2, 7

4 C. Tendero, C. Tixier, P. Tristant, J. Desmaison, P. Leprince, *Spectrochimica Acta Part B: Atomic Spectroscopy* **2006**, 61, 2

5 M. J. Druyvesteyn, F. M. Penning, *Rev. Mod. Phys.* **1940**, 12, 87

6 A. P. Napartovich, *Plasmas and Polymers* **2001**, 6, 1

7 F. Massines, D. Mary, C. Laurent, C. Mayoux, *Journal of Physics D-Applied Physics* **1993**, 26, 493

8 Y. P. Raizer, *Springer* **2001**, 1

9 U. Kogelschatz, *Plasma Chemistry and Plasma Processing* **2003**, 23, 1

10 L. B. Loeb, J. M. Meek, *Journal of Applied Physics* **1940**, 11, 438

11 M. M. Kekez, M. R. Barrault, J. D. Craggs, *Journal of Physics D-Applied Physics* **1970**, 3, 1886

12 S. Okazaki, M. Kogoma, M. Uehara, Y. Kimura, *Journal of Physics D-Applied Physics* **1993**, 26, 889

13 H. Shirakawa, E. J. Louis, A. G. MacDiarmid, A. J. Heeger, *Chem. Commun.* **1977**, 578

14 D. F. Shriver, P. W. Atkins, C. H. Langford, *Inorganic chemistry - second edition* **1994**, 91

15 R. E. Martin, F. Geneste, A. B. Holmes, *Comptes Rendus de l'Academie des Sciences - Series IV - Physics* **2000**, 1, 447

16 A. Dodabalapur, *Solid State Communications* **1997**, 102, 259

17 J.-M. Nunzi, *Comptes Rendus Physique* **2002**, 3, 523

18 V. Saxena, B. D. Malhotra, *Current Applied Physics* **2003**, 3, 293

19 B. Adhikari, S. Majumdar, *Progress in Polymer Science* **2004**, 29, 699

20 P. Zarras, J. D. StengerSmith, M. H. Miles, *Abstracts of Papers of the American Chemical Society* **1997**, 213, 354

21 A. Pron, P. Rannou, *Progress in Polymer Science* **2002**, 27, 135

22 K. Gurunathan, A. V. Murugan, R. Marimuthu, U. P. Mulik, D. P. Amalnerkar, *Materials Chemistry and Physics* **1999**, 61, 173

23 G. J. Cruz, J. Morales, M. M. CastilloOrtega, R. Olayo, *Synthetic Metals* **1997**, 88, 213

24 L. G. Paterno, S. Manolache, F. Denes, *Synthetic Metals* **2002**, 130, 85

25 G. A. Zaharias, H. H. Shi, S. F. Bent, *Thin Solid Films Proceedings of the Third International Conference on Hot-Wire CVD (Cat-CVD) Process* **2006**, 501, 341

26 C. J. Mathai, S. Saravanan, M. R. Anantharaman, S. Venkitachalam, S. Jayalekshmi, *Journal of Physics D-Applied Physics* **2002**, 35, 240, 27 C. J. Mathai, S. Saravanan, S. Jayalekshmi, S. Venkitachalam, M. R. Anantharaman, *Materials Letters* **2003**, 57, 2253

28 C. J. Mathai, S. Saravanan, M. R. Anantharaman, S. Venkitachalam, S. Jayalekshmi, *Journal of Physics D: Applied Physics* **2002**, 35, 2206

29 N. V. Bhat, N. V. Joshi, *Plasma Chemistry and Plasma Processing* **1994**, 14, 151

30 M. G. Olayo, J. Morales, G. J. Cruz, R. Olayo, E. Ordonez, S. R. Barocio, *Journal of Polymer Science Part B-Polymer Physics* **2001**, 39, 175

31 M. G. Olayo, G. J. Cruz, E. Ordonez, J. Morales, R. Olayo, *Polymer* **2004**, 45, 3565

32 C. Nastase, D. Mihaiescu, F. Nastase, A. Moldovan, I. Stamatin, *Synthetic Metals* **2004**, 147, 133

33 J. G. Wang, K. G. Neoh, L. P. Zhao, E. T. Kang, *Journal of Colloid and Interface Science* **2002**, 251, 214

34 X. Gong, L. Dai, A. W. H. Mau, H. J. Griesser, *Journal of Polymer Science Part A: Polymer Chemistry* **1998**, 36, 633

35 M. S. Silverstein, I. Visoly-Fisher, *Polymer* **2002**, 43, 11

36 K. J. Kim, N. E. Lee, M. C. Kim, J. H. Boo, *Thin Solid Films* **2001**, 398, 657

37 M. C. Kim, S. H. Cho, J. G. Han, B. Y. Hong, Y. J. Kim, S. H. Yang, J. H. Boo, *Surface & Coatings Technology* **2003**, 169, 595

38 M.-C. Kim, S.-H. Cho, S.-B. Lee, Y. Kim, J.-H. Boo, *Thin Solid Films* **2004**, 447, 592

39 M. Vasquez, G. J. Cruz, M. G. Olayo, T. Timoshina, J. Morales, R. Olayo, *Polymer* **2006**, 47, 7864

40 L. M. Groenewoud, A. E. Weinbeck, G. H. Engbers, J. Feijen, *Synthetic Metals* **2002**, 126, 143

41 L. M. H. Groenewoud, G. H. M. Engbers, J. Feijen, *Langmuir* **2003**, 19, 1368

42 L. M. H. Groenewoud, G. H. M. Engbers, J. G. A. Terlingen, H. Wormeester, J. Feijen, *Langmuir* **2000**, 16, 6278

43 L. M. H. Groenewoud, G. H. M. Engbers, R. White, J. Feijen, *Synthetic Metals* **2001**, 125, 429

44 I.-S. Bae, C.-K. Jung, S.-H. Jeong, S.-J. Cho, Y. J. Yu, J. G. Kim, J.-H. Boo, *Thin Solid Films Proceedings of the Eighth International Conference on Atomically Controlled Surfaces, Interfaces and Nanostructures and the Thirteenth International Congress on Thin Films - ACSIN-8/ICTF-13* **2006**, 515, 407

45 V. J. Rao, V. Manorama, S. V. Bhoraskar, *Applied Physics Letters* **1989**, 54, 1799

46 N. V. Bhat, D. S. Wavhal, *Journal of Applied Polymer Science* **1998**, 70, 203

47 N. V. Bhat, D. S. Wavhal, *Separation Science and Technology* **2000**, 35, 227

48 D. H. Shin, S. D. Lee, K. P. Lee, S. Y. Park, D. H. Choi, N. Kim, *Synthetic Metals* **1995**, 71, 2263

49 S.-M. Park, K. Ebihara, T. Ikegami, B.-J. Lee, K.-B. Lim, P.-K. Shin, *Current Applied Physics* **2006**, 7, 474

50 J. L. Delattre, R. d'Agostino, F. Fracassi, *Applied Surface Science* **2006**, 252, 3912

51 Y.-f. Zhou, Y.-b. Yuan, L.-f. Cao, J. Zhang, H.-q. Pang, J.-r. Lian, X. Zhou, *Journal of Luminescence* **2007**, 122-123, 602

52 J. Morales, M. G. Olayo, G. J. Cruz, M. M. Castillo-Ortega, R. Olayo, *Journal of Polymer Science Part B-Polymer Physics* **2000**, 38, 3247

53 J. Zhang, M. Z. Wu, T. S. Pu, Z. Y. Zhang, R. P. Jin, Z. S. Tong, D. Z. Zhu, D. X. Cao, F. Y. Zhu, J. Q. Cao, *Thin Solid Films* **1997**, 307, 14

54 L. Martin, J. Esteve, S. Borros, *Thin Solid Films, Proceedings of Symposium D on Thin Film and Nano-Structured Materials for Photovoltaics, of the E-MRS 2003 Spring Conference*, **2004**, 451, 74

55 G. J. Cruz, J. Morales, R. Olayo, *Thin Solid Films* **1999**, 342, 119

56 J. Wang, K. G. Neoh, E. T. Kang, *Thin Solid Films* **2004**, 446, 205

57 D. S. Kumar, Y. Yoshida, *Surface and Coatings Technology* **2003**, 169, 600

58 K. Hosono, I. Matsubara, N. Murayama, W. Shin, N. Izu, *Thin Solid Films* **2005**, 484, 396

59 R. K. John, D. S. Kumar, *Journal of Applied Polymer Science* **2002**, 83, 1856

60 S. Eufinger, W. J. vanOoij, T. H. Ridgway, *Journal of Applied Polymer Science* **1996**, 61, 1503

61 J. Morales, M. G. Olayo, G. J. Cruz, R. Olayo, *Journal of Applied Polymer Science* **2002**, 85, 263

62 T. Hirotsu, Z. Hou, A. Partridge, *Plasmas and Polymers* **1999**, 4, 1

63 F. Nastase, I. Stamatin, C. Nastase, D. Mihaiescu, A. Moldovan, *Progress in Solid State Chemistry Advanced Functional Nanomaterials: from NanoscaleObjects to Nanostructered Inorganic and Hybrid Materials* **2006**, 34, 191

64 J. Morales, M. G. Olayo, G. J. Cruz, R. Olayo, *Journal of Polymer Science Part B-Polymer Physics* **2002**, 40, 1850

65 O. Goossens, E. Dekempeneer, D. Vangeneugden, R. Van de Leest, C. Leys, *Surface & Coatings Technology* **2001**, 142, 474

66 Y. Sawada, S. Ogawa, M. Kogoma, *Journal of Physics D: Applied Physics* **1995**, 28, 1661

67 H. R. Lee, D. J. Kim, K. H. Lee, *Surface & Coatings Technology* **2001**, 142, 468

68 G. R. Prasad, S. Daniels, D. C. Cameron, B. P. McNamara, E. Tully, R. O'Kennedy, *Surface and Coatings Technology PSE 2004* **2005**, 200, 1031

69 F. Massines, N. Gherardi, A. Fornelli, S. Martin, *Surface and Coatings Technology, ICMCTF 2005* **2005**, 200, 1855

70 O. Goossens, S. Paulussen, D. Vangeneugden, H. Vrielinck, F. Callens, C. Leys, J. Meneve, *New Diamond and Frontier Carbon Technology* **2003**, 13, 221

71 A. Sonnenfeld, T. M. Tun, L. Zajcaronkov, K.V. Kozlov, H.-E. Wagner, J. F. Behnke, R. Hippler, *Plasmas and Polymers* **2001**, 6, 237

72 C. P. Klages, M. Eichler, R. Thyen, *New Diamond and Frontier Carbon Technology* **2003**, 13, 175

73 C.-P. Klages, K. Höpfner, B. Niklas Kläke AFFIL Fraunhofer Institute for Surface Engineering and Thin Films (IST), Germany, Rudolf Thyen, *Plasmas and Polymers* **2000**, 5, 79

74 L. J. Ward, W. C. E. Schofield, J. P. S. Badyal, A. J. Goodwin, P. J. Merlin, *Chemistry of Materials* **2003**, 15, 1466

Chapter 2

Plasma deposition of conjugated polymer coatings at atmospheric pressure

2.1 Introduction

Chemical or electrochemical synthesis of conjugated polymers is usually a batch process. Plasma deposition at atmospheric pressure is presented as an alternative coating method for in-line processing.

First, the reactor design will be explained in more detail. Plasma depositions are carried out in a dielectric barrier discharge reactor (DBD). Variations of the different plasma parameters have been studied in order to asses the effect on the coating properties. Parameters that can have an influence on the plasma deposition process and the coatings resulting therefrom are: power, frequency, gas flow, gas composition and precursor concentration. The parameters are discussed by doing experiments in a DBD reactor using several precursors. These precursors are aniline, pyrrole, thiophene and derivatives. Aniline is chosen because the application aimed at, is corrosion protection of metals. After all, polyaniline is known for its good anti-corrosion properties on steel. Also pyrrole and thiophene are used for corrosion protection of metals. Pyrrole is easily polymerized in electrochemical and chemical processes, while polymerization of thiophene is more difficult with conventional techniques.

The effect of the plasma parameters on the plasma coatings can be studied with conventional surface characterization techniques, such as Fourier transformed infrared spectroscopy (FT-IR), UV and visible light absorption spectroscopy (UV/VIS) and X-ray photo-electron spectroscopy (XPS). Also the conductivity of the plasma coatings is studied by measuring the electrical resistance.

2.2 The dielectric barrier discharge reactor

A schematic presentation of the used DBD reactor is presented in figure 2-1. It consists of two parallel aluminum electrodes. On the outside, these electrodes are insulated with PET. The lower electrode is covered with a 5 mm thick glass dielectric. The upper electrode is uncovered. The gap between the upper electrode and the dielectric is regulated by using spacers. This gap was varied between 1,5 and 2 mm, although larger gaps are also possible. A high voltage is used on the lower, covered electrode while the upper electrode is grounded. The voltage over the electrodes is regulated by adjusting the power delivered by the generator. This voltage is transformed up to high voltage by a transformer. The capacity and induction of the transformer is carefully tuned to minimize power losses for a certain frequency and reactor geometry. This is often referred to as matching. The voltage also depends on the used carrier gas, the reactor geometry and the frequency. This frequency is regulated on the power supply and can be varied between 1 and 100 kHz.

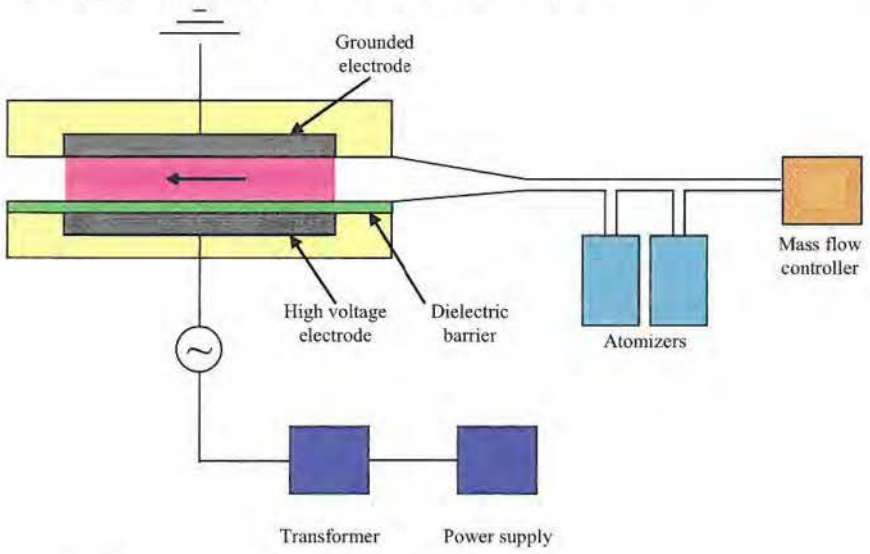

Figure 2-1: Schematic presentation of a DBD reactor.

The gas flow is adjusted by a mass flow controller. The flow usually varies between 1 and 50 l/min. The native of the gas has a strong influence on the plasma generation. When noble gases such as helium or argon are used, gas breakdown is easily realized. The voltage amplitude is relatively low, as is the power consumption. There are also less restrictions on the inter electrode gap (see Paschen breakdown curve, figure 1-5)[1]. However these gases are rather expensive. From an industrial point of view, it is more interesting to use nitrogen as discharge gas. Most experiments in this work are done in nitrogen. The discharge gas is also used to transport the precursor to the electrodes and hence also referred to as carrier gas. The precursor is injected into the carrier gas with an aerosol generator. This aerosol generator is pressure controlled and can generate aerosols of small dimensions. The working principle of these aerosols is explained in figure 2-2. Compressed gas is expanded through an orifice to form a high velocity jet. Liquid is drawn into the atomizing section through a vertical passage and is then atomized by the jet. By impact with the wall, opposite to the jet, large droplets are removed. The removed liquid is recirculated. With this system it is possible to create high aerosol concentrations (2 x 10^6 particles/cm^3) with droplet diameters around 0.3 µm.

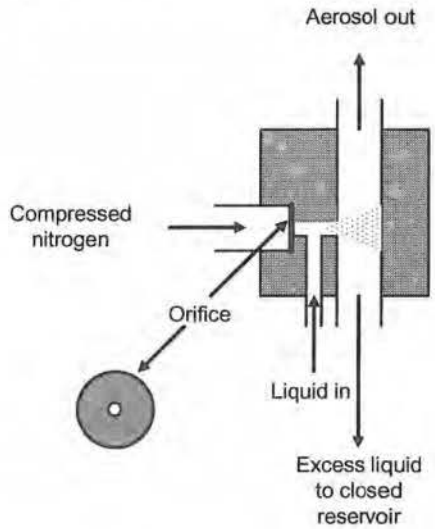

Figure 2-2: Working principle of a pressure controlled atomizer with recycling of excess liquid.

2.2 Plasma deposition of polyaniline coatings

About polyaniline

Polyaniline was first synthesized in 1835[2], and the term 'aniline black' was given to the resulting polymer. This type of structure is also found in melanin. Melanin is a pigment that gives skin and hair its natural color. It protects skin against UV light. Polyaniline differentiates itself from other conjugated polymers, as it can be doped by acids. It exists in four different states[3], presented in figure 2-3:

- The leucoemeraldine form: This is the completely reduced form of polyaniline. It absorbs light in the UV-region, which means that it has a transparent color. Usually, a yellow color is observed, probably because of the presence of radical species, deeply inserted in the polymer sites.
- The emeraldine base: This is the semi-oxidized state, with a blue-violet color.
- The pernigraniline form: In this state the polyaniline is completely oxidized. It has a violet color.
- The emeraldine salt: This is the (acid) doped state. Protonation of a (semi-) oxidized form of polyaniline results in charged polymer chains. It is the green colored conducting form of polyaniline.

Polyaniline is usually produced as emeraldine salt from (electro) chemical polymerization. The emeraldine base can be obtained by treatment with a base.

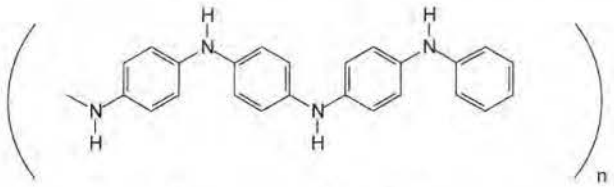

Leucoemeraldine form

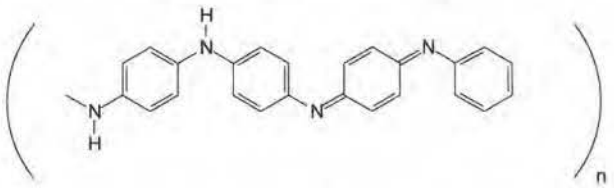

Emeraldine base

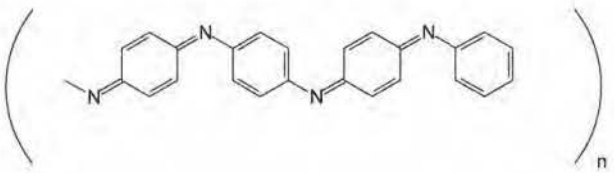

Pernigraniline form

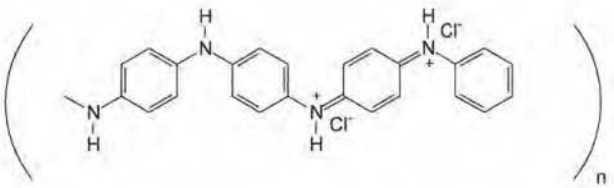

Emeraldine salt

Figure 2-3: The four different states of polyaniline.

Polyaniline is known as an active corrosion preventing pigment[4-8]. Because of its possibility for acid doping it performs excellent in acid media. Especially the double stranded polyaniline[9] is used, which is a stable helix structure of polyaniline and a polyanion such as the anion of poly(acrilic acid) or poly(styrene sulfonic acid).

Polymer precursor

The easiest way to produce a conjugated plasma polymer coating is by injecting the polymer into the plasma and cross linking it. Polyaniline is commercially available in powder form. Since low molecular weight emeraldine base polyaniline is soluble in some solvents, the first experiments were done by injecting an aerosol of polyaniline solution into the plasma.

The highest polyaniline concentration could be obtained with N-methyl pyrrolidone (NMP) as solvent. Even in this solvent, the solubility is low (max. 0.5% wt). Besides NMP, also an NMP/aniline (50/50) mixture and pure aniline were used as solvent. The experiments are summarized in table 2-1.

Solvent	Concentration	Plasma coating
NMP	0,5% wt*	No coating
NMP/aniline (1/1)	0,4% wt*	Yellow-brown coating
Aniline	0,4% wt*	Yellow-brown coating

Table 2-1: Different solutions of polyaniline, injected in a DBD reactor.

** Saturated solution*

No coating deposition was observed when a solution of polyaniline in NMP was injected into the plasma. Probably, the concentration of polyaniline in the plasma is too low. Furthermore, the polyaniline is protected from attack of energetic electrons because it is surrounded by NMP molecules. When polyaniline was dissolved in an aniline/NMP mixture, a yellow-brown plasma coating could be obtained although the maximum polyaniline concentration was even lower in this case. However, the original polyaniline emeraldine base has a blue color. It seems that the plasma coating was mainly formed by polymerization of the monomer aniline. A similar result was obtained when only aniline was used as solvent.

To study the effect of plasma treatments on polyaniline, the polymer was dip coated onto a substrate and brought into a nitrogen plasma for three minutes. The influence of plasma on the conjugated polymer film is shown in table 2-2. Polyaniline emeraldine base still showed a blue color after interaction with the

plasma which means that the conjugated system is retained. The absolute resistivity of the coating had even decreased which is probably due to the creation of charge carriers in the coating, resulting in a small doping effect.

Plasma treatment	color	resistivity (ohm)
Untreated	Blue	$2,5 \times 10^{11}$
Treated	Blue	$1,6 \times 10^{11}$

Table 2-2: Effect of plasma treatment on a polyaniline coating.

Effect of the power level on plasma polymerization of aniline

Generally, higher plasma power, which causes higher ionization degree, results in an increased deposition rate. However, higher ionization degree is usually also accompanied by an increased fragmentation of the monomer structure. It is thus important to find a good balance between reaction rate and structure retention, which results in maintenance of typical properties. Figure 2-4 shows the effect of the power level on the deposition rate. All depositions were done in air, which is a mixture of nitrogen and 21% oxygen. The deposition rate indeed increased with increased power level. However there seems to be a limit at high powers. Several factors might be responsible for this phenomenon, such as strong degradation, limited precursor availability or power losses.

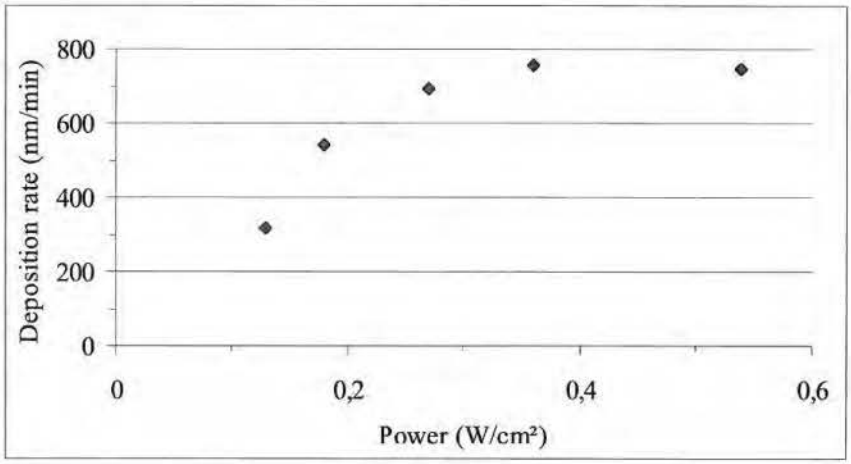

Figure 2-4: Effect of the power level on the deposition rate of plasma polyaniline.

The effect of the power level on the final structure of the polymer is studied with IR spectroscopy. For a better understanding of the differences between plasma polyaniline and conventional polyaniline, the spectra of aniline and polyaniline are discussed, first. Figure 2-5 shows the IR spectra of the monomer aniline and the emeraldine base form of polyaniline. A peak assignment is presented in table 2-2.

Aniline possesses some characteristic vibrations that absorb in the infrared region. The amine N-H stretching vibration is located around 3400 cm^{-1}. This vibration is intense and broad, because of hydrogen bonding. When strongly hydrogen bonded, the amine N-H stretch shifts to lower wavelengths, around 3200 cm^{-1}. The monomer shows two stretching vibrations around 3400 cm^{-1}, because primary amine stretches can be symmetrical and unsymmetrical. As polymerization results in secondary amines, only one peak is expected for the polymer. Furthermore the peak is less intense, because secondary amines absorb weak and the emeraldine base of polyaniline only consist of a few N-H bonds (figure 2-3). As all the aniline carbon atoms are sp^2 hybridized, the C-H stretches are all situated above 3000 cm^{-1}. The aromatic ring C-C stretches are situated at 1500 and 1600 cm^{-1} In the monomer spectra, an amine N-H bending vibration at 1619 cm^{-1} is observed as well as a ring deformation band at 510 cm^{-1}. The substitution pattern on the benzene ring can be determined by the

C-H out of plane bends between 650 and 900 cm^{-1}. The intense absorption at 834 cm^{-1} in the polymer spectrum can be assigned to two adjacent hydrogen atoms and thus para disubstitution. Peaks at 704 and 756 cm^{-1}, result from five adjacent hydrogen atoms or mono substitution. These absorptions result from the ends of the polymer chains.

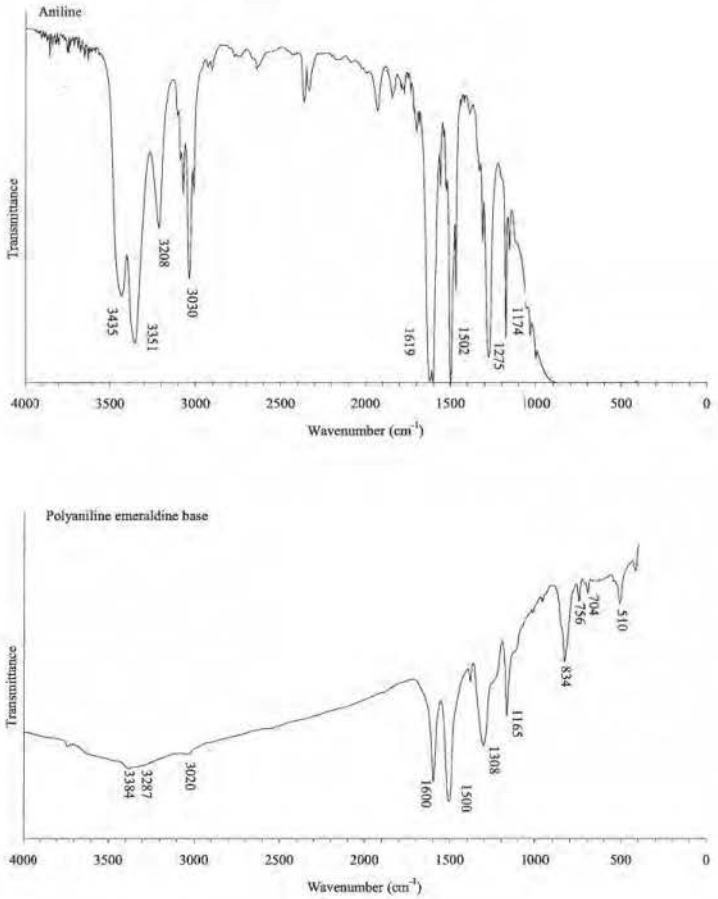

Figure 2-5: Infrared spectra of aniline and polyaniline (emeraldine base).

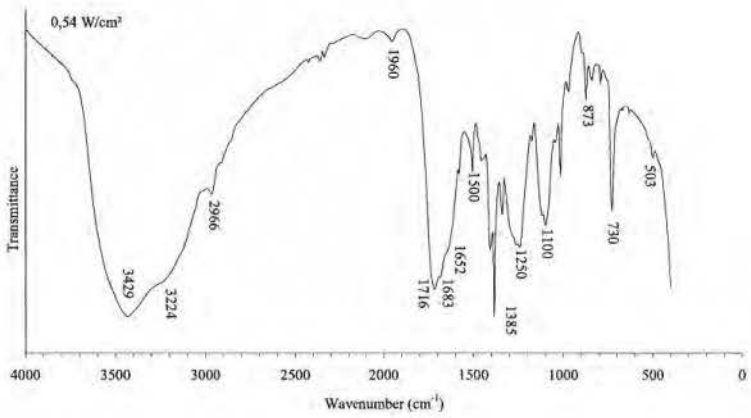
0,54 W/cm²
Transmittance
3429
3224
2966
1960
1716
1683
1652
1500
1385
1250
1100
873
730
503
4000
3500
3000
2500
2000
1500
1000
500
0
Wavenumber (cm⁻¹)

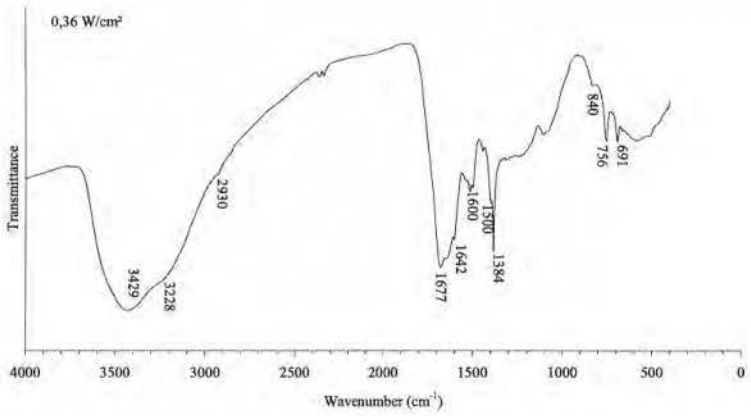
0,36 W/cm²
Transmittance
3429
3228
2930
1677
1642
1600
1500
1384
840
756
691
4000
3500
3000
2500
2000
1500
1000
500
0
Wavenumber (cm⁻¹)

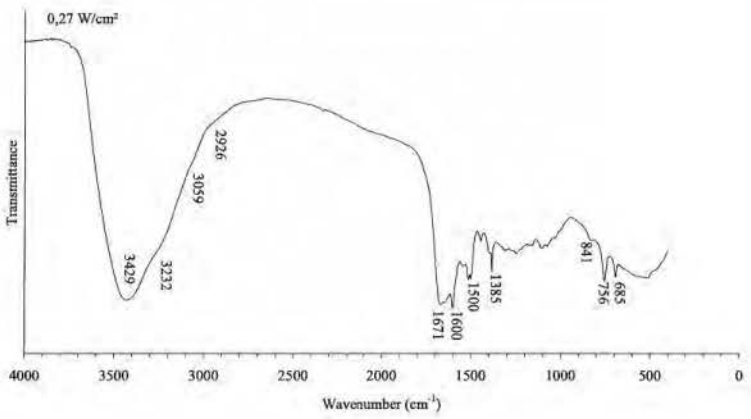
0,27 W/cm²
Transmittance
3429
3232
3059
2926
1671
1600
1500
1385
841
756
685
4000
3500
3000
2500
2000
1500
1000
500
0
Wavenumber (cm⁻¹)

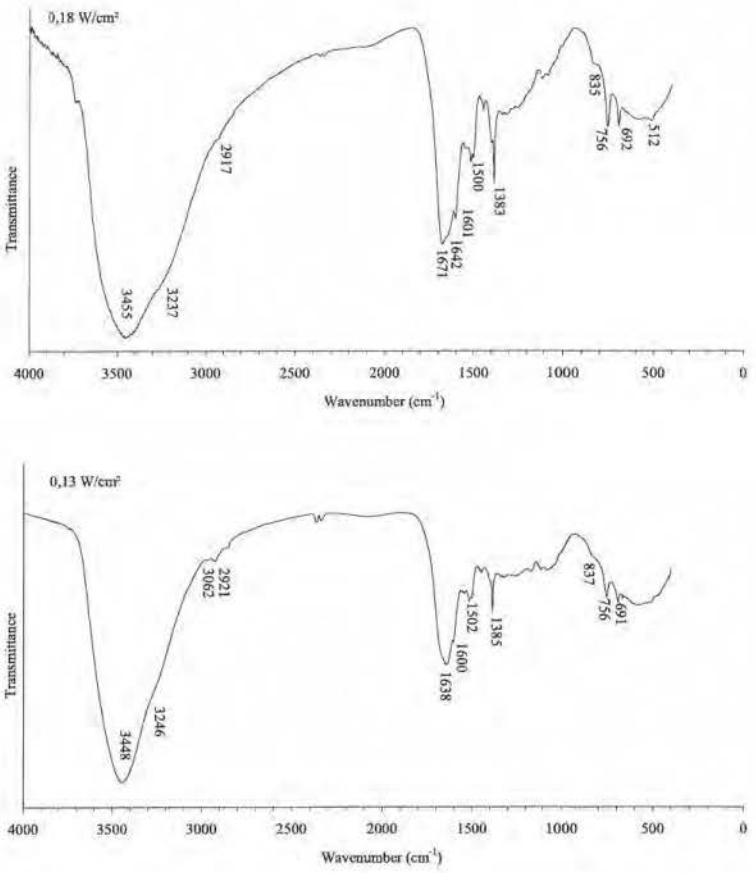

Figure 2-6: Infrared spectra of polyaniline, deposited at different power levels.

Vibration	Wavenumber (cm^{-1}) Aniline	Wavenumber (cm^{-1}) Polyaniline EB	Wavenumber (cm^{-1}) Plasma polyaniline
O-H stretch absorbed water	-	3600	overlap
N-H stretch amine	3351 3435	3384	3429
N-H stretch hydrogen bonded amine	3208	3287	3224
C-H stretch on double bond	3009 3030 3070	3020	3052
C-H stretch on saturated bond	-	-	2900
C≡C stretch	-	-	2100
Aromatic overtone band	1924	1888	1950
C=O stretch ketone	-	-	1720
C=O stretch secondary amide or conjugated ketone	-	-	1680
C=O stretch primary amide	-	-	1650
N-H bend	1619	-	1580
C=C stretch benzene ring	1502 1600	1500 1600	1500 1600
O-H bend absorbed water	-	1383	1380
C-N stretch aromatic amine	1275	1308	1250
C-H in plane bends	950-1200	950-1200	950-1200
C-H out of plane bend para disubstituted benzene	-	834	840
C-H out of plane bend mono substituted benzene	saturation	704 756	690 756
C-H out of plane bend benzene, other substitutions	-	-	680-900
C-H out of plane bend alkene	-	-	730
Ring deformation	saturation	510	510

Table 2-2: Detailed peak assignment for the infrared spectra of aniline, chemically polymerized polyaniline in its emeraldine base form and plasma deposited polyaniline[10, 11].

The IR spectra of plasma polyaniline coatings, deposited at different power levels are shown in figure 2-6. A detailed assignment of the absorption peaks is presented in table 2-2.

At a power level of 0.54 W/cm², there are some indications for structural retention. A strong absorption at 3429 cm^{-1} shows that there are still a lot of N-H bonds. Another intense absorption at 3224 cm^{-1} results from strongly hydrogen bonded N-H bonds. Also 6 ring aromatic C-C stretches at 1500 and 1600 cm^{-1} and ring deformations at 503 cm^{-1} are observed, illustrating that at least a part of the aromatic conjugated structure is retained. However, some peaks are not observed in the spectrum of pure polyaniline. Several absorptions around 2900 cm^{-1} show the existence of saturated carbons, while absorption around 2100 cm^{-1} is an indication for triple bonds in acetylenic or nitrillic functional groups. Strong absorptions around 1700 cm^{-1} indicate the presence of carbonyl functions. The carrier gas, which contains oxygen seems to have built in new functional groups. In the reactive plasma, oxygen forms ozone and oxygen radicals, which are able to break double bonds with formation of carbonyl functions[12]. The signal at 1716 cm^{-1} originates from isolated ketones and the one at 1683 cm^{-1} results from secondary amides and conjugated ketones. The C=O stretching vibration of primary amides is located at 1652 cm^{-1}. The amide functions in the plasma polymer are strongly hydrogen bonded and shift the N-H stretching band towards 3224 cm^{-1}. At 730 cm^{-1}, a C-H out of plane vibration, resulting from alkenes is found, indicating fragmentation of the aromatic ring. The presence of all these functional groups in the plasma polymer show that a large part of the original monomer structure is damaged in the highly reactive plasma. The substitution pattern on the remaining aromatic rings is complicated as can be derived from the many absorptions between 650 and 900 cm^{-1}. Remarkable is also the sharp and intense absorption at 1385 cm^{-1}. This peak is typical for O-H bending vibrations. The existence of many carbonyl functions in the coating makes it more hydrophilic and absorb water. This results in a broad absorption band around 3400 cm^{-1} which overlaps with the N-H stretching vibrations, and a sharp peak at 1385 cm^{-1}.

When the power is reduced to 0,36 W/cm², the IR spectrum is similar to the one at higher power. However, some important differences can be noticed. Peaks, resulting from structure degradation, such as triple bond stretches around 2100 cm^{-1}, C-H stretches on saturated carbons (2900 cm^{-1}) and C-H out of plane bends on alkenes (730 cm^{-1}) are less intense. Clearly, fragmentation of the monomer structure can be reduced by decreasing the plasma power. However, there is still a lot of oxygen built into the coating, as is shown by the absorptions around 1700 cm^{-1}. Only the peak resulting from isolated ketones around 1715 cm^{-1} is no longer present. This means that the ketones that are still present must be further conjugated, which is an indication for retention of the conjugated structure. Another difference at reduced power is the more clear substitution pattern on the aromatic ring. While para-disubstitution with the accompanying absorption at 840 cm^{-1} is expected to be the most important, it's absorption peak is not intense. The more important absorptions at 691 and 756 cm^{-1} show the presence of 5 adjacent hydrogen atoms and thus mono-substitution. Probably, the plasma deposition of polyaniline leads to small molecular weight polymers and unconventional polymerization.

Further decrease of the power towards 0,27; 0,18 and 0,13 W/cm², results in a decrease of the fragmentation by oxygen, as can be seen from the absorptions around 1700 cm^{-1} and 3200 cm^{-1}. At 0,13 W/cm², the ratio between the free standing N-H stretching peak at 3448 cm^{-1} and the hydrogen bonded N-H stretch at 3246 cm^{-1} has decreased, indicating a decreased amount of amide functions. Reduced power, however, does not lead to higher molecular weight polymers. The mono-substituted benzene rings (690 and 756 cm^{-1}) are still more important than the para-disubstituted (840 cm^{-1}).

Effect of the carrier gas on plasma polymerization of aniline

When air is used as discharge gas, carbonyl functions are present in the plasma polymer, which is an indication for degradation of the monomer structure. Other discharge gases that do not contain oxygen can also be used for plasma deposition. While nitrogen is the most interesting gas for industrial applications, the more expensive helium and argon are also used because they

have a low breakdown potential and do not form any bonds with organic materials.

Different gases have different breakdown voltages and create other reactive species in the plasma. Helium plasma's have a low ionization degree, because helium has a high ionization energy. Therefore, the applied electric field is not distorted by the charges formed in the plasma and the breakdown voltage stays low. Because their high ionization energy, helium ions also easily lose their charge in collisions and are therefore more aggressive. Nitrogen is more easily ionized and usually breaks down in filamentary discharges at atmospheric pressure. These filaments distort the applied electric field and increase the breakdown voltage. Because the different nature and concentrations of the plasma species in different gases, an effect of the discharge gas on the deposition rate is expected. Figure 2-7 presents the coating rate for the deposition of plasma polyaniline in a nitrogen, helium and nitrogen/oxygen plasma. Deposition rate is similar in helium and nitrogen when the same power is used. Addition of oxygen increases the deposition rate significantly. Even a small oxygen percentage in the nitrogen gas results in a 2,5 time increase of the deposition rate. In air, the deposition rate is 11 times faster. As oxygen is an oxidant, which forms the even more oxidative ozone and oxygen radicals in plasma, it is able to speed up the polymerization of aniline, which is know to react in an oxidative reaction mechanism, but it can also induce degradation.

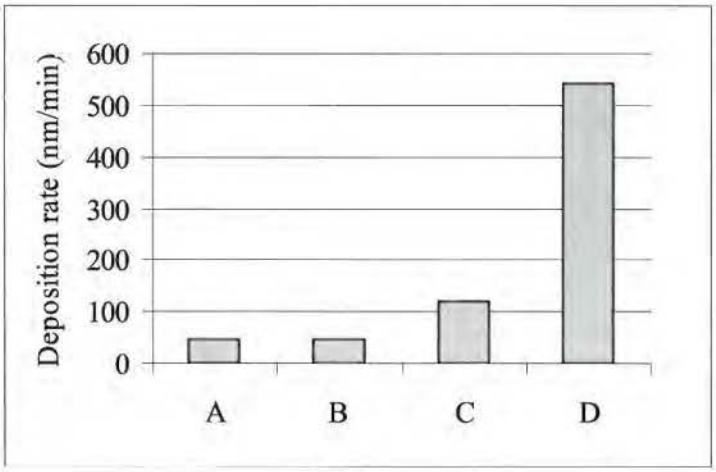

Figure 2-7: Deposition rate for plasma polymerization of polyaniline in: nitrogen (A), helium (B), nitrogen/oxygen (1%) (C) and air (D)

The influence of the carrier gas on the chemical structure of the plasma deposited polyaniline is studied with infrared spectroscopy. The IR spectra are presented in figure 2-8.

The IR spectrum of plasma polyaniline, deposited in nitrogen, clearly indicates that at least a part of the aniline structure is retained in the plasma polymer. The C-H stretch absorptions around 3050 cm^{-1} show that double bonds are present. This is confirmed by the presence of a ring deformation band at 507 cm^{-1} and of two intense peaks at 1497 and 1600 cm^{-1}, resulting from the aromatic benzene ring of polyaniline. Besides the expected peaks, other functionalities are observed in the spectrum. Peaks around 2929 cm^{-1}, show the presence of saturated C-H bonds. The absorption around 2186 cm^{-1} is an indication for triple bonds. Both functionalities do not occur in the monomer but are formed by fragmentation of the monomer in the reactive plasma. While a short peak at 825 cm^{-1} indicates para-disubstitution on the benzene ring, which is expected for conventional aniline polymerization, more intense peaks at 694 and 753 cm^{-1} are typical for mono-substituted benzene. This might indicate that the polymers, resulting from plasma polymerization have a low molecular weight.

Similar results are found when plasma polymerization was performed in helium. Also here, saturated and triple bonds show that a part of the monomer

structure is fragmented in the plasma. Although, there seem to be less triple bonds (2208 cm^{-1}) in helium than in nitrogen plasma discharges, the peak resulting from saturated bonds (2925 cm^{-1}) is more intense. Furthermore, another structural defect is observed at 1650 cm^{-1} (shoulder) where C=O stretches are situated. This is an indication for the presence of amides and ketones, probably resulting from reaction of oxygen from the environmental air with stable radicals that are left in the coating after plasma deposition.

When a small amount of oxygen (1%) is added to the nitrogen plasma, the carbonyl stretching absorption, is even more intense, than for plasma deposition in helium. The peaks at 695 and 754 cm^{-1} resulting from mono-substituted benzene, are less intense. These effects are even more pronounced when plasma deposition was done in air. Probably, the substitution pattern on benzene is more complex when oxygen is added. Furthermore, a large part of the aromatic rings might be destroyed in the plasma. In a low temperature plasma discharge, oxygen easily forms ozone which is able to break double bonds.

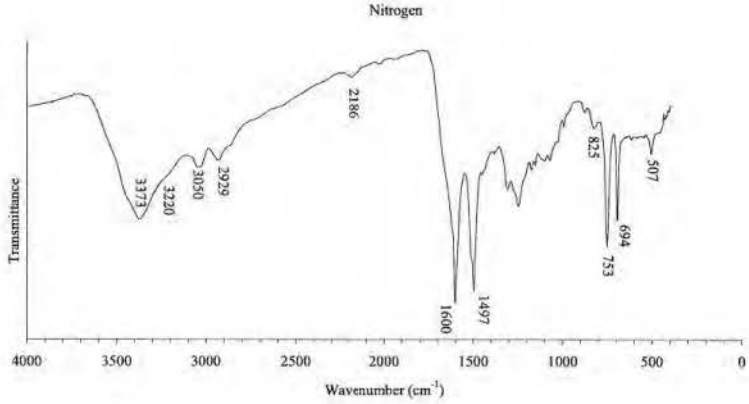
Nitrogen
Transmittance
3373
3220
3050
2929
2186
1600
1497
825
753
694
507
4000
3500
3000
2500
2000
1500
1000
500
0
Wavenumber (cm-1)

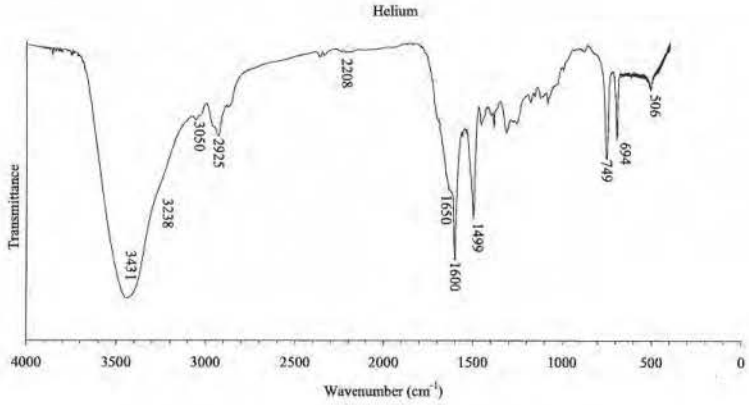
Helium
Transmittance
3431
3238
3050
2925
2208
1650
1600
1499
749
694
506
4000
3500
3000
2500
2000
1500
1000
500
0
Wavenumber (cm-1)

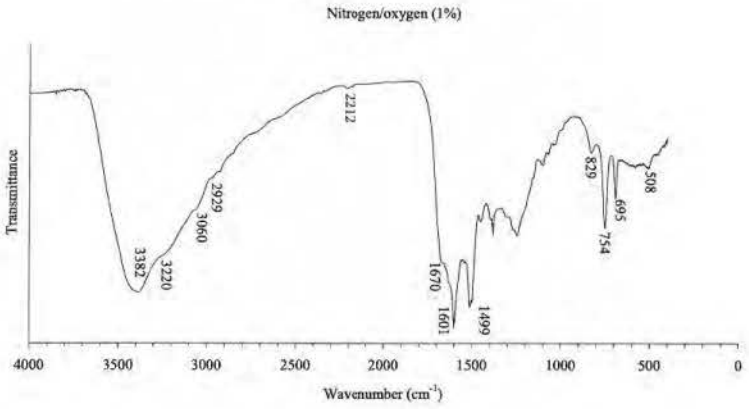
Nitrogen/oxygen (1%)
Transmittance
3382
3220
3060
2929
2212
1670
1601
1499
829
754
695
508
4000
3500
3000
2500
2000
1500
1000
500
0
Wavenumber (cm-1)

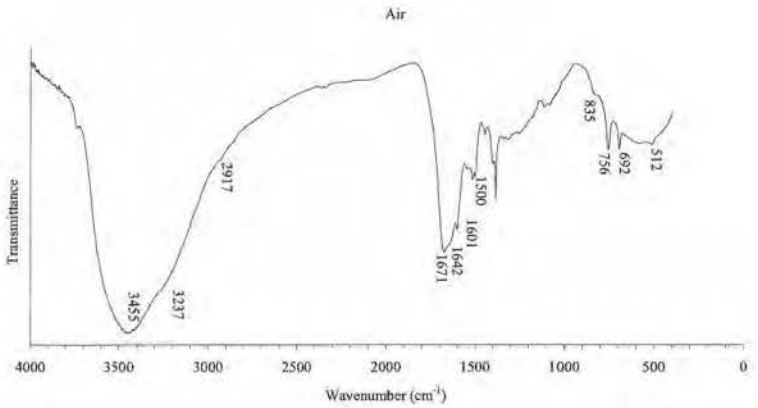

Figure 2-8: Infrared spectra of polyaniline, plasma deposited in different discharge gases.

Effect of the frequency on plasma polymerization of aniline

While the ionization degree in a plasma can be increased by increasing the power, this can also be accomplished by increasing the frequency. As an electron crosses the discharge gap more times at higher frequency, there are more collisions, leading to a higher ionization degree. The DBD reactor can work at lower voltage, when the frequency is increased (for the same power), while the current (electron density) increases. For this reason, a similar effect as was already seen for power changes, is also expected for the variation of the frequency.

The effect of a frequency increase on the coating thickness is presented in figure 2-9. The curve is similar to the one for power variation. At small frequencies, the coating thickness increases linearly with the frequency, while at higher frequency, the curve goes to a plateau.

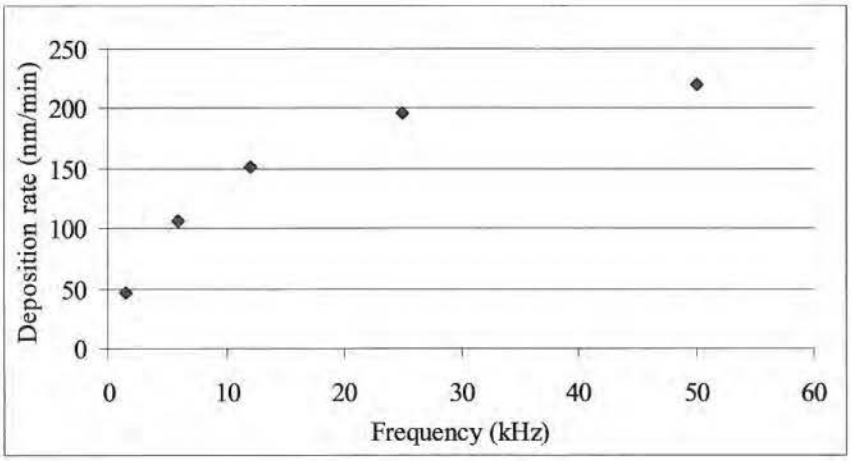

Figure 2-9: Deposition rate for aniline, plasma deposited at different frequencies.

Besides differences in the coating thickness, a visual effect is observed when frequency is changed. At low frequencies up to 12 kHz, the plasma coatings are smooth while at increased frequency (25 kHz and higher) a patterned surface morphology is observed (figure 2-10). A possible explanation for this phenomenon can be found in the low voltage that is necessary to ignite the plasma at these high frequencies. The discharge in the used DBD reactor is mostly filamentary. When a filament is formed, it will charge the dielectric during the first half cycle. When in the second half cycle the electric field is opposite, the filament will preferentially stay in the same position, because the electric field at that position in the discharge gap, is now the sum of the applied electric field and the charged dielectric. When the filament charges the dielectric in the first half cycle, this dielectric charge is usually spread out over a region that is larger than the filamentary channel itself, leaving a so called foot print. This reduces the electric field in this region (figure 2-11). Ignition of a second channel during the same half cycle, will preferentially occur on another position because the field is still high there. When the applied electric field is rather low, the formation of filamentary channels nearby will be suppressed and the separation distance between the filaments can be quite high[13]. Polymerization in the filaments, where the electron density is very high, leads to faster deposition than in between the filaments. The patterns seen

in the filamentary plasma are therefore also visible on the plasma coatings. Besides the formation of patterns, there is also some powder formation when higher frequencies are used.

Figure 2-10: Pictures of the surface of plasma polymerized polyaniline on glass substrates (24x24 mm). At 1,5 kHz the surface is smooth, while at 25 and 50 kHz, a pattern with nine spots is seen.

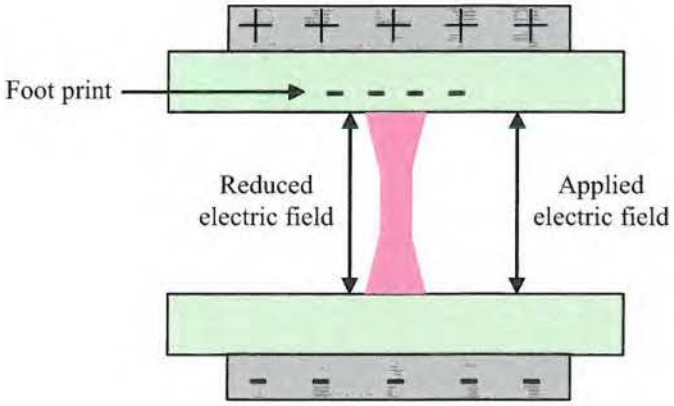

Figure 2-11: Schematic presentation of a filament in a DBD reactor. The filament charges the dielectric, leaving a foot print. These charges locally reduce the electric field rendering it unlikely that another streamer appears nearby.

The influence of the frequency on the chemical structure can be studied with infrared spectroscopy. IR spectra are presented in figure 2-12.

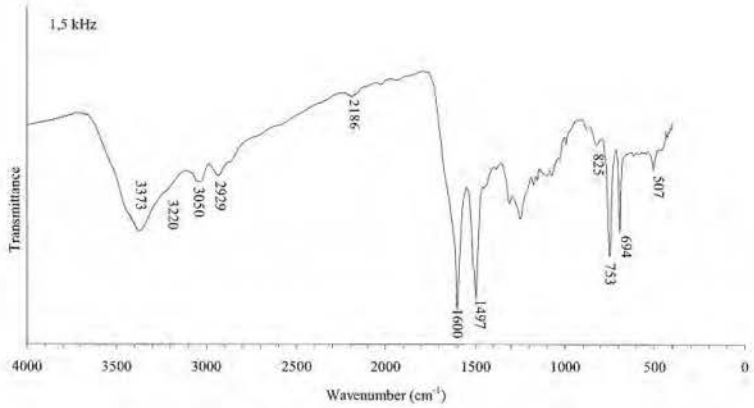
1,5 kHz
Transmittance
3373
3220
3050
2929
2186
1600
1497
825
753
694
507
4000
3500
3000
2500
2000
1500
1000
500
0
Wavenumber (cm-1)

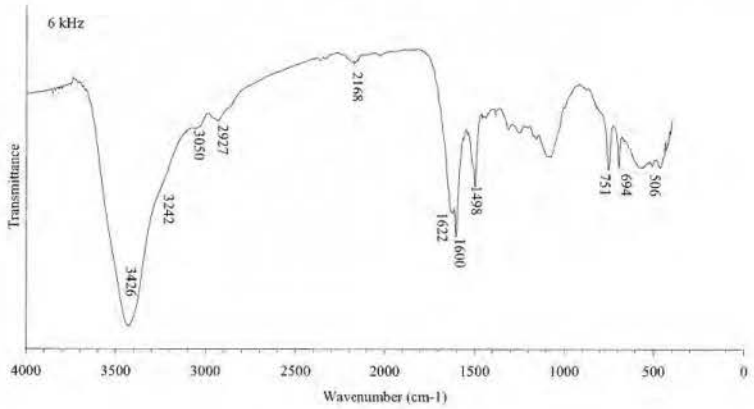
6 kHz
Transmittance
3426
3242
3050
2927
2168
1622
1600
1498
751
694
506
4000
3500
3000
2500
2000
1500
1000
500
0
Wavenumber (cm-1)

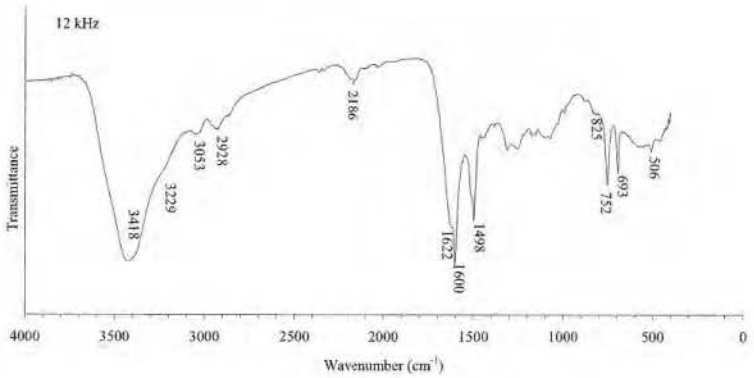
12 kHz
Transmittance
3418
3229
3053
2928
2186
1622
1600
1498
825
752
693
506
4000
3500
3000
2500
2000
1500
1000
500
0
Wavenumber (cm-1)

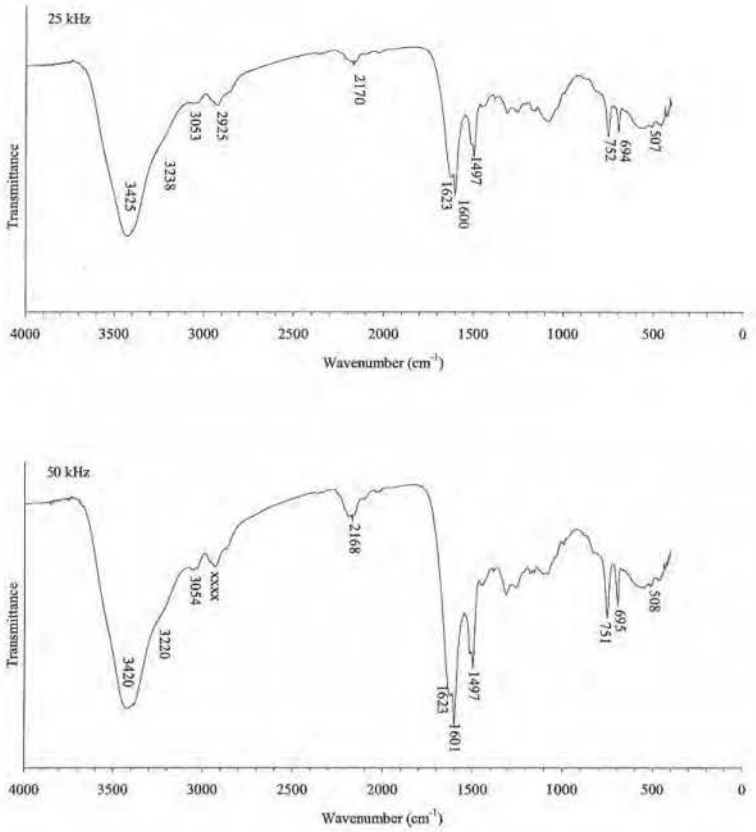

Figure 2-12: infrared spectra of plasma polymerized aniline at different frequencies.

All spectra show IR peaks around 3050 cm^{-1} indicating double bonds, while peaks around 507, 1500 and 1600 cm^{-1} confirm that at least part of the aromatic benzene ring is preserved in the plasma deposited layer. However, all spectra also show evidence of fragmentation of the monomer structure. Around 2900 cm^{-1}, several peaks are seen which result from C-H stretches on saturated bonds. Around 2200 cm^{-1}, triple bond stretches can be found. These structural defects indicate the incorporation of (partially) degraded aniline monomer in the plasma polymer.

Some differences between the spectra can be seen. At 6 kHz, a peak at 1622 cm^{-1} with several shoulders around 1650 cm^{-1} is observed. This peak is not present when plasma deposition is done at 1,5 kHz. The peak at 1622 cm^{-1} is

due to a primary amine N-H bend, which is not expected to be seen, since polyaniline mainly consists of secondary amines that absorb at lower wavenumber (weak absorption between 1500 and 1580 cm^{-1}). This means that aniline reacts in an unconventional manner at higher frequency. The shoulders around 1650 cm^{-1} result from carbonyl functions formed after plasma treatment when remaining radicals react with oxygen from the surrounding air. Peaks at 1620 and 1650 cm^{-1} are also seen when plasma reaction is done at even higher frequency. Also the degree of structural defects seems to be influenced by the plasma frequency. While absorption resulting from saturated carbon around 2925 cm^{-1} seems to have a constant intensity over the frequency range, absorption resulting from triple bonds around 2200 cm^{-1} increases in intensity with increased frequency. Plasma deposition at higher frequency thus results in more defects.

Influence of the gas flow on plasma polymerization of aniline

The gas flow is the last plasma parameter studied. The influence of the gas flow on the deposition rate of polyaniline is presented in figure 2-13. A higher gas flow results in slower deposition rates. Injection of a higher gas volume in the reactor will dilute the precursor and a lower reaction rate might therefore be expected. Furthermore, the plasma contact time is reduced which decreases the probability that the precursor will be activated by the plasma and also reduces the time to react.

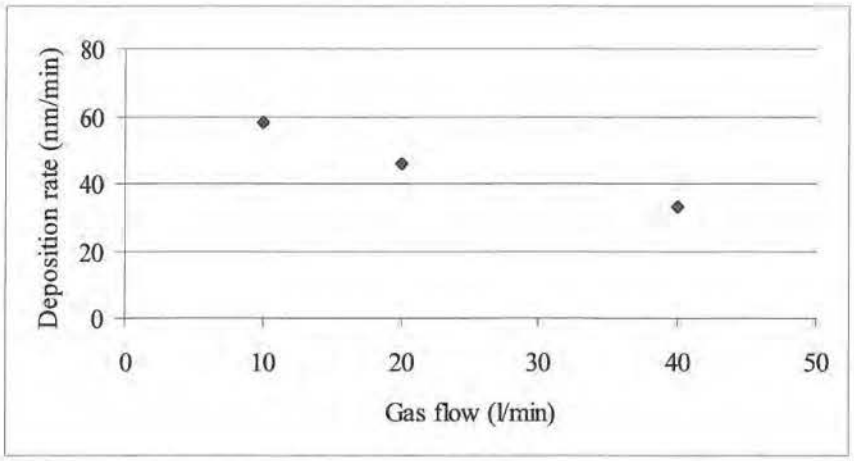

Figure 2-13: Deposition rate for the plasma polymerization of aniline at different gas flows.

The influence of the gas flow on the chemical structure of the plasma polymerized polyaniline can again be studied with infrared spectroscopy. These IR spectra are shown in figure 2-14. Since all the spectra are similar, the gas flow doesn't seem to have a big influence on the chemical structure of the deposited polyaniline. However, at 40 l/min, a shoulder peak around 1620 cm^{-1} is observed resulting form primary amines. As these primary amines normally only appear at the end of polyaniline chains, they are not expected to be detected by infrared spectroscopy. The presence of these signals in the spectrum at a gas flow of 40 l/min, is an indication for low molecular weight polymers, unconventional reactions or unreacted monomer.

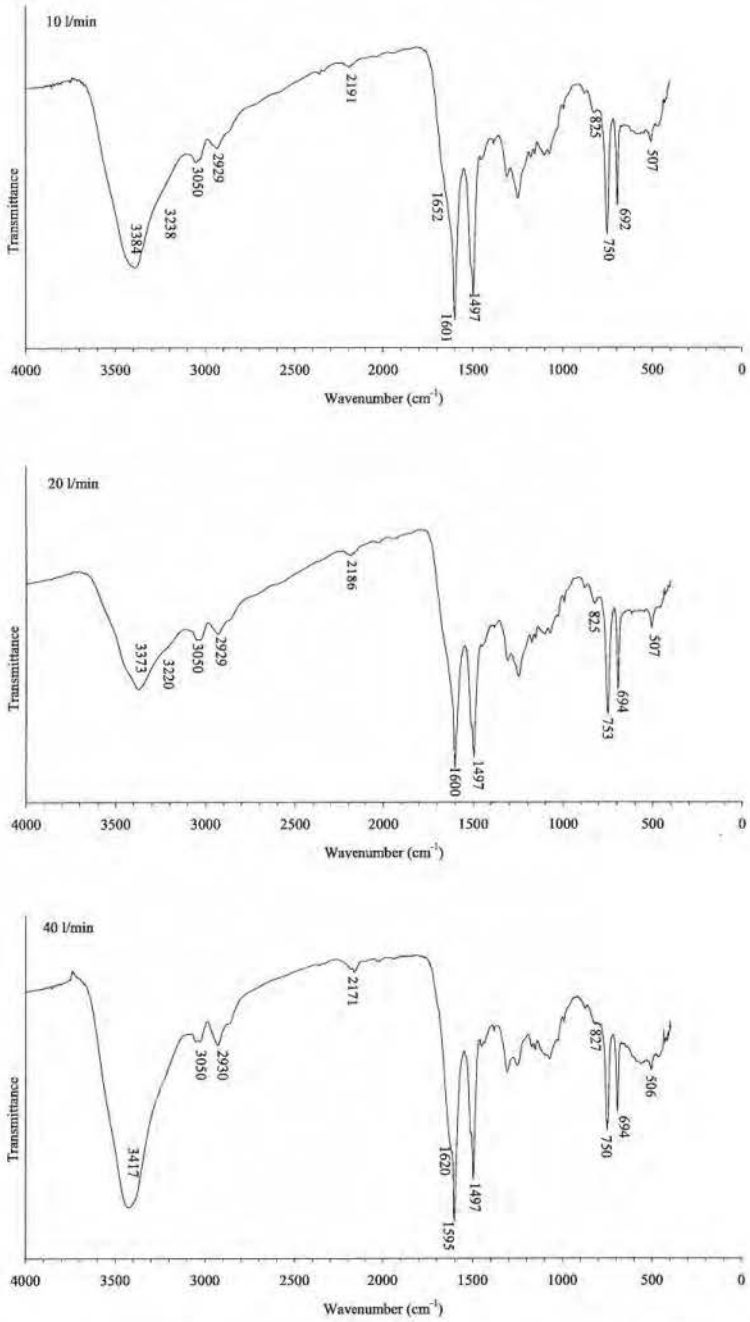

Figure 2-14: Infrared spectra of plasma polymerized aniline, deposited with different gas flows.

Properties

Typical properties of conjugated polymers are their color and (semi)conductivity after doping. (Electro)chemically polymerized polyaniline has a yellow color in its non-conjugated state (leucoemeraldine form), blue in its conjugated state (emeraldine base or pernigraniline form) and green in its doped state (emeraldine salt)[3].

While polyaniline synthesis usually leads to its blue emeraldine base form, plasma polymerization always resulted in yellow or brown coatings. An example of the absorption in the visible range of these plasma polyanilines is presented in figure 2-15. The expected absorption maximum in the visible range is not seen. There's only an absorption band close to the UV region, which means that the plasma polymer is either in the leucoemeraldine form or that its conjugated system is damaged. Since the plasma polyaniline does not show any conductivity after doping with an oxidant or an acid, one can conclude that the reactive plasma conditions result in too many structural defects to obtain an extended conjugated system.

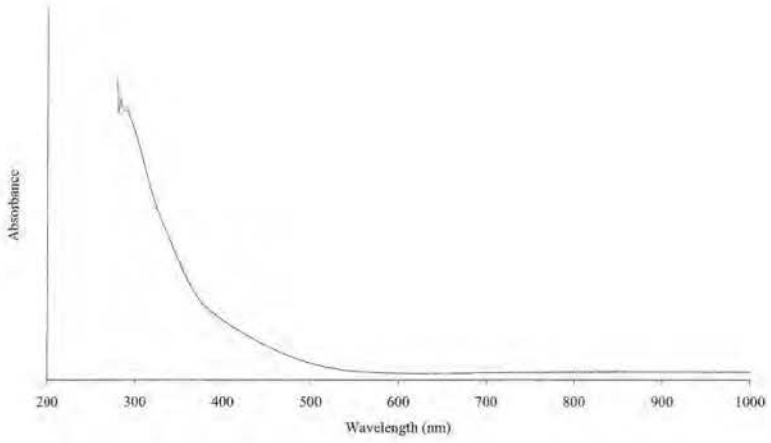

Figure 2-15: Absorption spectrum of plasma polymerized aniline.

Mechanical properties

In order to be useful in applications, the deposited polyaniline coatings should possess some mechanical stability. Anti-corrosion coatings for example, should not dissolve or delaminate from the substrate. It is known that plasma polymerization can offer better mechanical stability. Contact of the reactive plasma gas with the substrate, results in functionalization of the substrate and formation of radicals. Such activation of the substrate often leads to better adhesion of the coating. Furthermore, plasma deposited coatings can also be cross-linked due to unconventional cross-linking at radical sites[14].

The solubility and delamination of plasma polymerized polyaniline are studied by immersing coated glass substrates into solvents for 24 hours, followed by evaluation of the weight loss. The selected solvents are water, isopropyl alcohol and acetone. The results are presented in figure 2-16.

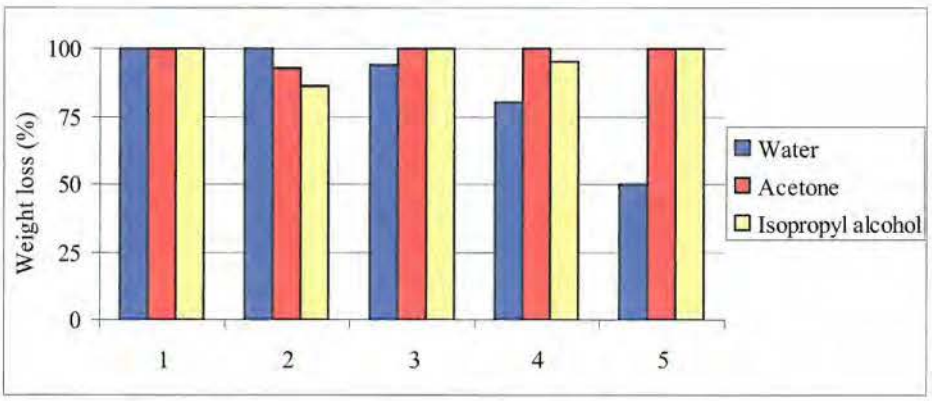

Figure 2-16: Weight loss of plasma polyaniline coatings after 24h immersion in selected solvents. The coatings are plasma deposited in different gases and at different power levels: 1) N_2, 0,13 W/cm²; 2) N_2, 0,27 W/cm²; 3) N_2/O_2 (1%), 0,13 W/cm²; 4) N_2/O_2 (1%), 0,27 W/cm²; 5) He, 0,18 W/cm²

The effect of the power and the carrier gas on the mechanical properties of plasma deposited polyaniline is studied. In water, the coating swells and delaminates almost completely from the substrate. The influence of the power and carrier gas is only small. Plasma deposition leads to incorporation of carbonyls and other functional groups, which make the coatings more

hydrophilic. In water they will have a high degree of swelling, which induces cracks and delamination from the substrate. When the plasma polyaniline coatings are immersed in acetone or isopropyl alcohol, the solvents turn yellow indicating dissolution of the coating. The weight loss is almost 100%, which means that the plasma polymers have a low molecular weight (oligomers).

Kinetics

The deposition rate of the plasma polymers depends on several factors. It can for example, be increased by the addition of oxygen. The monomers can react in an oxidative polymerization mechanism, so an increase in the reaction rate might be expected when an oxidative gas is added. This chapter contains a more detailed discussion of the reaction kinetics.

For industrial applications deposition rates must be as high as possible. One might expect that the deposition rate is also controlled by the concentration of the precursor. Figure 2-17 shows that the amount of precursor that is transported towards the plasma is linearly dependent on the pressure used on the atomizer. This means that it is possible to control the precursor concentration by adjusting the pressure.

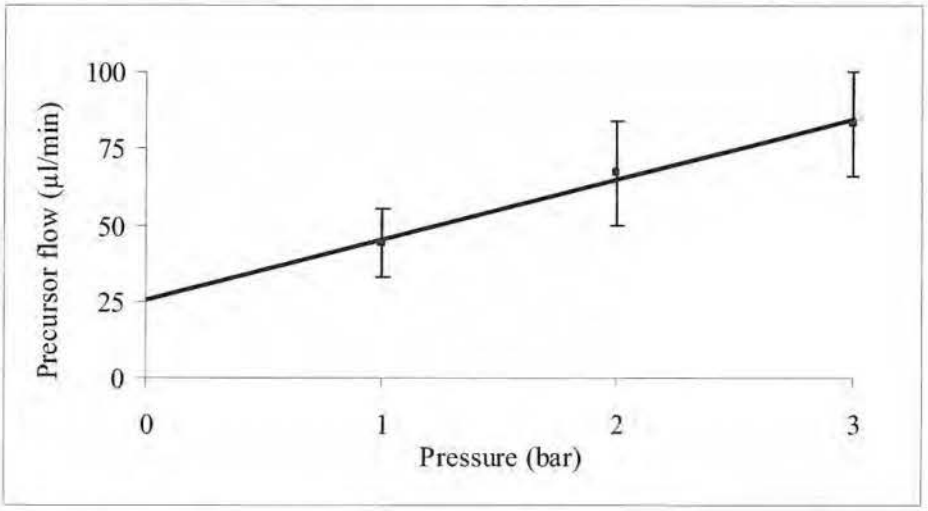

Figure 2-17: The consumption of aniline when atomized at different atomizing pressures.

Figure 2-18 shows the evolution of the thickness of the coating for three different atomizing pressures and two different carrier gases. The deposition rate at these different conditions is determined by the slope of the curves. The values of these slopes are presented in table 2-3. Although an increase in deposition rate is expected at higher precursor concentrations, almost no influence is observed. Also, when a small amount of oxygen (1%) is added, there is no effect of a higher precursor concentration. This probably means that an excess of precursor is present. When oxygen is added to the carrier gas, the deposition rate is higher than at the same conditions in pure nitrogen. It is known that aniline reacts in an oxidative mechanism to form polyaniline. As oxygen is an oxidant, which reacts in the plasma to form the even more oxidative ozone and oxygen radicals, this increase in deposition rate could be expected.

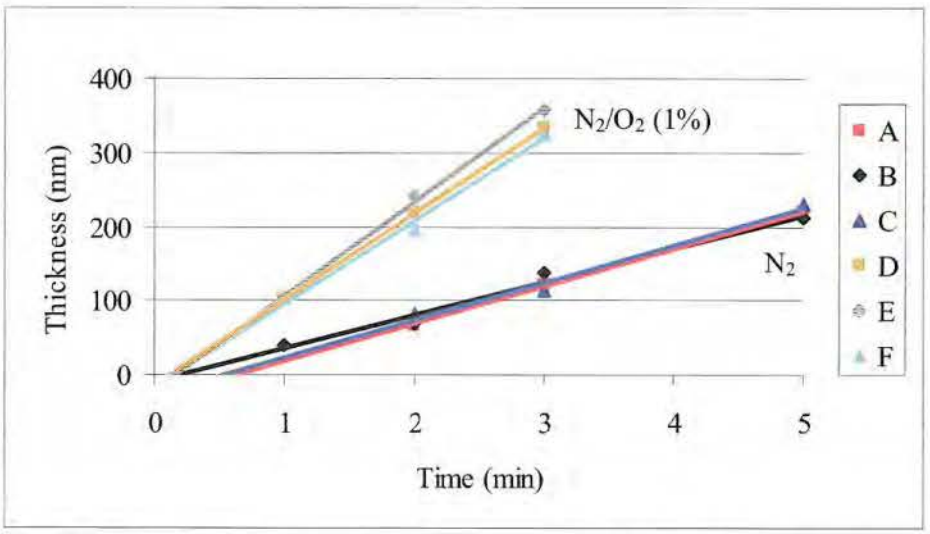

Figure 2-18: Coating thickness as a function of time, for the plasma deposition of polyaniline in different gases and at different atomizing pressures: A) N_2 1 bar; B) N_2 2 bar; C) N_2 3 bar; D) N_2+O_2 (1%) 1 bar; E) N_2+O_2 (1%) 2 bar; F) N_2+O_2 (1%) 3 bar.

Carrier gas	Pressure (bar)	Precursor flow µl/min	Deposition rate (nm/min)
N_2	1	44	51
N_2	2	67	45
N_2	3	83	50
N_2+O_2 (1%)	1	44	116
N_2+O_2 (1%)	2	67	128
N_2+O_2 (1%)	3	83	112

Table 2-3: Deposition rate and precursor consumption for the plasma deposition of polyaniline in nitrogen or a nitrogen/oxygen mixture and at different atomizing pressures.

Conclusions

The simplest way to deposit polyaniline coatings with a plasma seemed to be the injection of a low molecular weight form of polyaniline and crosslink it. However, the concentration of the polymer in the plasma was too low to obtain a deposition. A second approach was the injection of the monomer aniline and to polymerize it in the plasma.

The different plasma parameters have an influence on the thickness and the chemical structure of the deposited coatings. Higher power level results in higher deposition rate, but the monomer is more fragmented. Deposition rate can also be increased by the addition of small amounts of oxygen to the carrier gas. However, this also introduces unwanted carbonyl functions in the polyaniline layer. Better structural retention is observed when deposition is done in pure nitrogen or helium. Plasma coatings are thicker when higher frequency is used. However, higher frequencies again result in more fragmentation. While the coatings have a smooth surface at low frequency, patterns are seen in the coating morphology above 25 kHz. The gas flow has no large influence on the chemical structure of the deposition, but lower gas flow results in thicker coatings.

Variation of all these parameters results in many different plasma coatings. However, non of the experiments that have been performed, resulted in the

expected typical blue polyaniline coatings. All depositions had a yellow-brown appearance and absorbed light close to the UV range. Furthermore, no conductivity was measured after doping. When the coatings were immersed in water or other solvents, they delaminated from the substrate or dissolved.
In conclusion can be stated, that the desired polyaniline coating could not be deposited so far with a plasma discharge at atmospheric pressure. Best structure retention is realized at low power, low frequency and in an oxygen free environment.

2.3 Plasma deposition of polypyrrole

About polypyrrole

High conductivity in polypyrrole was first reported in 1963 by Weiss et al.[15] [16, 17] in a series of papers. For iodine doped polypyrrole, conductivities up to 1 S/cm were measured. While too early and eventually lost, this anticipated by many years the nobel prize winning discovery of high conductivity in iodine doped polyacetylene. In nature, polypyrrole or pyrrole black, is also found in some melanins in the form of a copolymer with polyacetylene and polyaniline.
Polypyrrole is formed by radical condensation of several pyrrole rings. It is synthesized in an oxidative reaction mechanism. Electrons are withdrawn from the aromatic ring by using an oxidant or an electrochemical cell (figure 2-19). Polypyrrole films are often used in organic sensors[20, 21]. Some papers also document on the successful application of polypyrrole coatings for the corrosion protection of metals[22, 23].

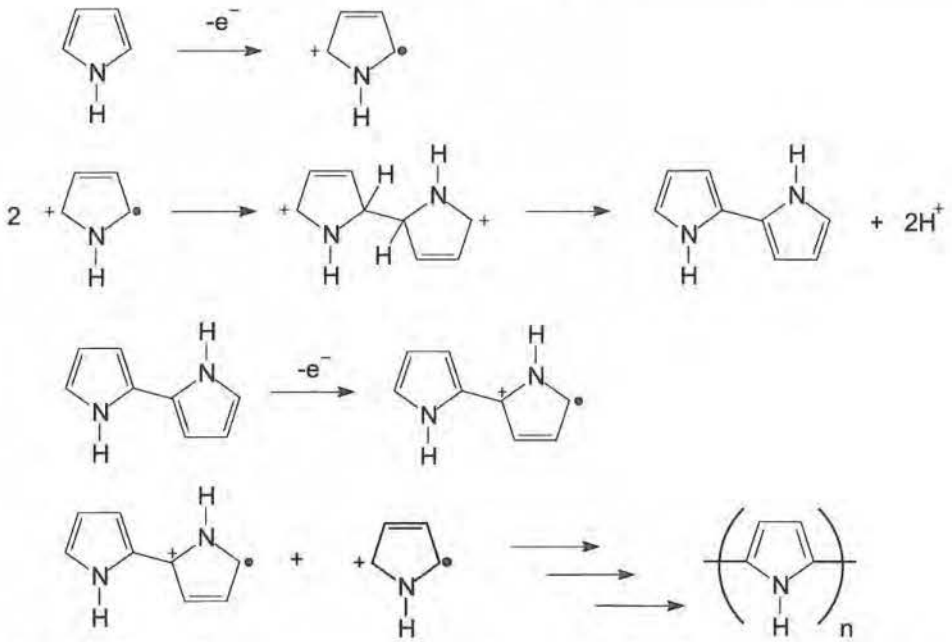

Figure 2-19: Mechanism for the electrochemical polymerization of polypyrrole[18, 19].

Chemical structure

Plasma deposited polypyrrole coatings are expected to be influenced by the different plasma parameters. Deposition rate and chemical structure of polypyrrole films, deposited in different plasma gases, at different powers and gas flows are studied in this section. The plasma parameters are summarized in table 2-4.

	Power (W/cm²)	Gas	Gas flow (l/min)
A	0,13	N_2	20
B	0,13	He	20
C	0,27	N_2	20
D	0,27	N_2	10
E	0,27	N_2+O_2 (1%)	20

Table 2-4: Different plasma parameters, used to deposit polypyrrole coatings.

The deposition rate for plasma polymerization of polypyrrole with different plasma parameters is presented in figure 2-20. Plasma polymerization in nitrogen or helium results in a similar coating thickness. When the plasma power is doubled, deposition rate is four times faster. The gas flow also has an effect on the deposition rate. A decreased gas flow increases the precursor concentration and the plasma contact time, resulting in thicker coatings. An even higher increase in deposition rate is accomplished by addition of a small oxygen concentration (1%) to the carrier gas. Like aniline, pyrrole is known to react in an oxidative mechanism (figure 2-19). For this reason it is expected that an oxidant like oxygen, which forms the even more oxidative ozone in a DBD reactor, would fasten the deposition.

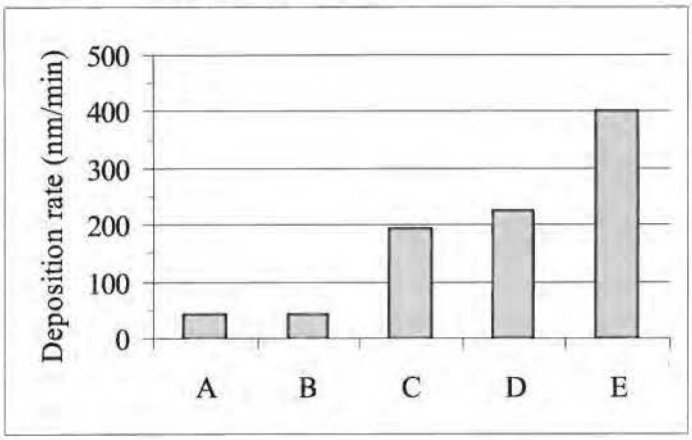

Figure 2-20: Deposition rate for plasma deposition of polypyrrole at different parameters. The parameters are presented in table 2-4.

The influence of the different plasma parameters on the chemical structure of the deposited polypyrrole is studied with infrared spectroscopy. Infrared spectra are presented in figure 2-21. A detailed peak assignment is shown in table 2-5.

Pyrrole has some very characteristic absorptions in the infrared range. At 3403 cm^{-1}, an intense N-H stretching band can be seen, accompanied by an N-H bending signal at 1569 cm^{-1}. C-H stretches are situated above 3000 cm^{-1}, at 3102 and 3128 cm^{-1} because the aromatic carbons are sp^2 hybridized. Three double bond stretches, typical for aromatic heterocycles are found at 1418,

1470 and 1528 cm^{-1}. C-N stretching results in peaks at 1015, 1048 and 1074 cm^{-1}. Finally a strong sp^2 hybridized C-H out of plane bend is observed at 737 cm^{-1}.

Vibration	Wavenumber (cm^{-1}) Pyrrole	Wavenumber (cm^{-1}) Plasma polypyrrole
Amine N-H stretch	3403	3400
Amide N-H stretch (hydrogen bonded)	-	3250
C-H stretch on double bond	3102 3128	3100 3130
C-H stretch on single bond	-	2870 2930 2960
C≡C or C≡N stretch	-	2200
5-ring ketones C=O stretch	-	1735
Ketone C=O stretch	-	1695
Amide C=O stretch	-	1670
Amide C=O stretch (conjugated)	-	1630
N-H bend	1569	1560
C=C or C=N stretch	1418 1470 1528	1400
C-H in plane bend	1142	1100
C-N stretch	1015 1048 1074	1000-1080
C-H out of plane bend	648 737	730 (several)

Table 2-5: Detailed peak assignment for infrared vibrations of pyrrole and plasma deposited polypyrrole[24].

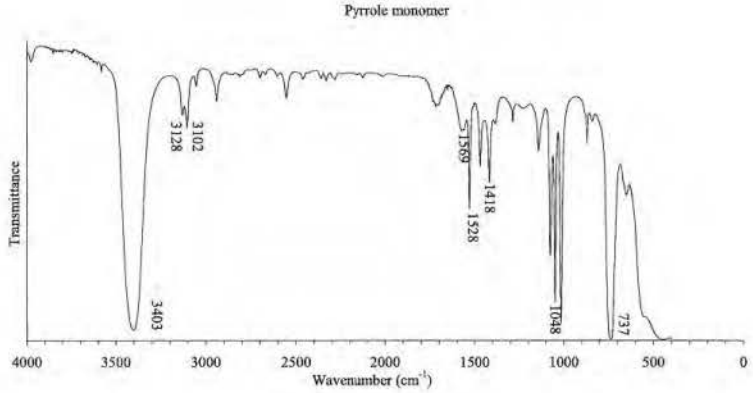
Pyrrole monomer
Transmittance
3403
3128
3102
1569
1528
1418
1048
737
4000
3500
3000
2500
2000
1500
1000
500
0
Wavenumber (cm-1)

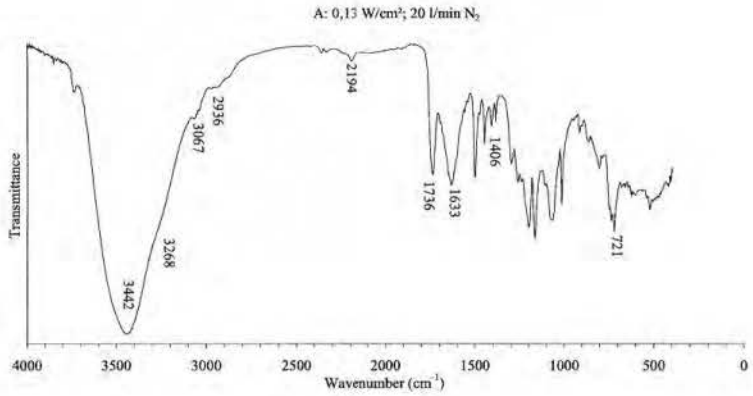
A: 0,13 W/cm²; 20 l/min N2
Transmittance
3442
3268
3067
2936
2194
1736
1633
1406
721
4000
3500
3000
2500
2000
1500
1000
500
0
Wavenumber (cm-1)

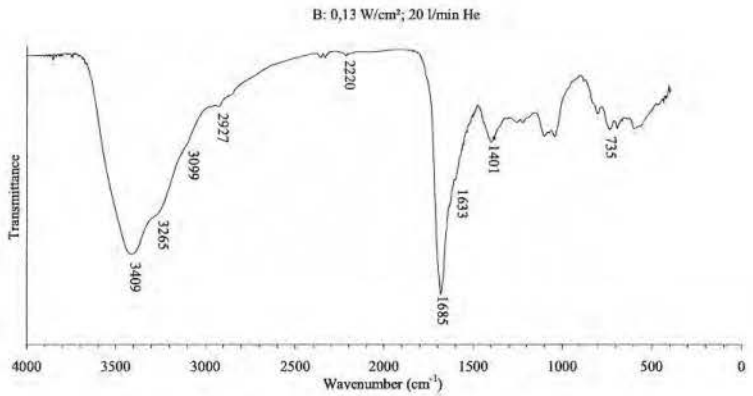
B: 0,13 W/cm²; 20 l/min He
Transmittance
3409
3265
3099
2927
2220
1685
1633
1401
735
4000
3500
3000
2500
2000
1500
1000
500
0
Wavenumber (cm-1)

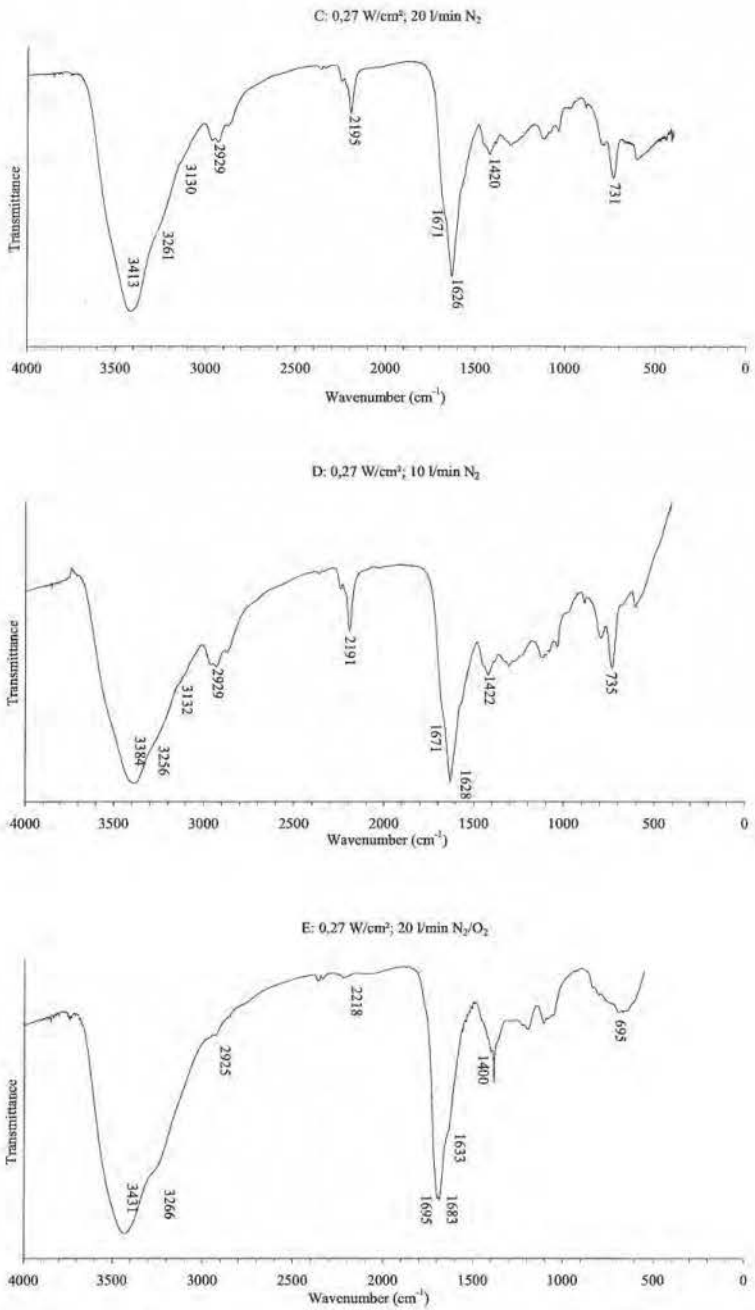

Figure 2-21: Infrared spectra of the pyrrole monomer and plasma polypyrrole, deposited using different plasma parameters.

When pyrrole is polymerized at low power in a nitrogen plasma, at least part of the typical pyrrole functionalities are retained, as can be seen in spectrum A. Peaks around 3067 cm^{-1} show that double bonds are still present. Absorption at 1406, 1449 and 1501 cm^{-1}, result from C=C stretches of the aromatic heterocycle. However, functionalities indicating structural degradation are also observed in the spectrum. At 2936 cm^{-1}, sp^3 hybridized C-H stretches are found. A peak at 2194 cm^{-1} shows the presence of triple bonds. Around 1700 cm^{-1} some carbonyl C=O stretches are seen. The peak at 1736 cm^{-1} results from 5-ring ketones and the one at 1633 cm^{-1} from conjugated amides. So, although no oxygen is added to the discharge gas, there are oxygen functionalities built into the plasma coatings. This oxygen comes from traces of oxygen in the plasma reactor or from reaction with the environmental air after plasma treatment. The appearance of all these functionalities shows that the pyrrole structure has partially degraded in the very reactive plasma. The presence of several bands around 736 cm^{-1} in stead of one (monomer spectrum) is an indication that the substitution pattern on the aromatic ring is indeed more complex.

When pyrrole is polymerized in helium (spectrum B) instead of nitrogen, the infrared spectrum is similar. However, some differences can be distinguished. While deposition in nitrogen led to 5-ring ketones, plasma polymerization in helium results in a strong absorption at 1685 cm^{-1}, which are typical for saturated amides. In helium, reaction with oxygen seems to be more aggressive, being able to destroy double bonds and the ring structure. At 1633 cm^{-1}, a shoulder is present, resulting from conjugated amides. Because of the higher defect degree in helium, the heterocycle stretches around 1401 cm^{-1} are also less intense.

When the power level is increased (spectrum C), the polypyrrole coatings show more saturated (2929 cm^{-1}) and triple bonds (2195 cm^{-1}). Higher power level thus increases the degree of fragmentation. A decrease of the gas flow (spectrum D) doesn't seem to have additional effects on the chemical structure of the polymer. The spectra are nearly identical.

Addition of a small amount of oxygen (1%) to the nitrogen plasma (spectrum E), suppresses the amount of saturated carbons and triple bonds. Then again,

saturated ketones (1695 cm^{-1}) and amides (1683 cm^{-1}) are found in the spectrum, indicating that some double bonds might have been destroyed by oxygen species in the plasma.

Properties

Conventional polymerization of pyrrole usually results in a black conductive coating which corresponds with the doped form of polypyrrole. Undoped polypyrrole has a green color. Since no doping agents are injected into the plasma, a green color can be expected when pyrrole is plasma polymerized. However, the plasma polypyrrole coatings all have a yellow-brown appearance. Figure 2-22 presents the absorption behavior of these coatings in the visible range. Indeed, all plasma polypyrrole films absorb close to the UV range, while an absorption maximum between 400 and 500 nm is expected[25]. This means that the conjugated system has only shortly extended. The many defects that were introduced in the polypyrrole coatings during plasma polymerization result in short conjugation lengths. For this reason, no conductivity was measured after doping.

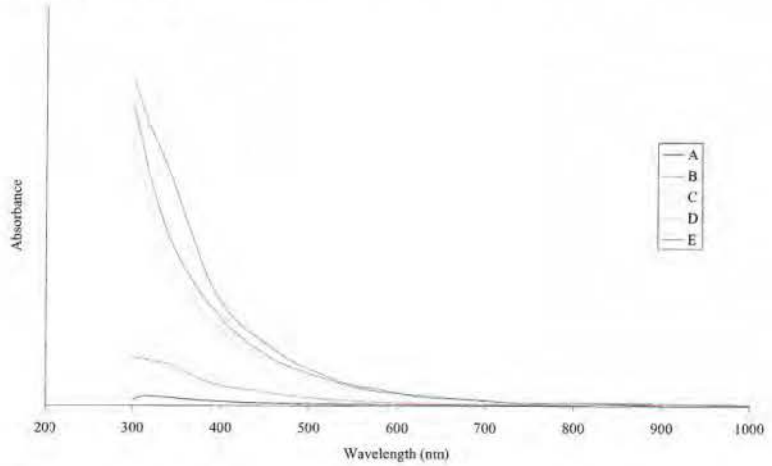

Figure 2-22: UV/VIS spectra of plasma polymerized polypyrrole coatings. The plasma parameters are presented in table 2-4.

Mechanical properties

As was already done for plasma deposited polyaniline, also immersion of plasma polymerized polypyrrole coatings in selected solvents is studied. The results are presented in figure 2-23.

All plasma polypyrrole coatings dissolved in acetone and isopropyl alcohol. The polypyrrole coatings that were deposited in a nitrogen/oxygen plasma also dissolved in water. This means that these coatings have small molecular weights. When no oxygen was added to the plasma gas, the coatings did not dissolve in water. However after 24h immersion, the films showed cracks and delaminated from the substrate due to the hydrophilic nature of the plasma coatings.

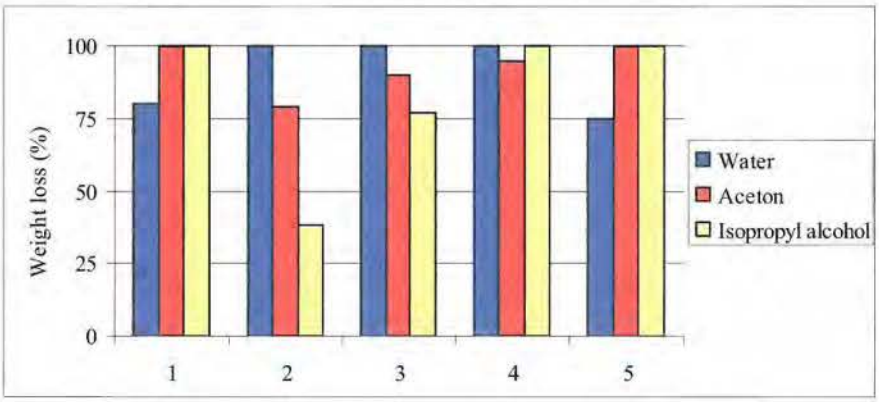

Figure 2-23: Weight loss of plasma polypyrrole coatings after 24h immersion in selected solvents. The coatings are deposited in different plasma gases and at different power levels: 1) N_2, 0,13 W/cm²; 2) N_2 0,27 W/cm²; 3) N_2/O_2 (1%), 0,13 W/cm²; 4) N_2/O_2 (1%), 0,27 W/cm²; 5) He, 0,18 W/cm²

Kinetics

The influence of oxygen addition to the plasma carrier gas and the influence of the precursor concentration on the deposition rate is studied in more detail. The dependence of the precursor consumption on the atomizing pressure is presented in figure 2-24. This graph shows that the precursor consumption can be controlled by adjusting the atomizing pressure.

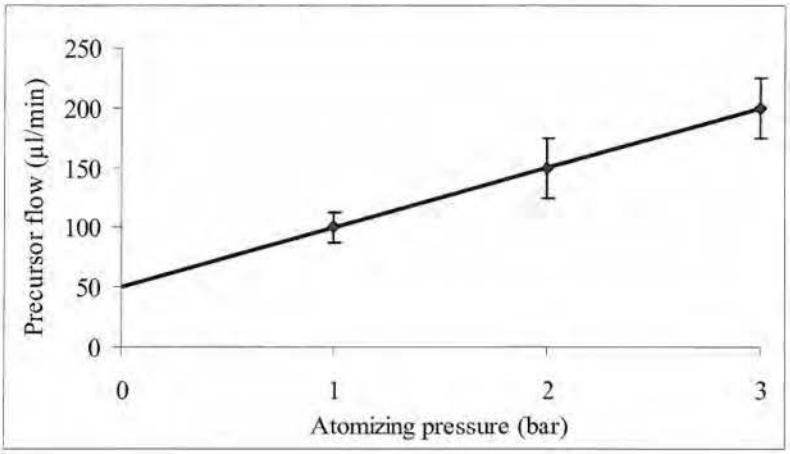

Figure 2-24: The consumption of pyrrole, when atomized at different atomizing pressures.

Figure 2-25 shows the evolution of the coating thickness of plasma polypyrrole, deposited at different atomizing pressures and in different carrier gases. The deposition rates are determined by the slopes of the curves which are presented in table 2-6. The deposition rate seems to be independent on the precursor concentration in both nitrogen and in a nitrogen/oxygen mixture. When a small oxygen concentration is added to the carrier gas, the deposition rate increases about three times. As expected, ozone and oxygen radicals formed in the plasma fasten the oxidative pyrrole polymerization.

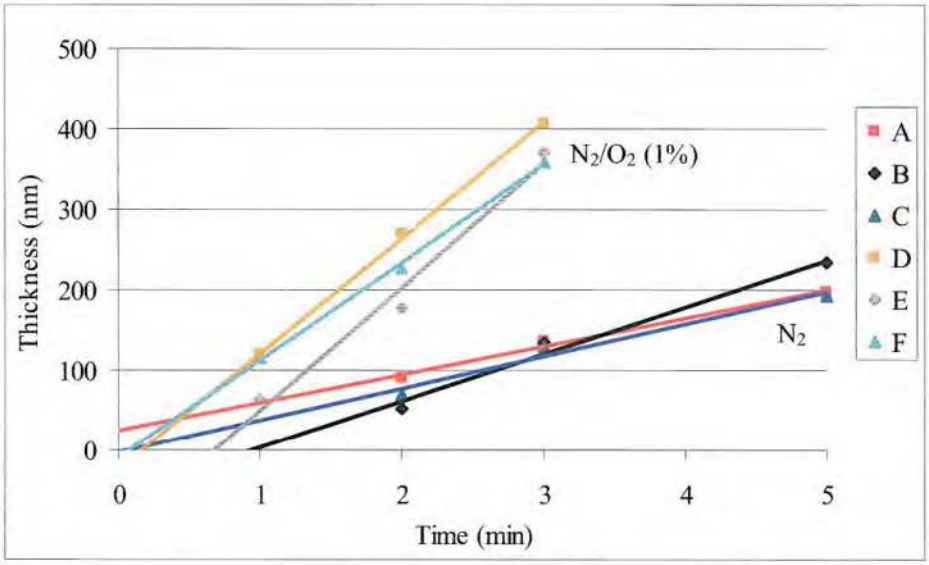

Figure 2-25: Coating thickness as a function of time, for the plasma deposition of polypyrrole in different gases and at different atomizing pressures: A) N_2 1 bar; B) N_2 2 bar; C) N_2 3 bar; D) N_2+O_2 (1%) 1 bar; E) N_2+O_2 (1%) 2 bar; F) N_2+O_2 (1%) 3 bar.

Carrier gas	Pressure (bar)	Precursor flow µl/min	Deposition rate (nm/min)
N_2	1	100	35
N_2	2	150	59
N_2	3	200	40
N_2+O_2 (1%)	1	100	144
N_2+O_2 (1%)	2	150	154
N_2+O_2 (1%)	3	200	122

Table 2-6: Deposition rate and precursor consumption for the plasma deposition of polypyrrole in nitrogen or a nitrogen/oxygen mixture and at different atomizing pressures.

Conclusions

IR spectra of plasma deposited polypyrrole coatings at atmospheric pressure show the presence of basic chemical functionalities of polypyrrole. However, other functionalities such as saturated bonds, triple bonds and carbonyl functions are also formed. These structural defects result in yellow-brown coatings instead of the expected green polypyrrole, because the conjugated system is shorter. A higher power level or addition of a small oxygen concentration to the carrier gas, increases the deposition rate significantly. However, this also increases the number of defects in the plasma coatings. Because of these defects, none of the plasma polypyrrole coatings showed conductivity after doping.

2.4 Plasma deposition of polythiophene

About polythiophene

Polythiophene (figure 2-26) results from the polymerization of thiophene, which is a five atom sulfur containing aromatic heterocycle. While polythiophenes may have been chemically synthesized by accident more than a century ago[26], the first planned chemical synthesis using metal-catalyzed polymerization of 2,5-dibromothiophene were reported by two groups independently in 1980. Yamamoto et al.[27] used magnesium in tetrahydrofuran and nickel(bipyridine) dichloride. Lin and Dudek[28] also used magnesium in tetrahydrofuran, but with a series of acetylacetonate catalysts. As with pyrrole (see figure 2-19), polymerization of thiophene can also be done electrochemically.

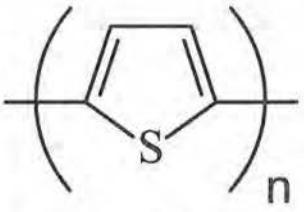

Figure 2-26: Chemical structure of polythiophene.

Polythiophene and its derivatives can be used in applications such as field-effect transistors, electroluminescent devices, solar cells, photochemical resists, nonlinear optic devices, batteries and diodes[29]. Also corrosion protection of metals is reported[30, 31]. The derivative 3,4-ethylenedioxythiophene is of special interest, because it can be made transparent in it's doped form[32, 33].

Chemical structure

Another interesting monomer for plasma deposition of conjugated polymers is thiophene. As with pyrrole and aniline, also the deposition of polythiophene will be influenced by the different plasma parameters. The plasma parameters studied are summarized in table 2-7. Figure 2-27 presents the deposition rate for these different conditions.

	Power (W/cm^2)	Gas	Gas flow (l/min)
A	0,13	N_2	20
B	0,13	He	20
C	0,27	N_2	20
D	0,27	N_2	10
E	0,27	N_2+O_2 (1%)	20

Table 2-7: Different plasma parameters, used to deposit polythiophene coatings.

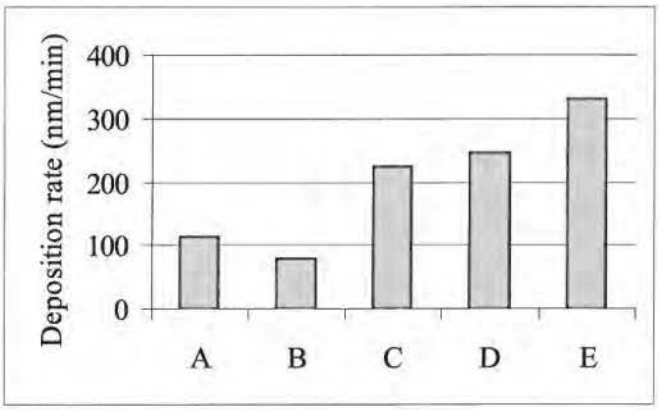

Figure 2-27: Deposition rate for the plasma polymerization of thiophene. The parameters are presented in table 2-7.

Plasma deposition of thiophene is faster in a nitrogen plasma (A) than in helium (B). However the difference is only small. When a higher power is used (C), more reactive species are formed in the plasma, leading to a higher deposition rate. An even faster deposition can be realized by decreasing the gas flow. A decreased gas flow, increases the contact time with the plasma of both the carrier gas and the precursor, which increases the probability that the precursor is activated by the plasma. Also the time to react is increased. Since thiophene reacts in an oxidative reaction mechanism, the increased deposition rate after addition of oxygen was expected. Although, the effect is not as pronounced for thiophene as for pyrrole and aniline.

The chemical structure of plasma polythiophene coatings can be studied with infrared spectroscopy. Spectra of the thiophene monomer and the plasma polymers are presented in figure 2-28. A detailed peak assignment is shown in table 2-8.

The infrared spectrum of thiophene shows two absorptions above 3000 cm^{-1}, which result from sp^2 hybridized C-H stretching vibrations. The C=C stretches in the aromatic heterocycle are found at 1408, 1558 and 1590 cm^{-1}. Besides some C-H in plane vibrations between 900 and 1260 cm^{-1}, which are of little diagnostic value, also a strong C-H out of plane vibration is found at 710 cm^{-1}. The C-S stretching vibration absorbs at 833 cm^{-1}.

When thiophene has passed through the plasma, the resulting deposition contains a lot of different features in the infrared spectrum. Spectrum A shows the absorptions of the plasma coating polymerized at low power in nitrogen gas. Aromatic C=C stretches can be found at 1401 and 1560 cm^{-1}, indicating that at least part of the aromatic ring is retained after plasma treatment. This is confirmed by the ring deformation peak at 589 cm^{-1}. Retention of double bonds is shown by sp^2 hybridized C-H stretches at 3025 and 3097 cm^{-1} (overlap with broad O-H stretching band) and C-H out of plane vibration at 702 cm^{-1}. However, only one C-H stretching band should be visible above 3000 cm^{-1} because conventional thiophene polymerization occurs in position 2 and 5 of the aromatic heterocycle, leaving only hydrogen atoms at the 3 and 4 positions. This could be an indication for low molecular weight polymers or cross-linking.

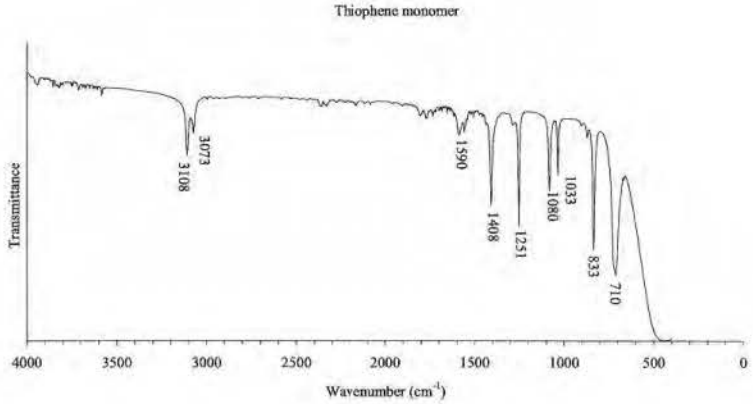
Thiophene monomer
Transmittance
3108
3073
1590
1408
1251
1080
1033
833
710
4000
3500
3000
2500
2000
1500
1000
500
0
Wavenumber (cm-1)

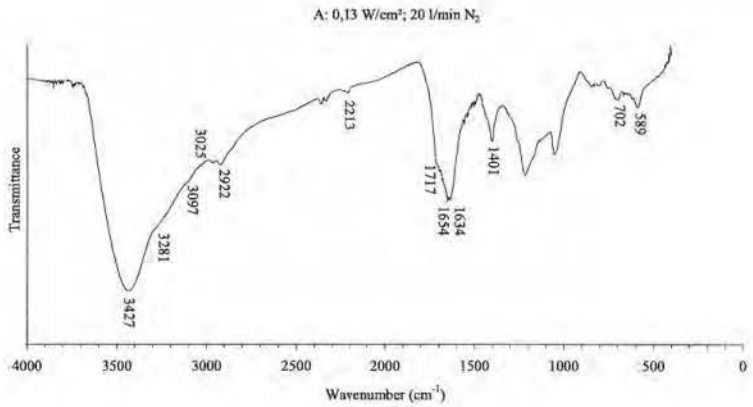
A: 0,13 W/cm²; 20 l/min N2
Transmittance
3427
3281
3097
3025
2922
2213
1717
1654
1634
1401
702
589
4000
3500
3000
2500
2000
1500
1000
500
0
Wavenumber (cm-1)

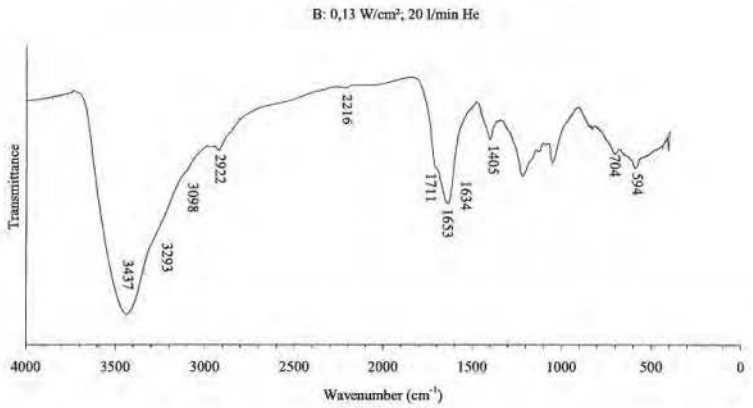
B: 0,13 W/cm²; 20 l/min He
Transmittance
3437
3293
3098
2922
2216
1711
1653
1634
1405
704
594
4000
3500
3000
2500
2000
1500
1000
500
0
Wavenumber (cm-1)

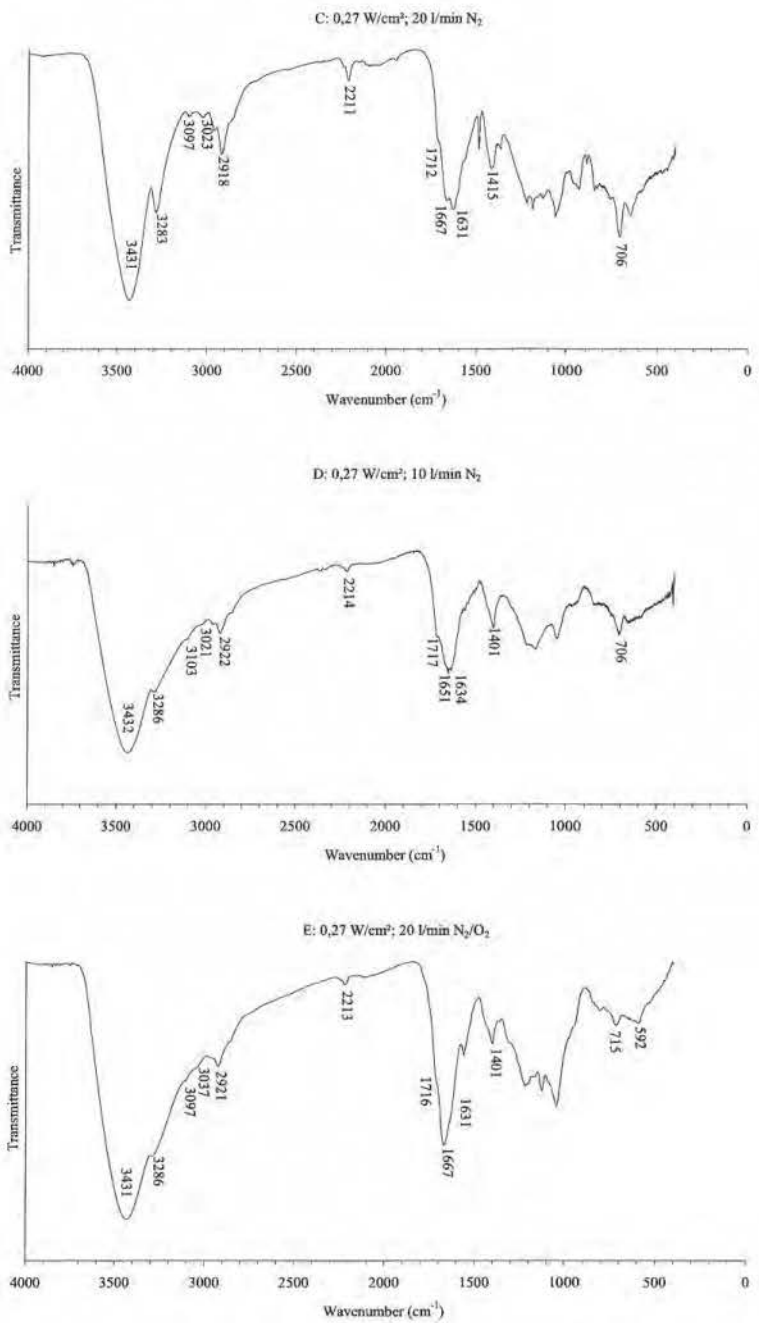

Figure 2-28: Infrared spectra of thiophene and plasma polythiophene, deposited under different conditions.

Vibration	Wavenumber (cm^{-1}) Thiophene	Wavenumber (cm^{-1}) Plasma polythiophene
O-H stretch absorbed water	-	3450
C-H stretch on triple bonded carbon	-	3290
C-H stretch on double bonded carbon	3073 3108	3030 3100
C-H stretch on saturated carbon	-	2900
C≡C stretch	-	2200
C=O stretch saturated ketone	-	1715
C=O stretch α,β-unsaturated ketone	-	1655
C=O stretch conjugated ketone	-	1635
C=C stretch	1408 1558 1590	1400 1560
C-H in plane bends	950-1250	950-1250
C-S stretch	833	833
C-H out of plane bend	710	705
Ring deformation	Saturation	590

Table 2-8: Detailed peak assignment for the infrared spectra of thiophene and plasma polymerized polythiophene[34].

Plasma polymerization of thiophene also results in additional peaks that are not observed when conventionally polymerized. C-H stretching bands around 2900 cm^{-1} show the presence of saturated carbons. Furthermore an absorption around 2200 cm^{-1} indicates that triple bonds are formed, while a C-H stretching band close to 3300 cm^{-1} (shoulder) is typical for terminal alkynes. The presence of these functionalities is an indication for structural degradation. Also the strong absorption around 1700 cm^{-1}, typical for carbonyl functions, results from degradation of the monomer structure. As there is no oxygen added to the plasma gas, these functions must be formed by reaction with traces of oxygen in the plasma reactor or by contact with oxygen from the air after plasma deposition. The absorption at 1717 cm^{-1} is typical for saturated ketones or aldehydes. When the ketones are conjugated or are involved in strong intramolecular hydrogen bonding, it's absorption frequency is lowered. This

explains the peaks at 1654 and 1634 cm^{-1}. As was already seen with pyrrole and aniline, the existence of oxygen functionalities in the films make them hydrophilic and absorb water, which causes a strong and broad O-H stretching band around 3427 cm^{-1}.

The infrared spectrum is almost identical when the thiophene polymerization is done in a helium plasma (spectrum B). Besides absorption peaks typical for the aromatic thiophene ring, indications for structural degradation are observed. This is also observed for plasma polymerization in nitrogen at a higher power (spectrum C). However, in this case, structural degradation of the monomer seems to be more pronounced. Indeed, C-H stretching vibration on saturated carbons around 2900 cm^{-1} and on terminal alkynes around 3300 cm^{-1}, as well as triple bond stretching around 2200 cm^{-1} are more intense than in the former spectra. The more reactive plasma at higher power level results in higher deposition rate but also in higher degree of degradation. In spectrum D, the effect of a decreased (nitrogen) carrier gas flow is studied. The spectrum is similar as the one with higher gas flow, although the intensities of the peaks indicating structure degradation seem to have decreased slightly. Addition of only a small percentage of oxygen (1%) to the carrier gas causes an important increase in deposition rate. However, the presence of oxygen in the carrier gas also increases the amount of carbonyl functions (around 1700 cm^{-1}, spectrum E), as could be expected.

A quantification of the amount of oxygen that is built in into the plasma coatings can be done with XPS spectroscopy. The atomic composition, as well as the structural formula of the polythiophene coatings deposited in nitrogen or a nitrogen/oxygen mixture are presented in table 2-9. The expected structural formula for polythiophene is C_4S. Besides carbon and sulfur, also nitrogen and oxygen are present in the plasma coatings, resulting from the discharge gas that has built in into the coating. While only a small amount of nitrogen is observed, the oxygen content in the plasma coatings is quite large. Even when no oxygen is added to the plasma gas, the oxygen amount still equals the sulfur amount. When a nitrogen/oxygen mixture is used, the oxygen content in the plasma coating is even higher. Since these oxygen amounts are measured on the surface of the coatings, it is possible that oxygen is mainly found on the surface

of the coatings and thus built in after plasma polymerization by contact with oxygen from the surrounding air.

Another difference between conventional polythiophene and plasma polythiophene is the carbon to sulfur ratio. Normally, a carbon tot sulfur ratio of 4 should be observed, but plasma polymerization leads to a slightly higher proportion. This is probably due to some elimination of sulfur during plasma deposition.

	Gas	%S	%C	%O	%N	Structural formula
C	N_2	15	66	16	3	$C_{4,4}SO_{1,1}N_{0,2}$
E	$N_2/O_2(1\%)$	15	63	20	2	$C_{4,2}SO_{1,3}N_{0,1}$

Table 2-9: Composition and structural formula of plasma polythiophene, deposited in two different gases.

Properties

As many other conjugated polymers, polythiophene absorbs light in the visible region. Because of this absorption, polythiophene typically has a red color in it's undoped form. After doping, it turns blue. However, the plasma deposited coatings all have a yellow or brownish color, which can be explained by the UV/VIS spectra presented in figure 2-29 for polythiophene deposited at different plasma conditions. The plasma parameters are shown in table 2-7. While an absorption peak between 400 and 500 nm is expected for polythiophene[35], the plasma polymers all show a broad band close to the UV region (300nm). A shift to shorter wavelengths corresponds with a higher energy gap between the valence and conduction band of the polythiophene and thus a shorter conjugation length. The reactive plasma results in coatings with many structural defects that cause an interruption of the conjugated system.

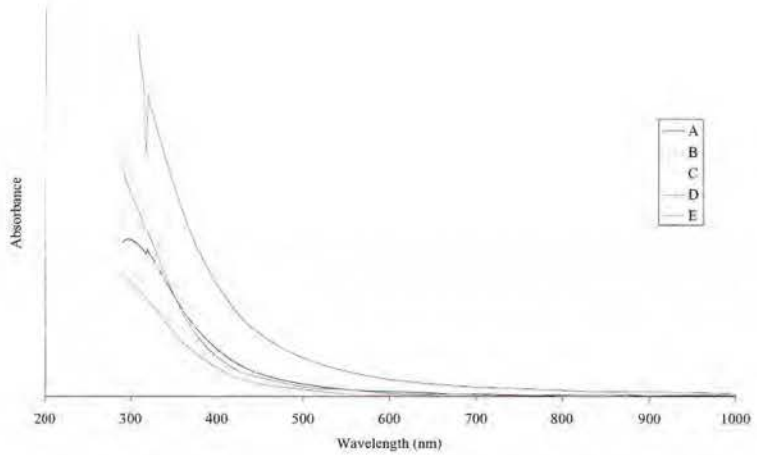

Figure 2-29: UV-Vis spectra of plasma polymerized polythiophene. The plasma conditions are presented in table 2-7.

Chemically synthesized polythiophene can reach quite high conductivities upon doping. In order to study the electrical properties of the plasma polymerized polythiophene, the samples are doped in an iodine chamber. Afterwards, the specific conductivity is measured under nitrogen atmosphere at 50% relative humidity. The results are presented in table 2-10. It shows that the conductivities of plasma polythiophene are much lower than its chemically synthesized form (up to 100 S/cm). The structural defects induced by the plasma damage the conjugated structure, which results in a decreased conductivity. Although it seems that the coating which was before assigned as the most damaged has the highest conductivity.

	Power W/cm²	**Gas**	**Gas flow l/min**	**Conductivity 10^{-4} S/cm**
A	0,13	N_2	20	0,1
B	0,13	He	20	<0,1
C	0,27	N_2	20	1,1
D	0,27	N_2	10	<0,1
E	0,27	N_2+O_2	20	0,1

Table 2-10: Conductivity of plasma deposited and iodine doped polythiophene.

Remarkable, is also that the conductivity decreases when measured in a dried atmosphere, as is shown in figure 2-30. When the humidity is increased, the conductivity also increases. Probably, the conduction in the coating is primary caused by ionic conductivity, which can be increased by absorption of water in the coating. Indeed, as was already observed before, the plasma polythiophene coatings are very hydrophilic and are able to absorb water from the environment. Therefore the differences in conductivity are in particular caused by the coatings ability to absorb iodine and water and not by the length of its conjugated system. This might be the explanation for the results summarized in table 2-10.

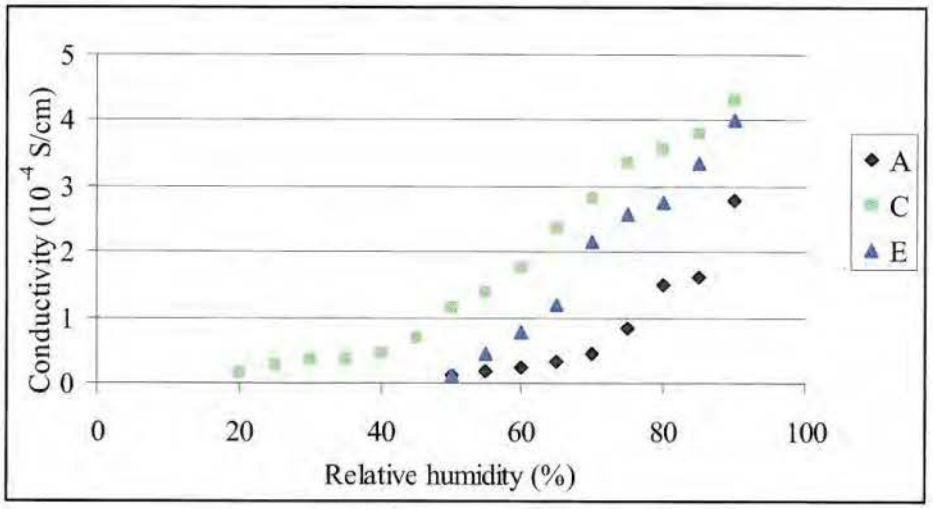

Figure 2-30: The relation between conductivity of plasma deposited and iodine doped polythiophene and the humidity. The plasma conditions are shown in table 2-7.

Mechanical properties

The application of plasma polythiophene as anti-corrosion layers not only requires the presence of some conjugation, the layers should also have some mechanical stability in wet environments. Therefore the samples are exposed to water, acetone and isopropyl alcohol for 24h. Afterwards the weight loss is measured, which is an indication for the amount of material that is dissolved or delaminated. The results are presented in figure 2-31.

When different plasma conditions are used, the plasma polythiophene films behave different in the selected solvents. A large difference is seen between the plasma depositions with an oxygen containing carrier gas and these in oxygen free gases. Addition of oxygen to the plasma makes the coatings more hydrophilic. In water the films swell, crack and delaminate from the substrate. In acetone, the coatings dissolve easily, indicating a low molecular weight and a low degree of cross-linking. Polythiophene depositions in nitrogen or helium plasmas perform better. When a higher power is used, the weight losses have even more decreased. Although, these coatings do not delaminate in water, there are some regions where they show some creases and small cracks, as is seen in picture 2-32. Also these films thus swell in water.

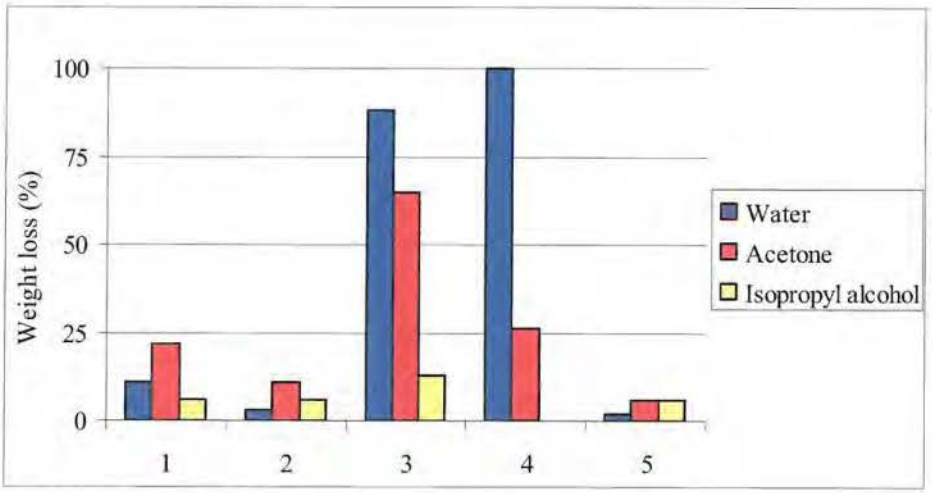

Figure 2-31: Weight loss of plasma polythiophene coatings after 24h immersion in selected solvents. The coatings are deposited in different plasma gases and at different power levels: 1) N_2 0,13 W/cm²; 2) N_2 0,27 W/cm²; 3) N_2/O_2 (1%), 0,13 W/cm²; 4) N_2/O_2 (1%), 0,27 W/cm²; 5) He, 0,18 W/cm²

Figure 2-32: Microscopic picture of a region with creases and cracks in a plasma polythiophene coating deposited in a helium plasma, after immersion in water for 24h.

Kinetics

The effect of oxygen addition and precursor concentration on the plasma deposition rate of polythiophene, is studied in this section. The concentration of thiophene aerosol in the plasma can be increased by raising the atomizing pressure as is shown in figure 2-33. In comparison with aniline and pyrrole, the thiophene monomer is able to produce higher aerosol concentrations.

Figure 2-34 presents the linear evolution of the coating thickness as a function of time. The slopes of these curves represent the deposition rates, which are shown in table 2-11. This deposition rate seems to be independent of the precursor concentration. Even when the concentration is doubled, the same reaction rate is found. Probably, there is an excess of precursor in the plasma gas, at these concentrations.

Addition of oxygen to the plasma gas increases the deposition rate. Even a small concentration of oxygen (1%) is able to raise the oxidative polymerization of thiophene. However the effect is less pronounced as with aniline or pyrrole.

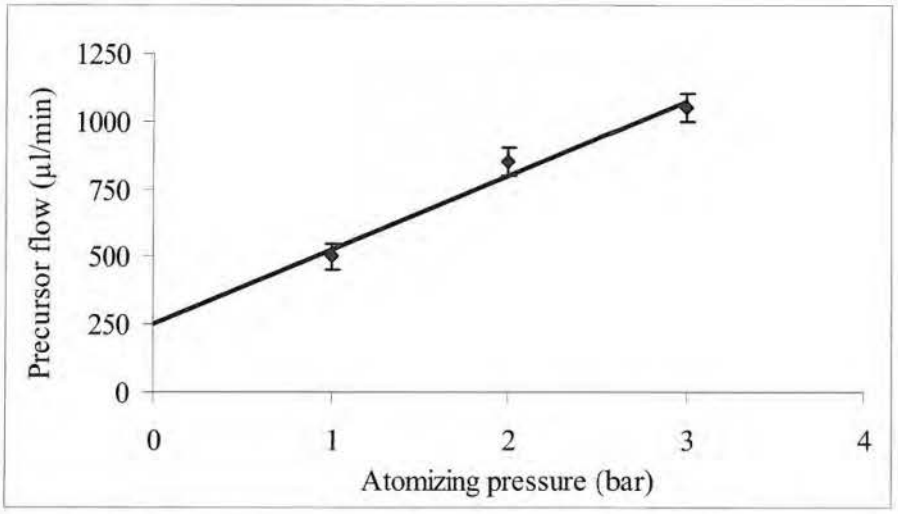

Figure 2-33: Consumption of thiophene, when atomized at different atomizing pressures.

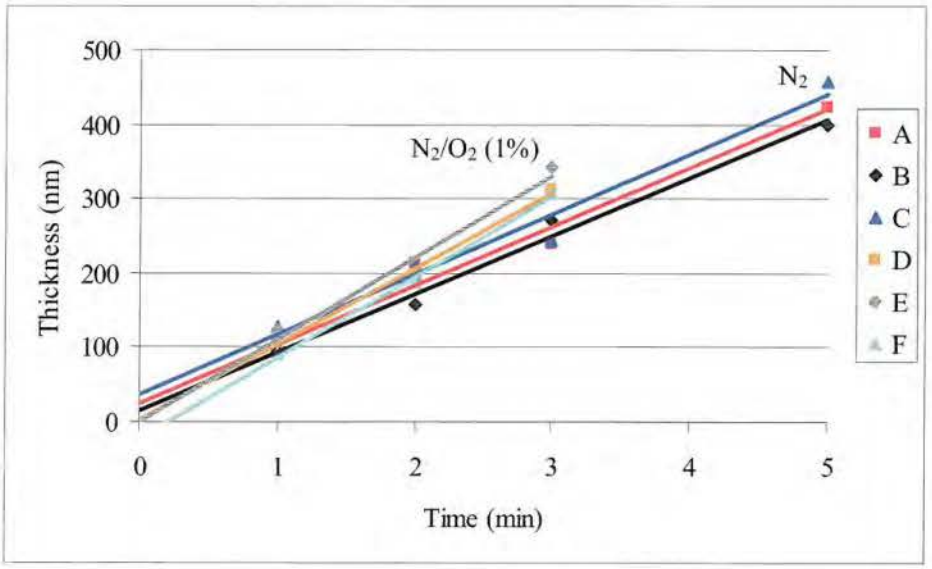

Figure 2-34: Coating thickness as a function of time, for the plasma deposition of polythiophene in different gases and at different atomizing pressures: A) N_2 1 bar; B) N_2 2 bar; C) N_2 3 bar; D) N_2+O_2 (1%) 1 bar; E) N_2+O_2 (1%) 2 bar; F) N_2+O_2 (1%) 3 bar.

	Carrier gas	Pressure (bar)	Precursor flow (µl/min)	Deposition rate (nm/min)
A	N_2	1	500	79
B	N_2	2	850	78
C	N_2	3	1050	81
D	N_2+O_2 (1%)	1	500	103
E	N_2+O_2 (1%)	2	850	110
F	N_2+O_2 (1%)	3	1050	109

Table 2-11: Deposition rate and precursor consumption for plasma deposition of thiophene in nitrogen or a nitrogen/oxygen mixture at different atomizing pressures.

Conclusions

Plasma deposition of polythiophene at atmospheric pressure results in yellow coatings. Although, the reactive plasma induces many structural defects which damage the conjugated system, conductivity could be measured after iodine doping. The measured conductivity is probably due to ionic conductivity and is dependent on the humidity of the surrounding air. Deposition rate can be increased by raising the power or by the addition of a small oxygen concentration. However, this also increases the number of structural defects. Furthermore, the polythiophene coatings deposited in a nitrogen/oxygen plasma swell and delaminate after being immersed in water, which make them less interesting for most applications.

2.5 Plasma deposition of a polythiophene derivative: poly(3-methyl thiophene)

In the former section, the possibility to deposit coatings from thiophene with an atmospheric pressure plasma has been shown. However, the reactive plasma resulted in many structural defects, which damaged the conjugated system. Section 2.5 and 2.6 will study the effect of substituents on the aromatic thiophene ring. Grounewoud et al.[36] already studied the effect of substituents

when they deposited thiophene derivatives in a vacuum plasma. In this work, it was shown that electron donating groups in the 3 and 4 positions of the thiophene rings led to less fragmentation and higher conductivities. In this section, the thiophene derivative 3-methylthiophene (figure 2.35) is deposited with an atmospheric pressure plasma. It is expected that the methyl group stabilizes the aromatic thiophene ring and will therefore lead to plasma polymerization with less defects. In section 2.6, plasma deposition of another thiophene derivative, 3,4-ethylenedioxythiophene, is discussed.

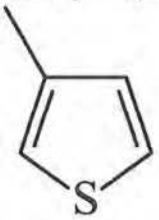

Figure 2-35: Chemical structure of 3-methylthiophene.

Chemical structure

The deposition rates for plasma polymerization of 3-methylthiophene are shown in figure 2-36. The same trends as with thiophene are seen. The reaction rate can be increased by using higher power or by addition of oxygen.

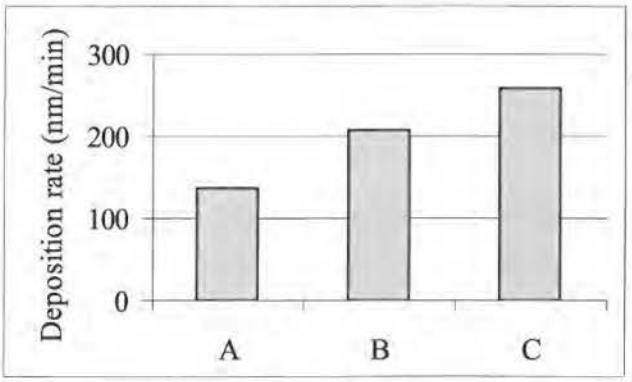

Figure 2-36: Deposition rate for plasma polymerization of poly(3-methylthiophene) at different power levels and with different discharge gases: A) N_2 0,13 W/cm²; B) N_2 0,27 W/cm²; C) N_2+O_2 (1%) 0,27 W/cm²

The chemical structure of plasma polymerized poly(3-methylthiophene) can be studied with infrared spectroscopy. The spectra are presented in figure 2-37. The monomer, as well as the plasma polymers are discussed. A detailed peak assignment is presented in table 2-12.

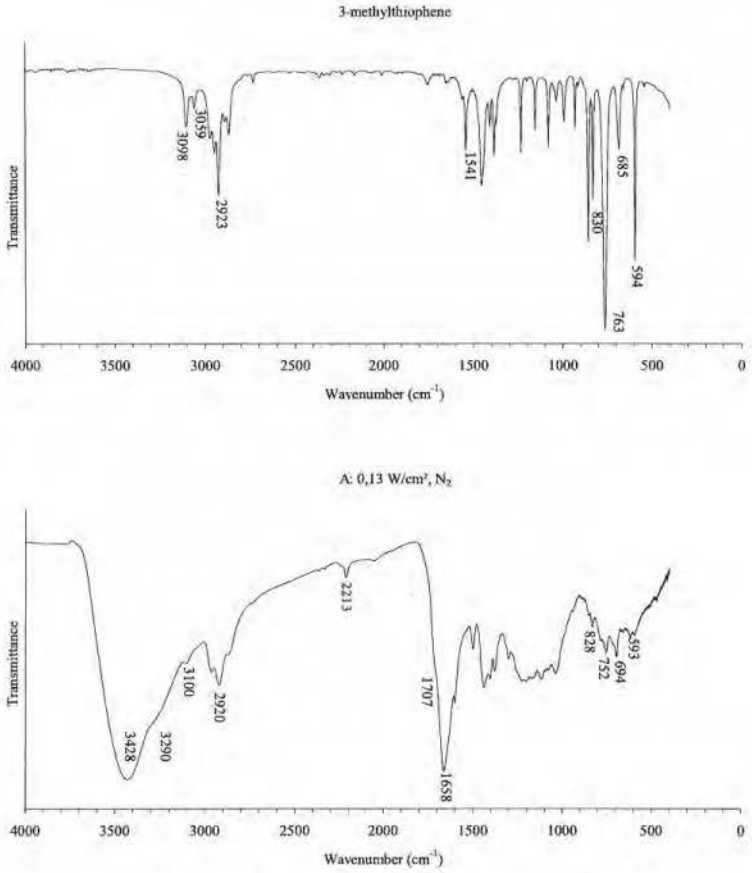

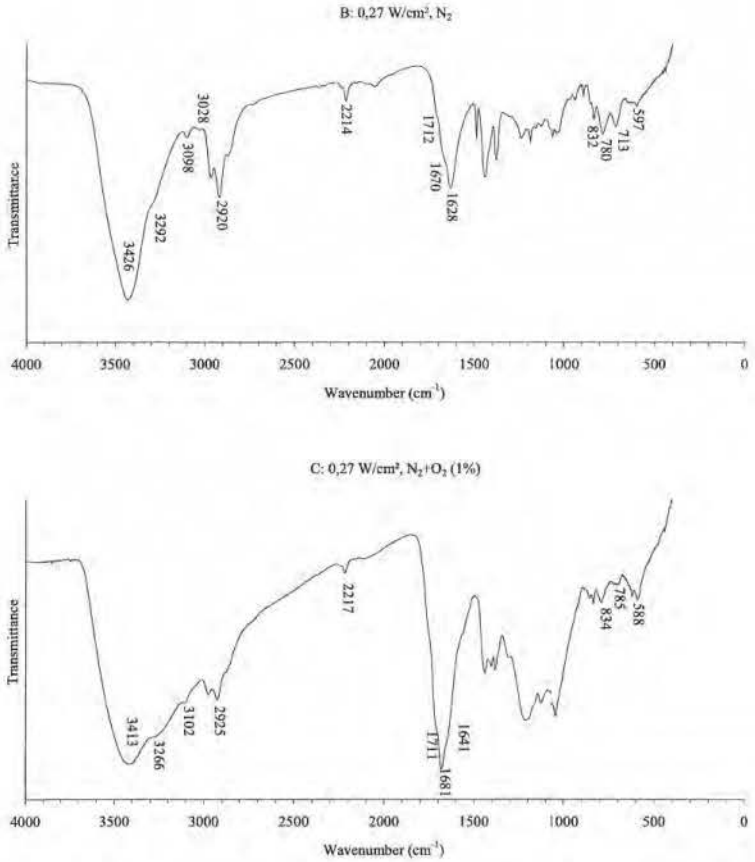

Figure 2-37: Infrared spectra of 3-methylthiophene and plasma polymerized poly(3-methylthiophene)s (A-C).

Vibration	Wavenumber (cm^{-1}) 3-methylthiophene	Wavenumber (cm^{-1}) Plasma poly-me-thiophene
O-H stretch absorbed water	-	3400
C-H stretch on triple bonded carbon	-	3290
C-H stretch on double bonded carbon	3059 3098	3030 3100
C-H stretch on saturated carbon	2900	2900
C≡C stretch	-	2215
C=O stretch saturated ketone	-	1710
C=O stretch α,β-unsaturated ketone	-	1670
C=O stretch conjugated ketone	-	1630
C=C stretch	1406 1541	1400 1560
C-H in plane bends	850-1450	850-1450
C-S stretch C-H out of plane bend	830 685 763	830 700 780
Ring deformation	594	590

Table 2-12: Detailed infrared peak assignment of 3-methylthiophene and plasma polymerized poly(3-methylthiophene).

The infrared spectrum of the 3-methylthiophene monomer resembles the one of thiophene. The major differences are the peaks around 2900 cm^{-1}, which result from the methyl substitute. Despite the presence of the substitute, the plasma deposited poly(3-methylthiophene) polymerized at low power level in nitrogen (A) still shows some structural defects. The absorptions at 2214 cm^{-1} and 3290 cm^{-1} indicate the presence of triple bonds. Also carbonyl stretches are found at 1658 and 1707 cm^{-1}, which may result from α,β unsaturated and saturated ketones. Some peaks are an indication for structure retention. The peaks around 3100 cm^{-1}, 1405 cm^{-1} and 593 cm^{-1} show that double bonds are present in the plasma polymers. The peak at 3100 cm^{-1}, resulting from C-H stretching in the 2 and 5 positions of the monomer, is not expected in the polymer spectrum, as

the monomer normally reacts in these positions. The fact that this peak is still present indicates that the plasma polymer has a low molecular weight or has reacted in an unconventional way.

When the power level has increased (B), the spectrum is similar. However, there are three carbonyl stretching peaks instead of two. The absorption at 1628 cm^{-1} is due to conjugated ketones which is an indication for retention of at least part of the conjugated structure. This is confirmed by the low intensity of the peaks resulting from saturated ketones (1712 cm^{-1}). Finally, a small amount of oxygen was added to the carrier gas during plasma polymerization. Besides the expected increase of the carbonyl content, oxygen addition doesn't seem to have a big effect on the structure of the polymer. Especially the saturated ketone peak has increased.

The results obtained from infrared spectroscopy can be confirmed by XPS spectroscopy (table 2-13). The structural formulas, calculated from these XPS data, show that the expected carbon to sulfur ratio of 5 is consistent with a methylthiophene structure. As was already seen from infrared, both the plasma polymer deposited in nitrogen, as well as the one deposited in a nitrogen/oxygen (1%) mixture have a considerable amount of oxygen incorporated. The amount of oxygen found in the plasma polymers is twice as high when oxygen is added to the plasma gas. This is in contrast with the results for plasma polythiophene, were the oxygen amount was also high when no oxygen was added to the plasma gas. The presence of the methyl group of 3-methylthiophene seems to hinder the reaction with oxygen in this case. In all these plasma depositions, a small amount of nitrogen is built in, resulting from reaction with the carrier gas.

	Gas	%S	%C	%O	%N	Structural formula
B	N_2	15	72	9	4	$C_{4,8}SO_{0,6}N_{0,3}$
C	$N_2/O_2(1\%)$	13	67	17	3	$C_{5,2}SO_{1,3}N_{0,2}$

Table 2-13: Composition and structural formula of poly(3-methylthiophene), plasma deposited in two different gases.

Properties

The presence of the methyl group in poly(3-methylthiophene) doesn't seem to have a large effect on it's absorption behavior. As well as polythiophene, it has a red color, that can be turned blue in it's doped state. However, the plasma deposited coatings again have a yellow-brown color. In figure 2-38, the UV/VIS spectra of the plasma polymerized poly(3-mehtylthiophene)s are shown. None of the spectra has an absorption maximum between 400 and 500 nm[37]. They all absorb close to the UV range, indicating that the conjugation length is rather short. Conjugation might be interrupted by the defects that were induced by the reactive plasma. After iodine doping, none of the plasma polymers were conducting.

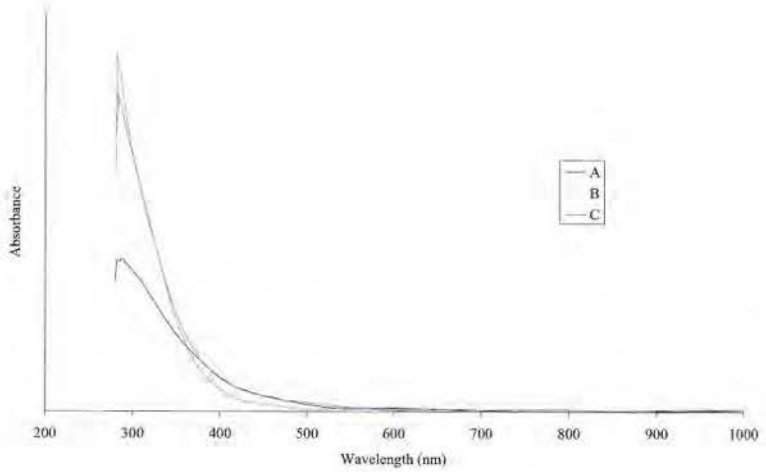

Figure 2-38: UV/VIS spectrum of plasma poly(3-methylthiophene) deposited in: (A) nitrogen at 0,13 W/cm², (B) nitrogen at 0,27 W/cm², (C) nitrogen/oxygen (1%) at 0,27 W/cm².

Mechanical properties

The influence of the methyl substitute on the mechanical properties of the plasma coating is studied by measuring the weight loss after immersion in various solvents. The results are presented in figure 2-39. As was already observed for plasma deposited polythiophene, plasma poly(3-methylthiophene)

coatings deposited in a nitrogen/oxygen plasma also swelled in water and delaminated from the substrate. Furthermore, they dissolved in acetone and isopropyl alcohol. In contrast with polythiophene, the methyl substituted derivative deposited in helium also delaminated from the substrate when immersed in water. All coatings showed high solubility in acetone, which is an indication for low molecular weight. The poly(3-methylthiophene) coatings deposited in a nitrogen plasma did not delaminate in water. However they did show cracks, which indicates swelling in water.

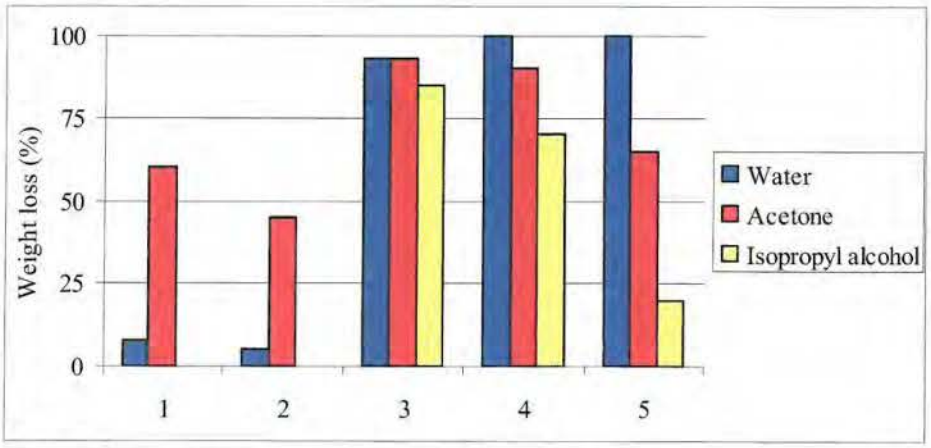

Figure 2-39: Weight loss of plasma poly(3-methylthiophene) coatings after 24h immersion in selected solvents. The coatings are deposited in different plasma gases and at different power levels: 1) N_2 0,13 W/cm²; 2) N_2 0,27 W/cm²; 3) N_2/O_2 (1%) 0,13 W/cm²; 4) N_2/O_2 (1%) 0,27 W/cm²; 5) He 0,18 W/cm²

Conclusions

Although electron donating substitutes on the thiophene ring increased structural retention in coatings plasma deposited at low pressure, this trend was not found when 3-methylthiophene was polymerized at atmospheric pressure. Infrared spectra showed the same defects as were seen in plasma polythiophene. The plasma poly(3-methylthiophene) even showed less conductivity after doping due to the short conjugation length, which is interrupted by the high amount of structural defects.

2.6 Plasma polymerization of a polythiophene derivative: poly(3,4-ethylenedioxythiophene)

Another thiophene derivative with electron donating substitutes on it's aromatic ring, is 3,4-ethylenedioxythiophene (EDOT). The aromatic heterocycle of EDOT is connected with a second six membered ring. This six membered ring is attached to the thiophene ring in the 3 and 4 positions by 2 electron donating oxygen atoms. What makes PEDOT (figure 2-40) special is that it can be made transparent in it's doped form, which makes it interesting for a lot of applications such as LCDs or solar cells. Furthermore, this polymer has a very stable doped state and is easily oxidized (doped). In applications, it is usually found as PEDOT/polystyrenesulfonic acid composite[38, 33, 39].

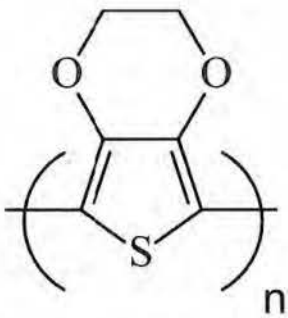

Figure 2-40: Chemical structure of PEDOT

Chemical structure

PEDOT that has been polymerized via an (electro)chemical method has a blue color in it's undoped state. We can make use of this color change to make a first evaluation of plasma deposited PEDOT layers. Some plasma parameters were studied and the effects on the appearance of the corresponding films are presented in table 2-14.

Plasma deposition of EDOT in a nitrogen plasma results in a very thin brown coating. Only the front of the electrode is coated. As was already observed for plasma polymerization of other thiophene derivatives, the conjugated system is severely damaged, resulting in a brownish deposition. When a small amount of

oxygen was added to the carrier gas, the coating had a green color. This is a first indication that an extended conjugated system has formed. It seems that addition of oxygen speeds up the polymerization reaction, making side reactions less important. However, deposition only occured at the front of the electrode. To increase the coated area, the same reaction was repeated, but now a block waved pulse mode was used, in which the plasma was sequentially turned on and off. Before turning on the plasma, the space between the electrodes was filled with the carrier gas and the precursor aerosol. After ten seconds the plasma was turned on for ten seconds. In a next sequence the electrode space was filled again, repeating the sequence several times. As intended, the electrode was completely covered with a coating. However the appearance of this coating changed. In the front there was a small amount of white powder, while further away from the gas inlet, a blue coating was formed. A possible explanation for this phenomenon is the occurrence of a concentration gradient. When the plasma is on, reaction occurs only at the front of the electrode, were the precursor concentration is highest, because the gas inlet (which continuously injects new precursor) is located at the front of the electrode. These high precursor concentrations seem to result in powder-like structures that are probably fragmented. When plasma is turned off, some activated but unreacted species are still present in the reactor. These activated species are mixed with new precursor that is injected into the gap. Reaction between these activated species and newly injected precursor, will result in deposition of the actual blue polymer with extended conjugated system. Since the reaction is slower than during the plasma on time, the complete electrode gap can be filled with precursor, resulting in deposition on the whole electrode area. When the pulse duration is reduced towards two seconds, the same result is found, but not the whole electrode area is covered because the diffusion time is too short. An intermediate pulse duration (5s) results in a somewhat different appearance. The white powder at the front of the electrode is no longer present, but a green coating is obtained instead. The ratio between activated and unactivated species is thus crucial. When the pulses are asymmetric, the results are similar. However, the white powder zone is broader when the on-time is longer than the off-time (2s on-1s off), confirming the assumption that this

white powder is formed during the on-time. When N_2O is mixed with the nitrogen discharge gas instead of oxygen, similar results can be obtained.

Gas	Pulse width		Appearance	
	On (s)	Off (s)	Front	Back
N_2	/	/	Brown	/
N_2+O_2 (1%)	/	/	Green	/
N_2+O_2 (1%)	10	10	White powder	Blue
N_2+O_2 (1%)	5	5	Green	Blue
N_2+O_2 (1%)	2	2	White powder	Blue
N_2+O_2 (1%)	2	1	White powder	Blue
N_2+O_2 (1%)	1	2	White powder	Blue
N_2+N_2O (1%)	5	5	White powder	Blue

Table 2-14: Appearance of PEDOT coatings deposited with different plasma parameters. A difference is made between deposition at the front or at the back of the electrode.

Besides the differences in appearance of the plasma PEDOT coatings plasma deposited at the front or at the back of the electrode, there's also a difference in deposition rate. This is shown in table 2-15 for the coating deposited in a nitrogen/oxygen mixture, and a power pulse with an on-time of 5s and an off-time of 5s. Deposition is more than 3 times faster at the front of the electrode.

Position	Deposition rate (nm/min)
Front of electrode	70
Back of electrode	20

Table 2-15: deposition rate of plasma deposited PEDOT at the front and at the back of the electrode.

The differences in chemical structure of the PEDOT coatings, deposited at the front and at the back of the electrode are studied with infrared spectroscopy (figure 2-41). In contrast with the other thiophene derivatives, plasma polymerization of PEDOT doesn't result in the formation of triple bonds (2200

cm^{-1}). However, carbonyl stretches are still found. The absorption around 1630 cm^{-1} indicates the formation of conjugated ketones. At 1730 cm^{-1} there's also a carbonyl stretch from a conjugated ester. These esters are formed when a carbonyl functionality is inserted next to oxygen in the six membered ring ether of EDOT.

The infrared spectrum of the plasma PEDOT coatings, deposited at the front and at the back of the electrode, are quite similar. However, there are some differences. First, plasma PEDOT deposited at the back of the electrode shows an absorption at 3115 cm^{-1}, which is absent for deposition at the front. One might expect that this C-H stretching band for unsaturated carbons in the 2 and 5 position should not be present in the spectrum, as EDOT normally polymerizes at these positions. However, when molecular weight is low, the head and tail of the polymer may still result in an absorption that's intense enough to be detected by infrared spectroscopy. This means that the polymer deposited at the front of the electrode has a higher molecular weight than the one at the back. Deposition during the more reactive plasma on-time, seems to result in higher molecular weight. In front of the electrode, the carbonyl stretches are also more intense. Especially the conjugated ester carbonyl stretch has a higher intensity. This is an indication that there are more structural defects at the start of the electrode than at the end, which is confirmed by the stronger absorption by the aromatic ring deformation at 589 cm^{-1} for plasma PEDOT deposited at the back of the electrode.

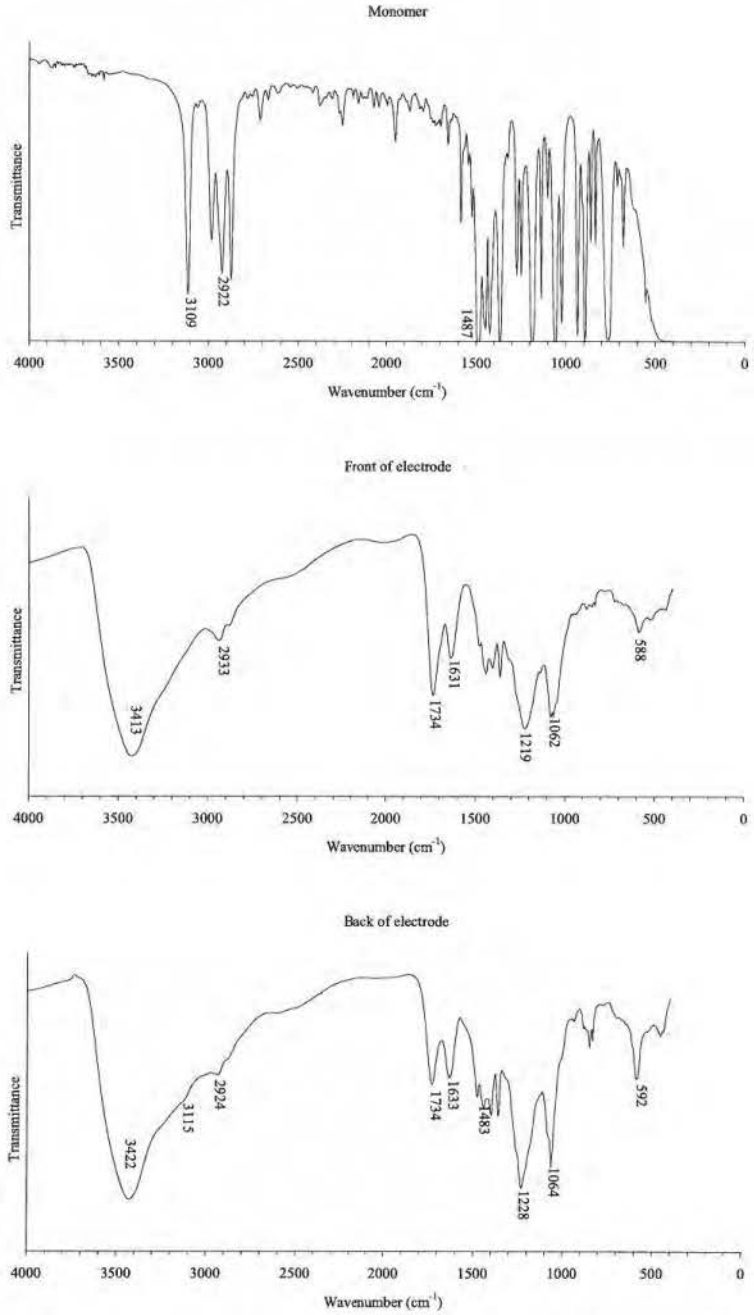

Figure 2-41: Infrared spectra of EDOT monomer and plasma PEDOT, deposited at the front and at the back of the electrode.

Vibration	Wavenumber (cm^{-1}) Monomer	Wavenumber (cm^{-1}) Front of electrode	Wavenumber (cm^{-1}) Back of electrode
O-H stretch absorbed water	-	3413	3422
C-H stretch on double bond	3109	-	3115
C-H stretch on saturated bond	2870 2922 2979	2933	2924
C=O stretch conjugated ester	-	1734	1734
C=O stretch conjugated ketone	-	1631	1633
C=C stretch	1487 1582	1479	1483
C-H in plane bends	950-1500	950-1500	950-1500
C-O stretch ether	1059 1188	1062 1219	1064 1228
C-H out of plane bends	700-1000	700-1000	700-1000
C-S stretch	833	832	832
Ring deformation	556	588	592

Table 2-16: Detailed infrared peak assignment for EDOT monomer and plasma PEDOT, deposited at the front and at the back of the electrode.

The atomic composition of the plasma PEDOT coatings is studied by XPS spectroscopy. The composition, as well as the structural formula are presented in table 2-17. The expected structural formula for PEDOT is C_6SO_2. At the front of the electrode, the PEDOT layer contains almost twice the amount of oxygen. Infrared spectra already showed that besides the expected ether functions, also carbonyl functions are present. Also the amount of carbon is much higher than in conventional PEDOT, which is an indication for fragmentation (elimination of sulfur). Plasma PEDOT deposited at the back of the electrode has a lower, but still very high oxygen content. The carbon amount however, is much lower which is an indication for a better retention of the aromatic structure (less sulfur elimination). All plasma PEDOT coatings also contain a small amount of nitrogen, coming from reaction with the carrier gas.

	Position	%S	%C	%O	%N	Structural formula
A	Front	8	60	30	2	$C_{7,5}SO_{3,8}N_{0,3}$
B	Back	9	58	31	2	$C_{6,4}SO_{3,4}N_{0,2}$

Table 2-17: Composition and structural formula of PEDOT, plasma deposited at the front and at the back of the electrode.

Properties

When polymerizing PEDOT, a blue coating is expected. For the first time, plasma deposition indeed results in the typical color for the conjugated polymer. Although, at the start of the electrode, close to the gas inlet, the plasma coating has a rather green appearance. This difference in color between deposition at the front and at the back of the electrode, should also be seen in UV/VIS spectroscopy. Figure 2-42 presents the absorption spectrum in the visible range for plasma PEDOT.

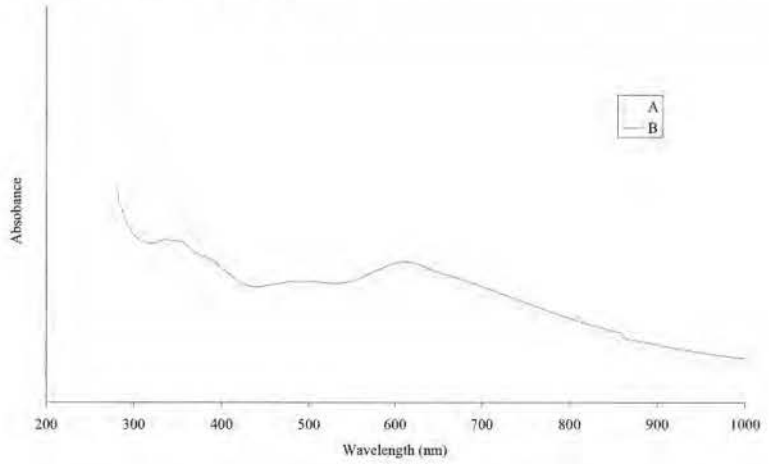

Figure 2-42: UV/VIS spectra of plasma polymerized PEDOT, deposited at the front of the electrode (A) or at the back (B).

Plasma PEDOT deposition at the back of the electrode (B) results in an expected absorption peak around 600 nm[32, 33]. At 350 nm, a second absorption maximum is found, which probably comes from some fragmentation that results in shorter conjugation length. Deposition at the front of the electrode

shows a similar spectrum (A). However, this time, the absorption peak at 350 nm has a higher intensity. This confirms the assumption that there is a higher fragmentation degree at the front of the electrode.

Doping of conjugated polymers results in a decrease of the energy gap between the valence and conduction band, which results in increased conductivity and color change. Conductivity of plasma deposited PEDOT coatings, before and after doping are presented in table 2-18.

	Position on electrode	**Conductivity (S/cm)**	
		Undoped	**Iodine doped**
A	Front	$2{,}8 \times 10^{-4}$	$5{,}4 \times 10^{-4}$
B	Back	$1{,}0 \times 10^{-2}$	$1{,}8 \times 10^{-3}$

Table 2-18: Conductivity of undoped and iodine doped plasma PEDOT, deposited at the front and at the back of the electrode. Conductivity is measured at room temperature at 50% humidity.

Both, plasma coatings at the front and at the back of the electrode already show semi-conductive behavior before doping. As expected, conductivity is higher in the less fragmented part of PEDOT plasma deposited at the back of the electrode. (B). When green PEDOT deposited at the front of the electrode is doped with iodine vapor, the conductivity increases with a factor 2. However, a higher increase upon doping is usually seen. The presence of the doping agent should also be seen in it's absorption spectrum. Indeed, doping decreases the bandgap and shifts the absorption maximum towards higher wavelengths. The absorption spectrum of plasma PEDOT deposited in front of the electrode is presented in figure 2-43. After doping the absorption maximum around 600 nm is broader and shows a small shift towards higher wavelengths, which is an indication for the formation of polarons and bipolarons. The presence of these charge carriers are probably responsible for the increased conductivity. Close to the UV-region two other peaks arise, resulting from the dopant itself. Indeed, iodine also absorbs light in the visible range. As an example, the absorption spectrum of a iodine solution in water is added to the graph. Three peaks can be seen. The one around 500 nm is the actual absorption of molecular iodine. This

peak can shift a bit depending on the interactions with the solvent molecules. In water, also ionic iodine (I_3^-) is formed, which absorbs at 290 nm and 350 nm[40]. In the doped plasma PEDOT spectrum, only the two I_3^- absorptions are found, which means that there's no molecular iodine present. So, all of the absorbed iodine must have interacted with the polymer.

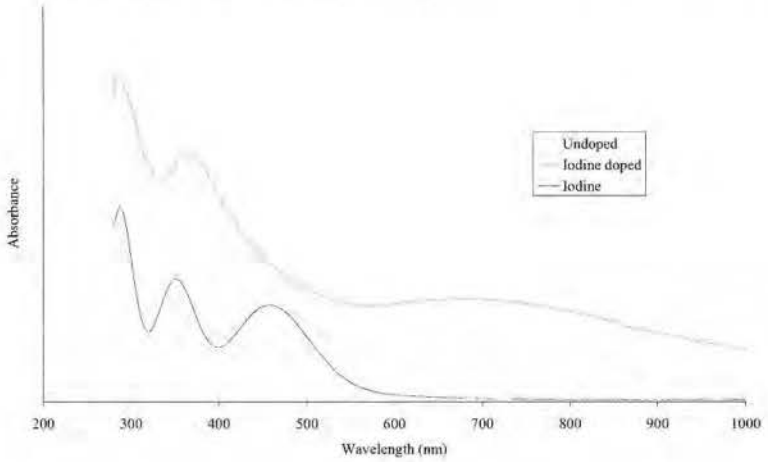

Figure 2-43: UV/VIS spectrum of undoped and iodine doped PEDOT, plasma deposited at the front of the electrode and of an aqueous iodine solution.

Surprisingly, iodine doping of the blue plasma PEDOT coating, deposited at the back of the electrode, results in a decreased conductivity. It is so far unclear why additional doping causes an actual decrease in conductivity. It may be possible that remaining radicals extended the conjugated system and so are partially responsible for the measured conductivity. Iodine doping may then cause a partial degradation of that conjugated system. The UV/VIS absorption spectra of undoped and iodine doped plasma PEDOT are compared in figure 2-44. Again the absorption maximum at 600 nm is broadened and slightly red shifted upon doping with iodine. While no molecular iodine is found in the coating (500 nm), two absorption peaks at 290 and 350 nm show the presence of the I_3^- ion.

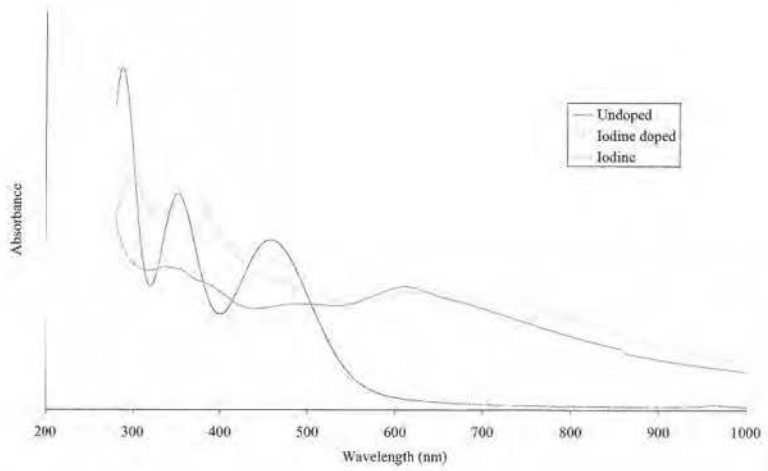

Figure 2-44: UV/VIS spectrum of undoped and iodine doped PEDOT, plasma deposited at the back of the electrode and of an aqueous iodine solution.

Figure 2-45 presents the conductivity of the plasma PEDOT coatings as a function of the relative humidity. Both, the plasma PEDOT film deposited at the front of the electrode as the one deposited at the back show an increased conductivity at higher humidity. The incorporation of carbonyl functions in the polymer structures make them more hydrophilic. Because of their high affinity for water, these plasma polymers are able to absorb water from the surrounding air. Water serves as a solvent for ionic products, left in the coating after plasma polymerization, which induces ionic conductivity.

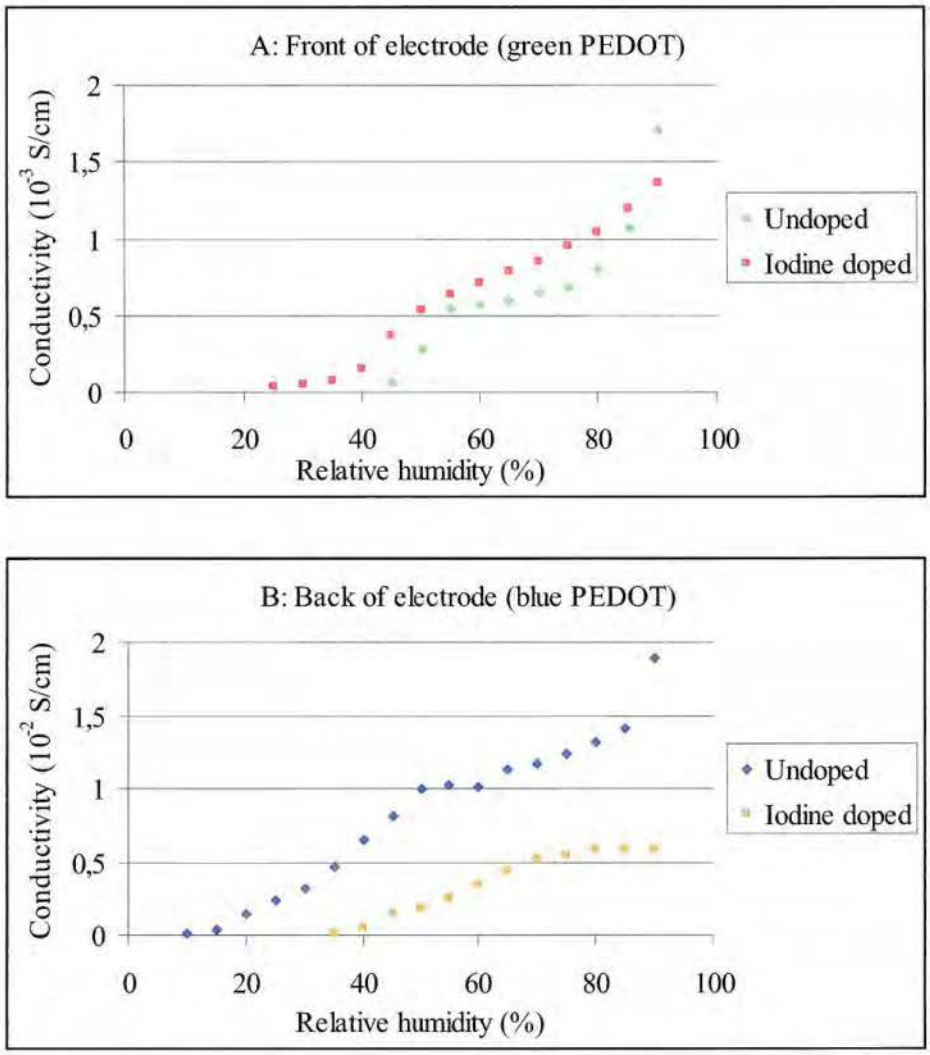

Figure 2-45: Conductivity as a function of humidity for plasma polymerized PEDOT, deposited at the front (A) and the back (B) of the electrode.

The conductivity of undoped plasma PEDOT seems to move to a plateau above 50% humidity. The coatings are probably close to saturation at this point. Above 80% of humidity the conductivity rises again, which is due to water that condensates on the coating surface, making the conduction channel (for ionic conductivity) wider. This behavior is not observed when the plasma PEDOT coatings are iodine doped.

Homogeneous PEDOT layers

Plasma polymerization of EDOT is possible when a small oxygen concentration is added to the discharge gas and a pulsed plasma is used. The plasma deposited coating is homogeneously distributed concerning both chemical structure and thickness along the entire width of the electrode, which is in contrast to it's distribution along the electrode length. At the front of the electrode, close to the gas inlet, the coating is more fragmented and therefore shows some different properties, compared to deposition at the back of the electrode. To overcome this problem, the same experiments were performed in a translating dielectric barrier discharge reactor, which moves across the substrate (figure 2-46). This system consists of a stationary earthed electrode and two translating high voltage electrodes. Discharge gas and precursor are injected in the middle of the two plasma zones. At the outside of the reactor, there are two air knives which cut of the environmental air by a double nitrogen flow. These air knives can be switched on and off in such a way that the one in the direction of the electrode translation is always on. This way, the environmental air is always kept out of the plasma and the precursor is blown into the plasma zone. It is expected that the use of such a translating reactor will mix the blue and green plasma PEDOT layers acquired with the stationary reactor, which will result in a more homogeneous coating. Furthermore, this reactor setup resembles more the industrial reel to reel approach with several reactors in line.

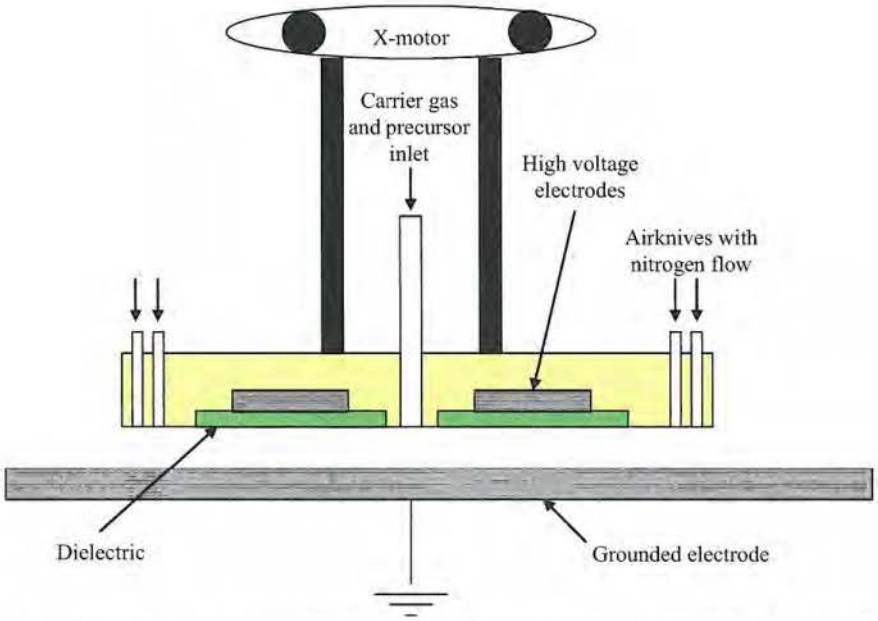

Figure 2-46: Schematic presentation of a DBD reactor with translating high voltage electrodes.

Two new parameters are introduced when a translating reactor is used, which are the speed of translation and the path length. Some experiments were set up to reproduce the blue coating that was deposited before with the stationary reactor. Therefore the carrier gas, the moving speed and path length of the reactor were adjusted. These experiments are summarized in table 2-19.
The first approach was to use nitrogen as discharge gas and a long path length, so that the samples would be exposed to environmental oxygen after every step. This resulted in a very thin brown coating, indicating that the conjugated system is severely damaged. In a second approach dinitrogenoxide was added to the plasma zone. Also the path length was shortened, to be sure that the sample was always in between the two air knives, so that less impurities would be able to enter the plasma zone. This also resulted in the undesired brown coating. Addition of oxygen didn't bring any improvements either.

	Gas	Moving speed (m/min)	Path length (mm)	Color
A	N_2	4	560	Brown
B	N_2/N_2O (5%)	4	360	Brown
C	N_2/O_2 (1%)	4	360	Brown
D	N_2/N_2O (5%)	2	360	Brown
E	N_2/O_2 (1%)	2	360	Blue

Table 2-19: Color of PEDOT coatings, plasma deposited in different gasses and with different moving speed and path length.

** Note that the gas mixture is injected in the middle between the two plasma zones. The gas mixtures reported might be diluted by nitrogen resulting from the air knives.*

In an attempt to imitate the reaction conditions of the stationary reactor as much as possible, the reactor speed was reduced from 4 to 2 m/min. At this speed, the samples are in the plasma zone for 5s, and out of the plasma zone for 5s, which resembles the pulsed plasma polymerization that gave the best results in the stationary reactor. When dinitrogenoxide was used as oxidant, this still resulted in a brown coating, but addition of oxygen to the plasma gas led to a homogeneous blue coating (figure 2-47).

Figure 2-47: Plasma deposition of PEDOT with a translating DBD reactor in: (A) nitrogen, (D) nitrogen/dinitrogenoxide (5%), (E) nitrogen/oxygen (1%)

To optimize these plasma PEDOT coatings, the influence of the different plasma parameters were studied. An evaluation of the conjugation is done with UV/VIS spectroscopy. Figure 2-48 shows the influence of the oxygen percentage in the nitrogen carrier gas on the absorption behavior of plasma

PEDOT. When the oxygen concentration is increased, the intensity of the absorption peak maximum around 600 nm also increases. As is shown in figure 2-49, this increase in intensity correlates well with an increase in thickness. Higher oxygen concentration thus results in a higher deposition rate. While the shape of the absorption curve is the same for oxygen concentrations of 1 and 2%, there is a difference when the oxygen concentration is further increased to 3%. At 490 nm, there's a second absorption maximum that is not seen at lower oxygen concentrations. This second peak might be due to the formation of other structures (such as thiophenes with another functional substitution) or shorter conjugation (oligomers). The use of 2% oxygen seems to be the optimum gas mixture and was always used hereafter.

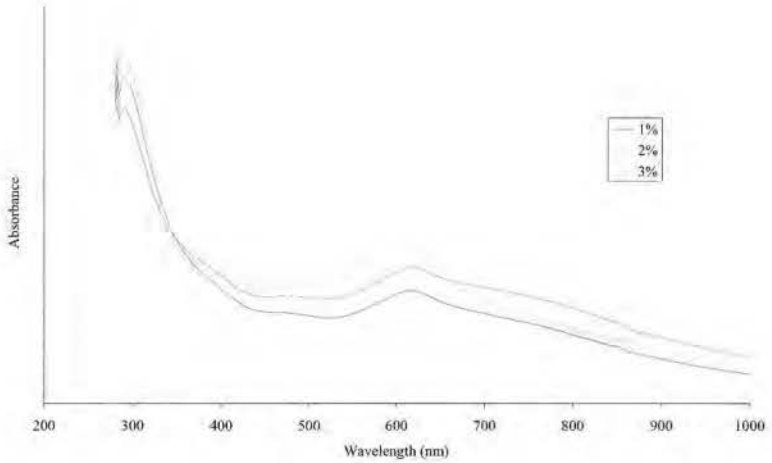

Figure 2-48: UV/VIS spectra of plasma PEDOT, deposited in a nitrogen/oxygen plasma with different oxygen concentrations.

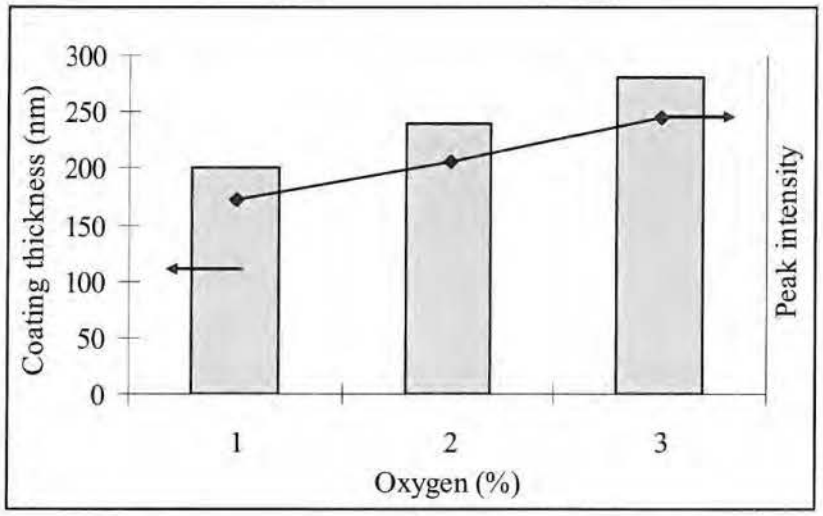

Figure 2-49: Coating thickness for plasma PEDOT, deposited in a nitrogen/oxygen plasma with different oxygen concentrations. The maximum peak intensity for absorption around 600 nm is also presented.

Figures 2-50 and 2-51 show the effect of power level and carrier gas flow on plasma deposition of PEDOT coatings. The power doesn't seem to have a large effect on the coating thickness nor on the absorption behavior. This is a surprising result because the deposition rate of other thiophene derivatives increased when higher power levels were used. In first instance an explanation for this phenomenon could be that the yield for plasma polymerization of EDOT is already close to 100% at lower power. However, as is shown in figure 2-49, an increase in oxygen concentration is actually able to increase the deposition rate. So the assumption of high yield is not correct. Another possible explanation could be related to the plasma regime. When a conducting layer like plasma PEDOT is formed, the plasma contains more streamers. In these conducting channels electron density is very high and ionization is very efficient. Probably, ionization of EDOT molecules close to these streamers is very efficient with yields close to 100%. Higher power does not necessarily result in more streamers, but in a higher electron density in these streamers, were the ionization degree was already very high. If this assumption is correct and the time scale for diffusion of all molecules towards the streamers is too

short, EDOT molecules further away from the streamers are not ionized directly by the plasma.

The fact that higher power does not lead to thicker coatings might be explained by streamer formation in the plasma. But what happens when more oxygen is added to the plasma? Oxygen forms ozone and oxygen radicals in the plasma. These species are strong oxidants which are able to oxidize EDOT. Thus ozone and oxygen radicals provide another oxidation mechanism, which is also able to oxidize the EDOT molecules further away from the streamers. Probably, ozone and oxygen radicals are also responsible for the polymerization reaction to continue after the samples have moved out of the plasma zone.

While increasing the power level didn't affect the deposition rate, an increase of the gas flow did. Higher gas flow leads to thinner coatings, which could be expected since this higher gasflow dilutes the precursor and decreases the plasma contact time. The shape of the absorption curve is not affected by a difference in gas flow. Again, the intensity of the absorption maximum correlates well with the coating thickness.

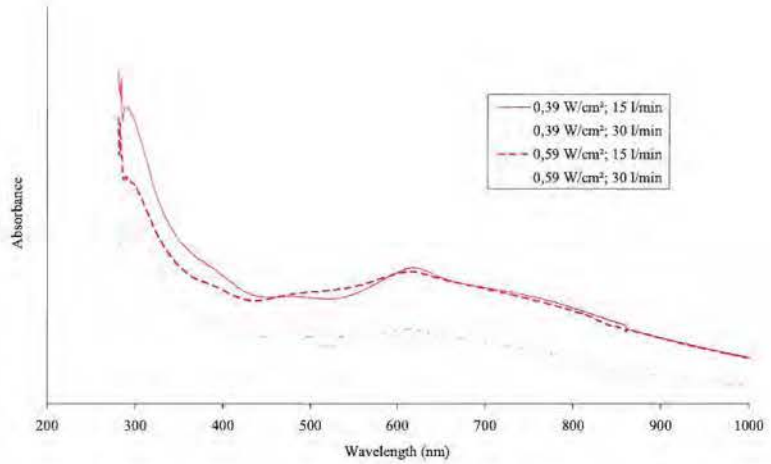

Figure 2-50: UV/VIS spectra of plasma PEDOT, deposited at different plasma powers and with different gas (nitrogen/oxygen -2%) flows.

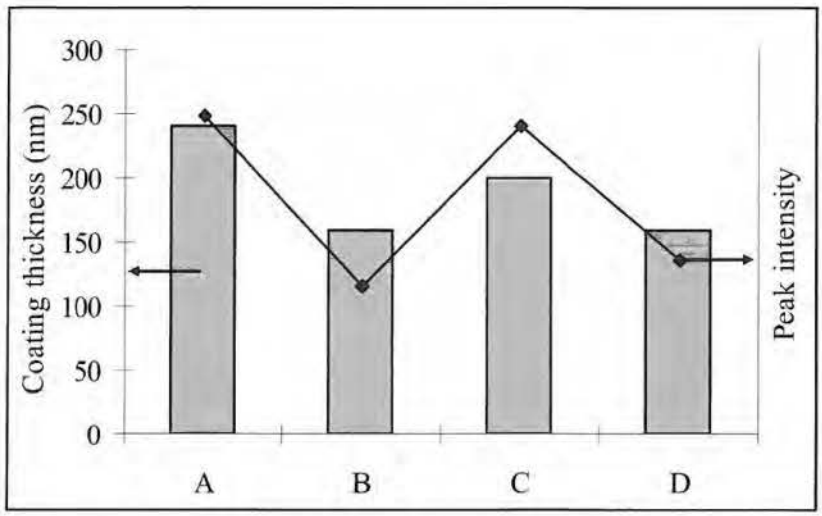

Figure 2-51: Coating thickness for plasma PEDOT, deposited at (A) 15 l/min N_2/O_2 (2%), 0,39 W/cm²; (B) 30 l/min N_2/O_2 (2%), 0,39 W/cm²; (C) 15 l/min N_2/O_2 (2%), 0,59 W/cm²; (D) 30 l/min N_2/O_2 (2%), 0,59 W/cm². The maximum peak intensity for absorption around 600 nm is also presented.

Figures 2-52 and 2-53 show the influence of the precursor concentration on the coating thickness and absorption behavior of the plasma PEDOT coatings. The precursor concentration can be controlled by adjusting the pressure on the atomizer. In contrast with other thiophene derivatives, the deposition rate of plasma PEDOT is dependent on the precursor concentration. An explanation could be the low consumption of EDOT by the atomizer (50µl/min) or also the streamer like plasma regime. Indeed, if assumed that only EDOT close to the streamers would polymerize efficiently, a higher precursor concentration would bring more EDOT close to this streamers, resulting in a higher deposition rate.
The intensity of the absorption maximum around 600 nm corresponds well with the coating thickness. At 3 bar atomizing pressure, however a second absorption peak is found around 490 nm. Probably, this peak is due to the formation of an oligomer fraction. Indeed, stepwise polymerization mechanisms (same as pyrrole polymerization - figure 2-19) generally result in lower molecular weight when the concentrations are higher.

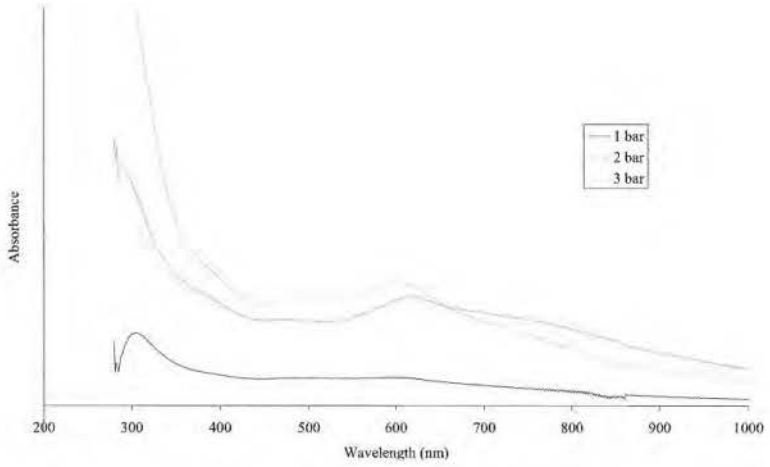

Figure 2-52: UV/VIS spectra of plasma PEDOT, deposited at different atomizing pressures (precursor concentrations).

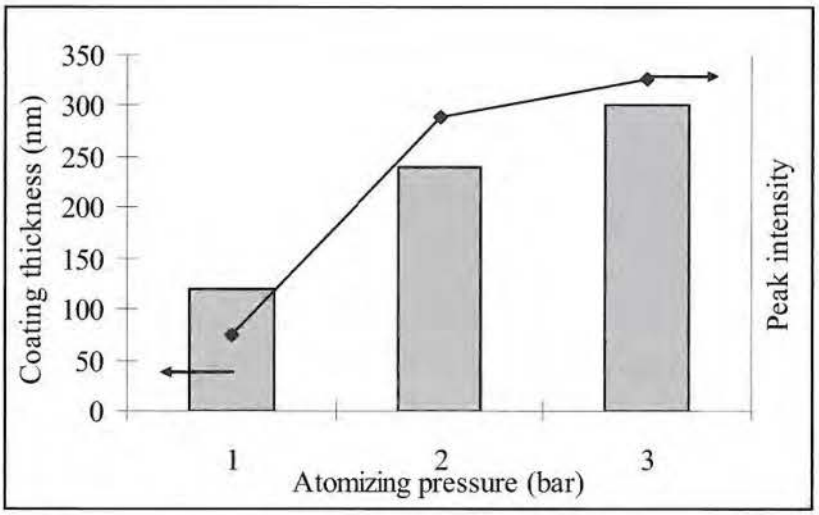

Figure 2-53: Coating thickness for plasma PEDOT, deposited at different atomizing pressures (precursor concentrations). The maximum peak intensity for absorption around 600 nm is also presented

All PEDOT coatings deposited with the translating DBD plasma reactor are very homogeneous and have smooth surfaces. An example of such PEDOT

coating is presented in figure 2-54, which shows a SEM picture of such plasma deposited PEDOT film.

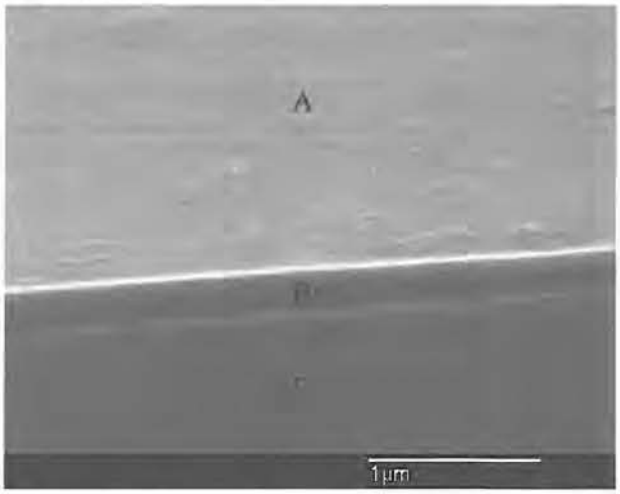

Figure 2-54: SEM picture (25° tilt) of a plasma deposited PEDOT coating, deposited with a moving DBD reactor: (A) coating surface, (B) coating cross-section, (C) substrate cross-section.

Conclusions

Plasma polymerization of PEDOT at atmospheric pressure resulted in colored coatings when a small oxygen concentration was added to the plasma gas. When an on-off block wave pulsed plasma was used, structural defects could be decreased, resulting in a blue coating, which is a typical color for PEDOT. Probably, the blue coating is formed during the off-times of the plasma. Conductivities up to 1 x 10^{-2} S/cm were obtained without doping. It is so far unclear why doping causes a decrease in conductivity. Possibly, remaining radicals cause a degradation of the conjugated system. While the coatings deposited in a stationary DBD reactor were inhomogeneous across the length of the electrode, the application of a translating DBD reactor resulted in homogeneous films. Reaction rate could be increased by applying a higher oxygen concentration. However, at a concentration of 3%, a second absorption maximum in the visible range was seen, indicating side reactions or low molecular weight fractions. While an increased power level did not have any

effect on the coating thickness, nor on the absorption behaviour, an increased gas flow did decrease the reaction rate. Finally, the coating rate could also be increased by increasing the pressure on the aerosol generator (higher aerosol concentrations). At a pressure of 3 bar, a second absorption maximum was seen again, probably due to the formation of an oligomeric fraction.

2.7 Experimental part

Characterization methods

The thickness of the plasma deposited coatings was measured with an UBC 14 profilometer of UBM, using the diamond probe.

The composition of the plasma deposited coatings was studied with an x-ray photoelectron spectrometer (XPS) from Thermo with a theta probe. Monochromatic soft X-rays of Al Kα at 1486.6 eV were used to irradiate the coatings deposited on glass substrates. Spectra were obtained at 100 W with a spot size of 400 μm. To determine the elemental composition of each surface, survey spectra were recorded at 300 eV pass energy and 1 eV step size. To compensate for the charging of non-conductive polymers, an argon flood gun was used at 6 eV and 25 μA emission. The photoelectron spectral peak areas were scaled to deal with instrument sensitivity and ionization probabilities affording surface concentrations in atom percent.

The chemical structure of the plasma deposited coatings was studied with a Nexus Fourier transformed infrared spectrometer from Thermo. The samples were prepared by scraping off the coating from the glass substrate, mixing it with potassium bromide and pressing it into a pellet. The potassium bromide (99+, FTIR grade) was purchased from Sigma Aldrich and used after drying at 120°C.

The absorption of UV and visible light by plasma deposited coatings was measured on coatings deposited on glass slides, with a Lambda 900 UV/VIS/NIR spectrometer from Perkin Elmer.

The conductivity of the plasma deposited coatings was calculated from their resistance. Two silver electrodes were coated onto the coating surface with

silver paste. The resistance of the coating was measured under a nitrogen atmosphere (50% humidity) with a Fluke 189 True RMS multimeter. Specific conductivity was calculated from these resistance measurements. The influence of the humidity on the conductivity was tested in a humidity chamber. The humidity is adjusted by a nitrogen flow which has passed through water.
For analysis of the coating's morphology, scanning electron microscopy (SEM) was used. Photographs of cross-sections of coated samples were taken with a JSM-6340F SEM of JEOL. To have a picture of both the coating surface and the cross section of the coatings, the samples were tilted under an angle of 25°. The cross-section of the coating also shows the coating thickness.

Chemicals

All chemicals used were obtained from Sigma Aldrich and used without further purification. The following chemicals were used in this chapter: aniline (99%), polyaniline (Mw: 10000 g/mol), pyrrole (98%), thiophene (99+%), 3-methylthiophene (98%), 3,4-ethylenedioxythiophene, N-methylpyrrolidone (99,5%).

Plasma reactor

The plasma is generated with a dielectric barrier discharge between two horizontally placed electrodes. The lower electrode is covered by a glass dielectric of 5 mm thickness, while the upper electrode is uncovered. A high ac voltage is used on the lower electrode, which has an area of 560 cm^2 (21,5 x 26 cm). Power is supplied by a G10 S-V AFS generator, that is carefully tuned for the used frequency and the specific electrode configuration, in order to minimize power losses. The upper electrode is grounded. The gap between the glass dielectric and the uncovered electrode is 2 mm. The gas flow rate is controlled with an MKS mass flow controller. The precursors are injected into the plasma as an aerosol, generated with a TSI constant output atomizer type 3076. Before entering the plasma the aerosol is mixed with the carrier gas which is used to transport the aerosol towards the plasma. The coatings where deposited onto glass substrates which were placed onto the dielectric.

When a translating reactor is used, the fixed lower electrode was grounded, while a high voltage was applied on two moving upper electrodes, which have an area of 256 cm^2 (2x). The upper electrodes were covered with a 2,2 mm thick glass dielectric. To keep environmental oxygen out of the plasma zone, two airknives are situated at the edges of the plasma zone. While nitrogen flows out of the outer airknive at a rate of 20 l/min, the inner airknive has a flow rate of 15 l/min.

Plasma parameters

All plasma parameters used, are presented in the tables below. The different parameters shown are:

- **Chemicals**: the precursors or precursor solutions that are injected into the plasma as an aerosol
- **Press**: the gas pressure used to generate the aerosols
- **Power**: the power per square cm, used on the high voltage electrode
- **Time**: the total reaction time
- **Gas**: the gasses used to create the plasma and their concentration
- **Flow**: the total gas flow rate in standard liters per minute
- **Freq**: the high voltage frequency
- **Pulse**: The on and off times of the plasma, when the power is applied in the block wave pulsed mode.
- **Speed**: The speed at which the translating reactor moves over the samples.
- **Range**: The translation range of the moving reactor.
- **Steps**: The number of passes of the translating reactor above the samples.

2.2: plasma deposition of polyaniline
Polymer precursor

Chemicals	Pressure (bar)	Power (W/cm²)	Time (s)	Gas	Flow (sl/min)	Freq (kHz)
Polyaniline (0,5%) in NMP	2	0,27	300	N_2	5	1,5
Polyaniline (0,4%) in NMP/aniline (1/1)	2	0,27	300	N_2	5	1,5
Polyaniline (0,4%) in aniline	2	0,27	180	N_2	20	1,5

2.2: plasma deposition of polyaniline
Effect of the power level on plasma polymerization of aniline

Chemicals	Pressure (bar)	Power (W/cm²)	Time (s)	Gas	Flow (sl/min)	Freq (kHz)
Aniline	2	**0,54**	180	N_2 O_2(21%)	20	1,5
Aniline	2	**0,36**	180	N_2 O_2(21%)	20	1,5
Aniline	2	**0,27**	180	N_2 O_2(21%)	20	1,5
Aniline	2	**0,18**	180	N_2 O_2(21%)	20	1,5
Aniline	2	**0,13**	180	N_2 O_2(21%)	20	1,5

2.2: plasma deposition of polyaniline

Effect of the carrier gas on plasma polymerization of aniline

	Chemicals	Pressure (bar)	Power (W/cm²)	Time (s)	Gas	Flow (sl/min)	Freq (kHz)
A	Aniline	2	0,18	180	N_2	20	1,5
B	Aniline	2	0,18	180	**He**	20	1,5
C	Aniline	2	0,18	180	N_2 **O_2(1%)**	20	1,5
D	Aniline	2	0,18	180	N_2 **O_2(21%)**	20	1,5

2.2: plasma deposition of polyaniline

Effect of the frequency on plasma polymerization of aniline

Chemicals	Pressure (bar)	Power (W/cm²)	Time (s)	Gas	Flow (sl/min)	Freq (kHz)
Aniline	2	0,18	180	N_2	20	**1,5**
Aniline	2	0,18	180	N_2	20	**6**
Aniline	2	0,18	180	N_2	20	**12**
Aniline	2	0,18	180	N_2	20	**25**
Aniline	2	0,18	180	N_2	20	**50**

2.2: plasma deposition of polyaniline

Effect of the gas flow on plasma polymerization of aniline

Chemicals	Pressure (bar)	Power (W/cm²)	Time (s)	Gas	Flow (sl/min)	Freq (kHz)
Aniline	2	0,18	180	N_2	**10**	1,5
Aniline	2	0,18	180	N_2	**20**	1,5
Aniline	2	0,18	180	N_2	**40**	1,5

2.2: plasma deposition of polyaniline
Mechanical properties

	Chemicals	Pressure (bar)	Power (W/cm²)	Time (s)	Gas	Flow (sl/min)	Freq (kHz)
1	Aniline	2	0,13	180	N_2	20	1,5
2	Aniline	2	0,27	180	N_2	20	1,5
3	Aniline	2	0,13	180	N_2 O_2(1%)	20	1,5
4	Aniline	2	0,27	180	N_2 O_2(1%)	20	1,5
5	Aniline	2	0,18	180	He	20	1,5

2.2: plasma deposition of polyaniline: Kinetics

Chemicals	Pressure (bar)	Power (W/cm²)	Time (s)	Gas	Flow (sl/min)	Freq (kHz)
Aniline	1	0,18	60	N_2	20	1,5
Aniline	1	0,18	120	N_2	20	1,5
Aniline	1	0,18	180	N_2	20	1,5
Aniline	1	0,18	300	N_2	20	1,5
Aniline	2	0,18	60	N_2	20	1,5
Aniline	2	0,18	120	N_2	20	1,5
Aniline	2	0,18	180	N_2	20	1,5
Aniline	2	0,18	300	N_2	20	1,5
Aniline	3	0,18	60	N_2	20	1,5
Aniline	3	0,18	120	N_2	20	1,5
Aniline	3	0,18	180	N_2	20	1,5
Aniline	3	0,18	300	N_2	20	1,5
Aniline	1	0,18	60	N_2 O_2(1%)	20	1,5
Aniline	1	0,18	120	N_2 O_2(1%)	20	1,5
Aniline	1	0,18	180	N_2 O_2(1%)	20	1,5
Aniline	2	0,18	60	N_2 O_2(1%)	20	1,5
Aniline	2	0,18	120	N_2 O_2(1%)	20	1,5
Aniline	2	0,18	180	N_2 O_2(1%)	20	1,5
Aniline	3	0,18	60	N_2 O_2(1%)	20	1,5
Aniline	3	0,18	120	N_2 O_2(1%)	20	1,5
Aniline	3	0,18	180	N_2 O_2(1%)	20	1,5

2.3 Plasma deposition of polypyrrole
Chemical structure

	Chemicals	Pressure (bar)	Power (W/cm²)	Time (s)	Gas	Flow (sl/min)	Freq (kHz)
A	Pyrrole	2	0,13	180	N_2	20	1,5
B	Pyrrole	2	0,13	180	He	20	1,5
C	Pyrrole	2	0,27	180	N_2	20	1,5
D	Pyrrole	2	0,27	180	N_2	10	1,5
E	Pyrrole	2	0,27	180	N_2 O_2(1%)	20	1,5

2.3 Plasma deposition of polypyrrole
Mechanical properties

	Chemicals	Pressure (bar)	Power (W/cm²)	Time (s)	Gas	Flow (sl/min)	Freq (kHz)
1	Pyrrole	2	0,13	180	N_2	20	1,5
2	Pyrrole	2	0,27	180	N_2	20	1,5
3	Pyrrole	2	0,13	180	N_2 O_2(1%)	20	1,5
4	Pyrrole	2	0,27	180	N_2 O_2(1%)	20	1,5
5	Pyrrole	2	0,18	180	He	20	1,5

2.3: plasma deposition of polypyrrole: Kinetics

Chemicals	Pressure (bar)	Power (W/cm²)	Time (s)	Gas	Flow (sl/min)	Freq (kHz)
Pyrrole	1	0,18	60	N_2	20	1,5
Pyrrole	1	0,18	120	N_2	20	1,5
Pyrrole	1	0,18	180	N_2	20	1,5
Pyrrole	1	0,18	300	N_2	20	1,5
Pyrrole	2	0,18	60	N_2	20	1,5
Pyrrole	2	0,18	120	N_2	20	1,5
Pyrrole	2	0,18	180	N_2	20	1,5
Pyrrole	2	0,18	300	N_2	20	1,5
Pyrrole	3	0,18	60	N_2	20	1,5
Pyrrole	3	0,18	120	N_2	20	1,5
Pyrrole	3	0,18	180	N_2	20	1,5
Pyrrole	3	0,18	300	N_2	20	1,5
Pyrrole	1	0,18	60	N_2 O_2(1%)	20	1,5
Pyrrole	1	0,18	120	N_2 O_2(1%)	20	1,5
Pyrrole	1	0,18	180	N_2 O_2(1%)	20	1,5
Pyrrole	2	0,18	60	N_2 O_2(1%)	20	1,5
Pyrrole	2	0,18	120	N_2 O_2(1%)	20	1,5
Pyrrole	2	0,18	180	N_2 O_2(1%)	20	1,5
Pyrrole	3	0,18	60	N_2 O_2(1%)	20	1,5
Pyrrole	3	0,18	120	N_2 O_2(1%)	20	1,5
Pyrrole	3	0,18	180	N_2 O_2(1%)	20	1,5

2.4 Plasma deposition of polythiophene
Chemical structure

	Chemicals	**Pressure (bar)**	**Power (W/cm²)**	**Time (s)**	**Gas**	**Flow (sl/min)**	**Freq (kHz)**
A	Thiophene	2	0,13	180	N_2	20	1,5
B	Thiophene	2	0,13	180	He	20	1,5
C	Thiophene	2	0,27	180	N_2	20	1,5
D	Thiophene	2	0,27	180	N_2	10	1,5
E	Thiophene	2	0,27	180	N_2 O_2(1%)	20	1,5

2.4 Plasma deposition of polythiophene
Mechanical properties

	Chemicals	**Pressure (bar)**	**Power (W/cm²)**	**Time (s)**	**Gas**	**Flow (sl/min)**	**Freq (kHz)**
1	Thiophene	2	0,13	180	N_2	20	1,5
2	Thiophene	2	0,27	180	N_2	20	1,5
3	Thiophene	2	0,13	180	N_2 O_2(1%)	20	1,5
4	Thiophene	2	0,27	180	N_2 O_2(1%)	20	1,5
5	Thiophene	2	0,18	180	He	20	1,5

2.4: plasma deposition of polythiophene: Kinetics

Chemicals	Pressure (bar)	Power (W/cm²)	Time (s)	Gas	Flow (sl/min)	Freq (kHz)
Thiophene	1	0,18	60	N_2	20	1,5
Thiophene	1	0,18	120	N_2	20	1,5
Thiophene	1	0,18	180	N_2	20	1,5
Thiophene	1	0,18	300	N_2	20	1,5
Thiophene	2	0,18	60	N_2	20	1,5
Thiophene	2	0,18	120	N_2	20	1,5
Thiophene	2	0,18	180	N_2	20	1,5
Thiophene	2	0,18	300	N_2	20	1,5
Thiophene	3	0,18	60	N_2	20	1,5
Thiophene	3	0,18	120	N_2	20	1,5
Thiophene	3	0,18	180	N_2	20	1,5
Thiophene	3	0,18	300	N_2	20	1,5
Thiophene	1	0,18	60	N_2 O_2(1%)	20	1,5
Thiophene	1	0,18	120	N_2 O_2(1%)	20	1,5
Thiophene	1	0,18	180	N_2 O_2(1%)	20	1,5
Thiophene	2	0,18	60	N_2 O_2(1%)	20	1,5
Thiophene	2	0,18	120	N_2 O_2(1%)	20	1,5
Thiophene	2	0,18	180	N_2 O_2(1%)	20	1,5
Thiophene	3	0,18	60	N_2 O_2(1%)	20	1,5
Thiophene	3	0,18	120	N_2 O_2(1%)	20	1,5
Thiophene	3	0,18	180	N_2 O_2(1%)	20	1,5

2.5 Plasma deposition of poly(3-methylthiophene) Chemical structure

	Chemicals	Pressure (bar)	Power (W/cm²)	Time (s)	Gas	Flow (sl/min)	Freq (kHz)
A	3-methylhiophene	2	0,13	180	N_2	20	1,5
B	3-methylhiophene	2	0,27	180	N_2	20	1,5
C	3-methylhiophene	2	0,27	180	N_2 O_2(1%)	20	1,5

2.5 Plasma deposition of poly(3-methylthiophene) Mechanical properties

	Chemicals	Pressure (bar)	Power (W/cm²)	Time (s)	Gas	Flow (sl/min)	Freq (kHz)
1	3-methylhiophene	2	0,13	180	N_2	20	1,5
2	3-methylhiophene	2	0,27	180	N_2	20	1,5
3	3-methylhiophene	2	0,13	180	N_2 O_2(1%)	20	1,5
4	3-methylhiophene	2	0,27	180	N_2 O_2(1%)	20	1,5
5	3-methylhiophene	2	0,18	180	He	20	1,5

2.6 Plasma deposition of PEDOT

Chemical structure

Chemicals	**Press**	**Power**	**Pulse (s)**		**Time**	**Gas**	**Flow**	**Freq**
	(bar)	**(W/cm²)**	**On**	**Off**	**(s)**		**(sl/min)**	**(kHz)**
EDOT	2	0,36	-	-	180	N_2	20	1,5
EDOT	2	0,27	-	-	120	N_2 O_2(1%)	10	1,5
EDOT	2	0,27	**10**	**10**	300	N_2 O_2(1%)	10	1,5
EDOT	2	0,27	**5**	**5**	300	N_2 O_2(1%)	10	1,5
EDOT	2	0,27	**2**	**2**	300	N_2 O_2(1%)	10	1,5
EDOT	2	0,27	**2**	**1**	300	N_2 O_2(1%)	10	1,5
EDOT	2	0,27	**1**	**2**	300	N_2 O_2(1%)	10	1,5
EDOT	2	0,27	**5**	**5**	300	N_2 N_2O(1%)	10	1,5

2.6 Plasma deposition of PEDOT

Homogeneous PEDOT layers

Chemicals	**Press**	**Power**	**Gas**	**Flow**	**Freq**	**Speed**	**Range**	**steps**
	bar	**W/cm²**		**sl/min**	**kHz**	**m/min**	**mm**	
EDOT (A)	2	0,39	N_2	15	1,5	4	560	24
EDOT (B)	2	0,39	N_2 N_2O(5%)	15	1,5	4	360	24
EDOT (C)	2	0,39	N_2 O_2(1%)	15	1,5	4	360	24
EDOT (D)	2	0,39	N_2 N_2O(5%)	15	1,5	2	360	24
EDOT (E)	2	0,39	N_2 O_2(1%)	15	1,5	2	360	24
EDOT	2	0,39	N_2 O_2(2%)	15	1,5	2	360	24
EDOT	2	0,39	N_2 **O_2(3%)**	15	1,5	2	360	24
EDOT	2	0,39	N_2 O_2(2%)	**30**	1,5	2	360	24
EDOT	2	**0,59**	N_2 O_2(2%)	15	1,5	2	360	24
EDOT	2	**0,59**	N_2 O_2(2%)	**30**	1,5	2	360	24
EDOT	**1**	0,39	N_2 O_2(2%)	15	1,5	2	360	24
EDOT	**3**	0,39	N_2 O_2(2%)	15	1,5	2	360	24

2.8 References

1 Y. P. Raizer, *Springer* **2001**, 1

2 B. Sari, M. Talu, *Turkish Journal of Chemistry* **1998**, 22, 301

3 M. Malta, E. R. Gonzalez, R. M. Torresi, *Polymer* **2002**, 43, 5895

4 B. C. Berry, A. U. Shaikh, T. Viswanathan, *Electroactive Polymers for Corrosion Control* **2003**, 843, 182

5 S. C. Yang, R. Brown, R. Racicot, Y. Lin, F. McClarnon, *Electroactive Polymers for Corrosion Control* **2003**, 843, 196

6 X. H. Wang, J. L. Lu, J. Li, X. B. Jing, F. S. Wang, *Electroactive Polymers for Corrosion Control* **2003**, 843, 254

7 T. Wang, Y. J. Tan, *Materials Science and Engineering: B Science and Technologies of Advanced Materials and Polymers for Defence and Aerospace Applications* **2006**, 132, 48

8 A. T. Ozyilmaz, M. Erbil, B. Yazici, *Thin Solid Films* **2006**, 496, 431

9 S. Yang, R. Brown, J. Sinko, *European coatings conference* **2005**,

10 A. Pielesz, A. Wlochowicz, *Spectrochimica Acta Part A: Molecular and Biomolecular Spectroscopy* **2001**, 57, 2637

11 Milton A J, A. P. Monkman, *Journal of Physics D: Applied Physics* **1993**, 26, 1468

12 J. Nowaczyk, W. Czerwinski, E. Olewnik, *Polymer Degradation and Stability* **2006**, 91, 2022

13 U. Kogelschatz, *HAKONE VII* **2000**, 1, 1

14 F. S. Denes, S. Manolache, *Progress in Polymer Science* **2004**, 29, 815

15 R. Mc. Neill, R. Studak, J. H. Wardlaw, D. E. Weiss, *Australian Journal of Chemistry* **1963**, 16, 1056

16 B. A. Bolto, D. E. Weiss, *Australian Journal of Chemistry* **1963**, 16, 1076

17 B. A. Bolto, R. Mc. Neill, D. E. Weiss, *Australian Journal of Chemistry* **1963**, 16, 1090

18 S. Sadki, P. Schottland, N. Brodie, G. Sabouraud, *Chemical Society Reviews* **2000**, 29, 283

19 J. Rodriguez, H.-J. Grande, T. F. Otero, *Handbook of organic conductive molecules and polymers volume 2: conductive polymers: synthesis and electrical properties* **1997**, 2, 415

20 A. Ramanavicius, A. Ramanaviciene, A. Malinauskas, *Electrochimica Acta ChargeTransfer at Electrochemical Interfaces "Two Hundred Years of Electrlysis"* **2006**, 51, 6025

21 A. Ramanaviciene, A. Ramanavicius, *Critical Reviews in Analytical Chemistry* **2002**, 32, 245

22 J. I. Martins, T. C. Reis, M. Bazzaoui, E. A. Bazzaoui, L. Martins, *Corrosion Science* **2004**, 46, 2361

23 M. A. L. Garcia, M. A. Smit, *Journal of Power Sources* **2006**, 158, 397

24 E. Geidel, F. Billes, *Journal of Molecular Structure: THEOCHEM* **2000**, 507, 75

25 R. Cabala, J. Skarda, K. Potje-Kamloth, *Physical Chemistry Chemical Physics* **2000**, 2, 3283

26 V. Meyer, *Ber. Dtsch. Chem. Ges.* **1883**, 16, 1465–1478

27 T. Yamamoto, K. Sanechika, A. Yamamoto, *Journal of Polymer Science Part C-Polymer Letters* **1980**, 18, 9

28 J. W. P. Lin, L. P. Dudek, *Journal of Polymer Science Part a-Polymer Chemistry* **1980**, 18, 2869

29 J. D. Stenger-Smith, *Progress in Polymer Science* **1998**, 23, 57

30 T. Tuken, B. Yazici, M. Erbil, *Progress in Organic Coatings* **2004**, 51, 205

31 C. Ocampo, E. Armelin, F. Liesa, C. Aleman, X. Ramis, J. I. Iribarren, *Progress in Organic Coatings* **2005**, 53, 217

32 S. Sindhu, K. Narasimha Rao, S. Ahuja, A. Kumar, E. S. R. Gopal, *Materials Science and Engineering: B* **2006**, 132, 39

33 B. L. Groenendaal, F. Jonas, D. Freitag, H. Pielartzik, J. R. Reynolds, *Advanced Materials* **2000**, 12, 481

34 K. Pasterny, R. Wrzalik, T. Kupka, G. Pasterna, *Journal of Molecular Structure* **2002**, 614, 297

35 C. A. Cutler, A. K. Burrell, D. L. Officer, C. O. Too, G. G. Wallace, *Synthetic Metals* **2002**, 128, 35

36 L. M. H. Groenewoud, G. H. M. Engbers, J. Feijen, *Langmuir* **2003**, 19, 1368

37 Y. A. Udum, K. Pekmez, A. Yildiz, *European Polymer Journal* **2004**, 40, 1057

38 P. Anderson, D. Nilsson, P. O. Svensson, M. Chen, A. Malmstrom, T. Remonen, T. Kugler, M. Berggren, *advanced materials* **2002**, 14, 1460

39 W. A. Daoud, J. H. Xin, Y. S. Szeto, *Sensors and Actuators B: Chemical* **2005**, 109, 329

40 Z. Kebede, S.-E. Lindquist, *Solar Energy Materials and Solar Cells* **1999**, 57, 259

Chapter 3

Plasma polymerization of in situ doped conjugated polymers at atmospheric pressure

3.1 Introduction

Plasma polymerization of conjugated polymers at atmospheric pressure results in depositions with many structural defects. To retain the typical properties of conjugated polymers in these plasma coatings, the number of defects should be decreased. A possibility to prevent these defects is the addition of an oxidant. The monomers discussed above all react in an oxidative reaction mechanism. This way, a second polycondensation pathway is available. Furthermore, the rate of the polymerization reaction would be higher, which could diminish the importance of the side reactions. The addition of an oxidant was already studied in the former chapter, with the addition of oxygen. Oxygen indeed increased the reaction rate, however it also reacts with the precursor to form stable carbonyl functions, increasing the number of defects. In this chapter, other oxidants than oxygen will be studied. Especially soft oxidants are used that do not have the potential to form new functionalities in the polymer structure.

Another advantage of this approach is the possibility for in-situ doping. Since conjugated polymers can be doped with oxidants, simultaneous injection of an oxidant and the precursor in the plasma could lead to the deposition of an in-situ doped conjugated polymer coating. This offers two major advantages:

- Homogeneous doping: When doping is done after coating deposition the dopant must diffuse into the coating. Doping degree will then be higher close to the surface than at the substrate interface (figure 3-1 A). In situ doping will equally distribute the dopant over the entire bulk of the coating (figure 3-1 B). The doping degree is therefore also higher[1].

- Stable doping: As the dopant must diffuse through the pores of the coating when doped after deposition, there are some restrictions on the dopant. Indeed, the dopant must be small enough to be able to diffuse through the pores. Of course, if the dopant is able to move inside the coating, the opposite motion is also possible, making the doping unstable. Now, when the coating is in situ doped, larger dopants can be used (figure 3-1 C), that are not able to diffuse out of the coating, resulting in more stable doping[2, 3].

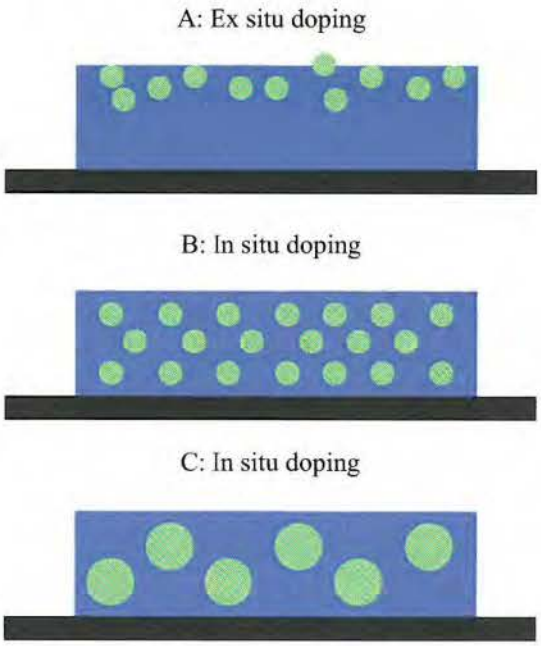

Figure 3-1: In contrast with ex situ doping (A), in situ doping results in a homogenous doping degree (B). When large dopants (C) are used, doping is also expected to be more stable.

This chapter will discuss the plasma polymerization of conjugated polymers, with simultaneous doping. Pyrrole and aniline were used as precursors.

3.2 Plasma polymerization of in situ doped polypyrrole

Doping of conjugated polymers is often done with the oxidant iodine[4-6]. Iodine has a relatively high vapor pressure and sublimates easily when heated slightly above room temperature. This way, conjugated polymers can be doped in iodine vapor without the need for any solvents. In its gas phase, iodine can easily be mixed with the plasma carrier gas, making it an interesting agent for in situ plasma doping. A possible disadvantage is the fact that iodine can also easily come out of the coating again, which results in unstable doping.

More stable doping can be achieved with larger oxidants, such as nitrosonium tetrafluoroborate ($NOBF_4$ - figure 3.2). When mixed with a conjugated polymer like polypyrrole, the very oxidative nitrosonium part will extract electrons from the polymer backbone, leaving a positive charge. The negatively charged tetrafluoroanion will associate with the positive charge on the polymer backbone[7]. This voluminous anion will not easily diffuse out of the coating resulting in a more stable doping level.

For the above mentioned reasons, both iodine and $NOBF_4$ are used for the plasma polymerization of in situ doped polypyrrole. Plasma depositions with these two dopants are compared in the next sections after discussing the dopant injection mechanism.

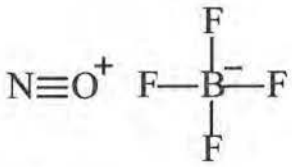

Figure 3-2: chemical structure of nitrosonium tetrafluoroborate ($NOBF_4$).

Injection of the dopant

Since pyrrole polymerizes when it is dissolved in an oxidant solution, it might also form a coating on the walls of the transportation tubes, due to condensation of monomer and oxidant aerosols. To prevent early reaction in the tubes of the plasma system, the injection channels of both precursor and oxidant are completely separated. The compounds are mixed just in front of the electrodes.

Iodine will be injected into the plasma as iodine gas. It is heated up to 60°C into a closed reservoir. Since iodine sublimates at this temperature, it's vapor can easily be mixed with the carrier gas stream.

$NOBF_4$ is a salt and therefore more difficult to inject. It has to be dissolved first. Therefore, 5% solutions were made in ethanol and injected into the plasma by means of an aerosol generator.

In situ doped plasma polypyrrole: chemical structure

The aim of the work described in this chapter was to decrease the structural defects in plasma polymerized polypyrrole coatings. Therefore, the influence of co-injection of an oxidant during plasma deposition is studied. The addition of iodine or $NOBF_4$ to the carrier gas is compared with plasma pyrrole polymerization, without additives. It is expected that the addition of an oxidant will have an influence on the deposition rate, as pyrrole is known to polymerize in contact with such oxidants[8-10]. Figure 3-3 confirms that the deposition is faster in the presence of iodine or $NOBF_4$.

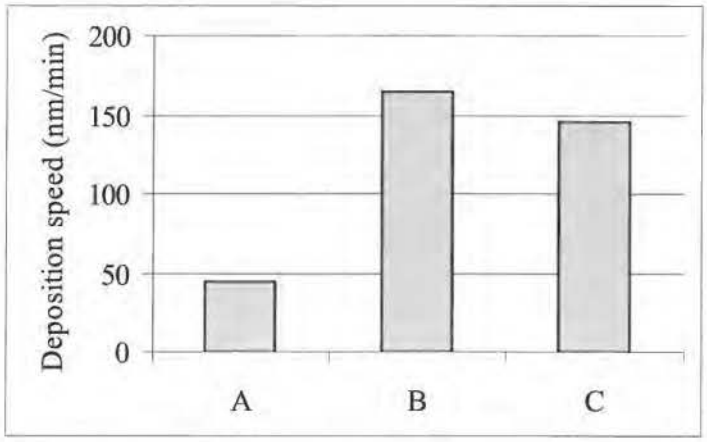

Figure 3-3: Deposition rate for plasma polymerized polypyrrole, with simultaneous injection of: A) no dopant, B) iodine, C) $NOBF_4$.

The influence of the different oxidants on the chemical structure of plasma polypyrrole is studied with infrared spectroscopy. The spectra are presented in figure 3-4. A detailed peak assignment is shown in table 3-1.

In section 2.3 plasma polymerization of polypyrrole without addition of an oxidant (or dopant) was already described. This resulted in many structural defects such as saturated bonds (2900 cm^{-1}), triple bonds (2200 cm^{-1}) and carbonyl functions (1700 cm^{-1}). When iodine is added to the plasma carrier gas, the same structural defects are present, although the intensity of the C-H stretch on saturated carbons has decreased. At 1775 cm^{-1} a carbonyl stretching band is found, which was not present in plasma polypyrrole polymerized without dopant. It can be assigned to an acid iodide, which means that iodine has also bonded chemically (when used as a dopant, iodine forms I_3^-). It is clear that the addition of the oxidant iodine to the carrier gas still results in a plasma polymer with many structural defects.

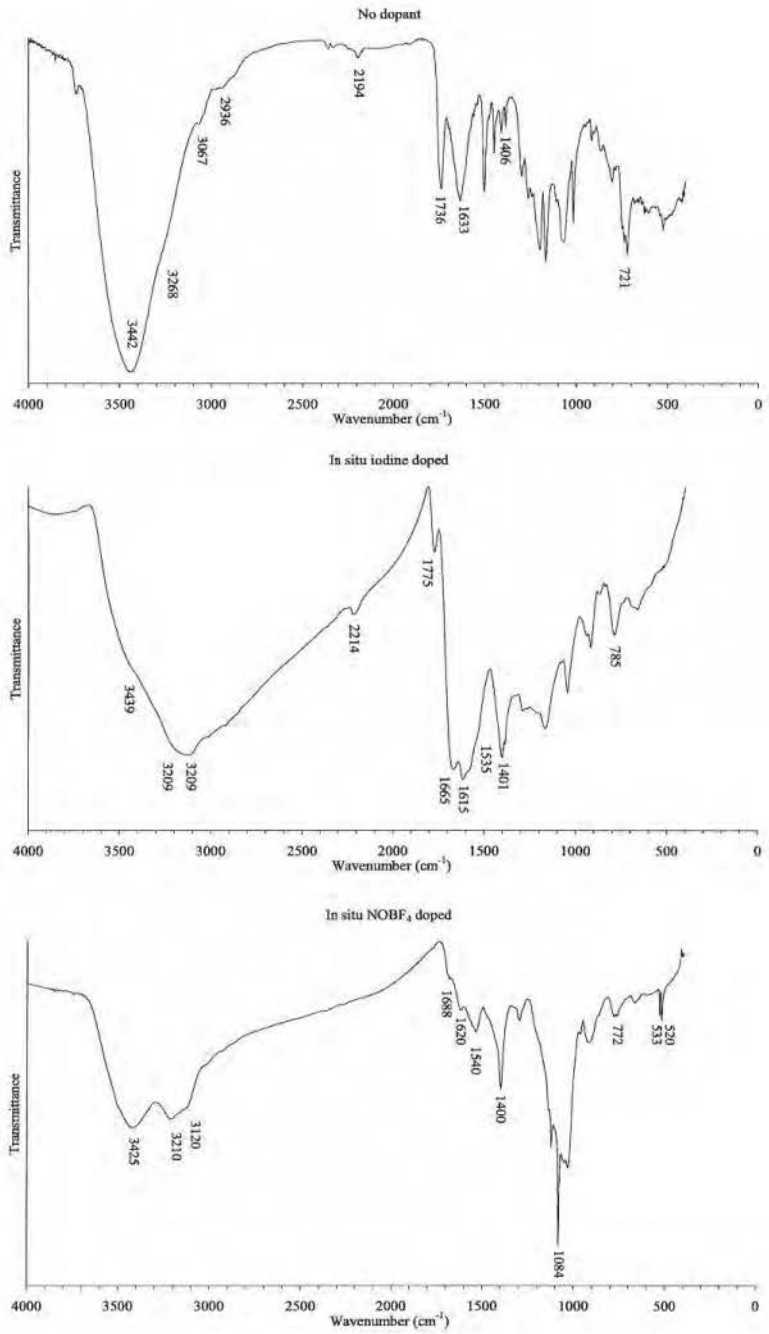

Figure 3-4: Infrared spectra of plasma polymerized polypyrrole, with simultaneous addition of no dopant, iodine or $NOBF_4$.

Vibration	Wabenumber (cm^{-1}) no dopant	Wavenumber (cm^{-1}) iodine doped	Wavenumber (cm^{-1}) $NOBF_4$ doped
Amine N-H stretch	3442	3439	3425
Amide N-H stretch	3268	3209	3210
=C-H stretch	3037 3067	3008 3120	3008 3120
-C-H stretch	2936	2917	2923
C≡C or C≡N stretch	2194	2214	-
acid iodide C=O stretch	-	1775	-
amide C=O stretch	1682	1665	1688
amide C=O stretch (conj.)	1633	1615	1620
N-H bend	1559	1535	1540
C=C/C=N stretch	1406	1401	1400
B-F stretch	-	-	1299 1126 1084 1034
C-H in plane bend	1167	1164	overlap
C-N stretch	1070	1043	overlap
C-H out of plane bend	721 736 747	915 785 660	916 772 669
B-F bend	-	-	520 533

Table 3-1: Detailed peak assignment for the infrared spectra of undoped plasma polypyrrole and in situ doped with iodine or $NOBF_4$.

Finally, the even stronger oxidant $NOBF_4$ was added to the plasma carrier gas. Plasma polymerization of polypyrrole then results in a completely different infrared spectrum. Triple bonds (2200 cm^{-1}) are not seen. Peaks around 1700 cm^{-1} are small, indicating that only a small amount of carbonyl functions has been built in. Also the C-H stretch on saturated bonds has decreased. An intense absorption around 1400 cm^{-1} shows retention of the aromatic pyrrole ring. The doublet at 520 and 533 cm^{-1} and the multiplet around 1084 cm^{-1} originate from the BF_4^- anion. Indeed, when $NOBF_4$ oxidizes polypyrrole, the

NO^+ part of the salt is reduced, while the BF_4^- anion stays in the coating to act as the counter ion for the positive charges created in the polymer chain. Because boron exist as two different isotopes, the B-F stretching band around 1084 cm^{-1} split up in a complex multiplet[11].

The infrared spectra show that plasma polymerization of polypyrrole with simultaneous $NOBF_4$ doping, results in a doped conjugated polymer with less structural defects. The structural formula as well as the doping degree, can be calculated from XPS data. A comparison between the iodine doped and $NOBF_4$ doped plasma polypyrrole is made in table 3-2, which presents the composition and the structural formula of these coatings.

Oxidant	%C	%N	%O	%B	%F	%I	Structural formula
Iodine	74	13	9	-	-	4	$C_4N_{0,8}O_{0,5}I_{0,3}$
$NOBF_4$	32	13	5	11	39	-	$C_4N_{1,6}O_{0,6}\,(BF_{3,6})_{1,4}$

Table 3-2: Composition and structural formula, calculated from XPS spectra, for in situ iodine and $NOBF_4$ doped plasma polypyrrole.

While the structural formula of pyrrole is C_4N, in situ iodine doped plasma polypyrrole shows a higher carbon/nitrogen ratio. This means that elimination of nitrogen functionalities has occurred, which is only possible by breaking the aromatic heterocycle. There's also a high amount of oxygen present in the coating. This confirms the results obtained from infrared spectroscopy. Carbonyl functions are formed by reaction with traces of oxygen in the plasma reactor during plasma treatment or with the oxygen in the environmental air after plasma treatment. The iodine content in the coating is rather low. Regarding that all the incorporated iodine is in the I_3^- form and thus acts as a counter ion for the charges injected in the polymer backbone, there would only be 1 charge for 10 monomer units. One must keep in mind, however that a lot of the iodine amount might have got lost in the vacuum chamber of the XPS spectrometer. The iodine content measured, is probably mainly chemically bonded.

In contrast with the in situ iodine doped plasma polypyrrole coatings, the $NOBF_4$ doped coatings have a high nitrogen content. Also the oxygen content

is high, although the infrared spectrum shows that only few carbonyl functions are formed. These high oxygen and nitrogen contents might originate from the dopant. Indeed, the dopant also contains nitrogen and oxygen in its chemical structure. When $NOBF_4$ is used as an oxidant, it is the NO^+ part that acts as the oxidizing agent. NO^+ extracts an electron from the polypyrrole chain, forming NO, which is not expected to further react with the coating. The BF_4^- cation will stay in the coating as the counter ion for the injected charges. Since the NO function is also found in the coating, there must also be unreacted $NOBF_4$ present in the coating. Part of the $NOBF_4$ might be incorporated in the plasma deposition as crystallites, when the solvent evaporates. Assuming that all the oxygen present comes from these crystals, the real structural formula of the plasma deposited polypyrrole coating would be $C_4N(BF_{3,6})_{0,8}$. The carbon/nitrogen ratio is four, which means that nitrogen elimination has not occurred. The estimated doping degree is 0,8 charges per monomer unit. However, the fluor content is lower than expected. Boron and fluor are thus not only incorporated into the coating as BF_4^-. The doping degree might therefore be overestimated.

Properties

Section 2.3 already showed that plasma polymerization of polypyrrole without dopant addition, results in yellow brown coatings. They absorb light close to the UV range, indicating that there is only little conjugation. Addition of iodine to the carrier gas during plasma polymerization results in green coatings, which is the typical color for undoped polypyrrole. In situ $NOBF_4$ doping produces black coatings, that are typical for doped polypyrrole. The absorption spectra of all these plasma polypyrrole coatings are presented in figure 3-5.

The iodine doped polymer shows two new absorption peaks besides the one close to the UV range. The peak at 350 nm, probably comes form the I_3^- anion. I_3^- has two absorption peaks, at 290 (possible overlap with polypyrrole absorption) and 350 nm[12]. Another small absorption is seen at 650 nm, which might come from a small portion of doped polypyrrole.

When $NOBF_4$ is used as in situ doping agent, the absorption behavior completely changes. This time, a broad absorption over the entire visual range is seen, with peaks at 500 and 600 nm. The decrease in structural defects results in longer conjugation lengths. Longer conjugation results in a decrease of the energy gap between the valence and conduction band. The absorption maximum then shifts to higher wavelengths. Several absorption maxima might be seen because doping results in the formation of polarons and bipolarons, decreasing the energy gap even more[13, 14].

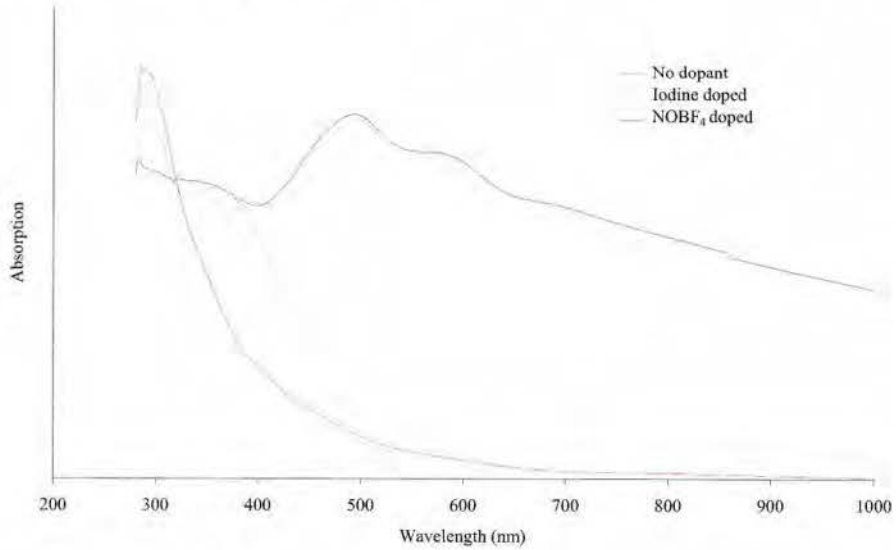

Figure 3-5: UV/VIS absorption of plasma polymerized polypyrrole, with no dopant addition and with in situ iodine or $NOBF_4$ doping.

Creation of charges on the polymer backbone by doping agents makes the conjugated polymers (semi-) conductive. Conductivity is therefore also expected for the in situ doped plasma polymers. The measured specific conductivities for in situ doped plasma polypyrrole are presented in table 3-3.

	Dopant	Conductivity (S/cm)	Thickness (nm)
1	Iodine	$< 1 \times 10^{-5}$	327
2	$NOBF_4$	$3{,}6 \times 10^{-3}$	290
3	$NOBF_4$	$1{,}8 \times 10^{-2}$	320

Table 3-3: Conductivity and coating thickness of in situ doped plasma polypyrrole.

In situ iodine doped plasma polypyrrole doesn't show significant conductivity. The high amount of structural defects interrupts the conjugated system, which results in a decreased conductivity. Specific conductivities up to $1{,}8 \times 10^{-2}$ S/cm are measured for in situ $NOBF_4$ doped plasma polypyrrole. The lower amount of structural defects results in an extended conjugation. After injection of charges in this conjugated system, the polypyrrole film becomes conductive. Experiments 2 and 3 in table 3-3 are done under the same conditions. Only the position on the electrode was different. The conductivity of experiment 3, however, is 5 times higher. This is a clear indication that the deposited coatings are not homogeneous. There's also a slight difference in the thickness. Furthermore, a color gradient can be seen. The coating is black close to the gas inlet and in the centre of the electrode. Everywhere else, the coating is yellow-brown. This means that there is an inhomogeneity in both the y (width of electrode) and x (length of electrode) direction. The inhomogeneity in the y direction is caused by a bad mixing of the precursor and the dopant. With the current injection system, the dopant concentration is higher in the centre than at the edges. To solve this problem modeling is necessary to adjust the injection equipment. The inhomogeneity in the x-direction is due to an efficient incorporation of the dopant into the coating. Therefore the dopant concentration is highest close to the gas inlet, and decreases further away from this inlet. At a certain point, the $NOBF_4$ concentration is too low to produce the desired black coating.

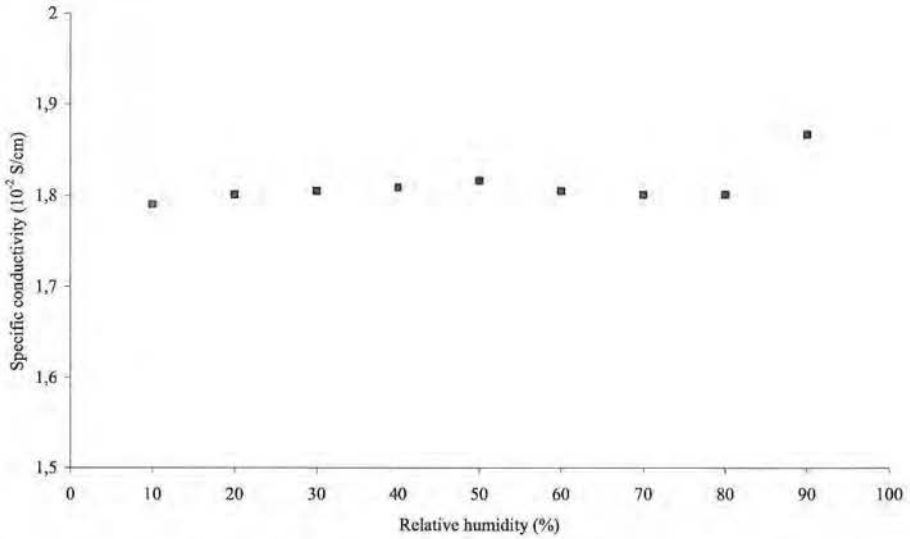

Figure 3-6: Dependence of the specific conductivity of in situ $NOBF_4$ doped plasma polypyrrole on the relative humidity.

Conductivity of iodine doped plasma polythiophene and plasma PEDOT were dependent on the relative humidity of the environmental air, as was already discussed in sections 2.4 and 2.6. Figure 3-6 shows the dependence of the conductivity of the $NOBF_4$ doped plasma polypyrrole films on the relative humidity. The conductivity of these coatings was constant over the entire humidity range. Only at very high humidity, a small increase can be measured, probably due to condensation of water on the coating surface. In contrast with plasma polythiophene and derivatives, only few carbonyl functions are built into the in situ $NOBF_4$ doped polypyrrole layers. Therefore, the coating has less affinity for water, decreasing its tendency to absorb water from the environment. Furthermore, the conjugation is responsible for the measured conductivity, which is not as dependent on the water absorption than ionic conductivity.

The advantage of in situ doping is that a more stable doping can be achieved when dopants with voluminous counter ions are used. The BF_4^- anion, that is incorporated in the coating when $NOBF_4$ is the oxidant, is already more voluminous than I_3^-. A more stable doping is thus expected. Figure 3-7 presents the aging of the conductivity of in situ $NOBF_4$ doped polypyrrole under ambient conditions. The normalized conductivity is presented as a function of time. This normalized conductivity is the ratio of the conductivity after a certain time (σ_t) and the initial conductivity (σ_0):

Normalized conductivity = σ_t/σ_0

After 25 days the conductivity of the $NOBF_4$ doped plasma polypyrrole coatings has been reduced to about 20% of the initial value. This result can be compared with electrochemically synthesized and in situ doped polypyrrole/BF_4^- coatings[7]. The decrease in conductivity is mainly caused by reaction of the polymer backbone with oxygen and water and also with the dopant anion[15].

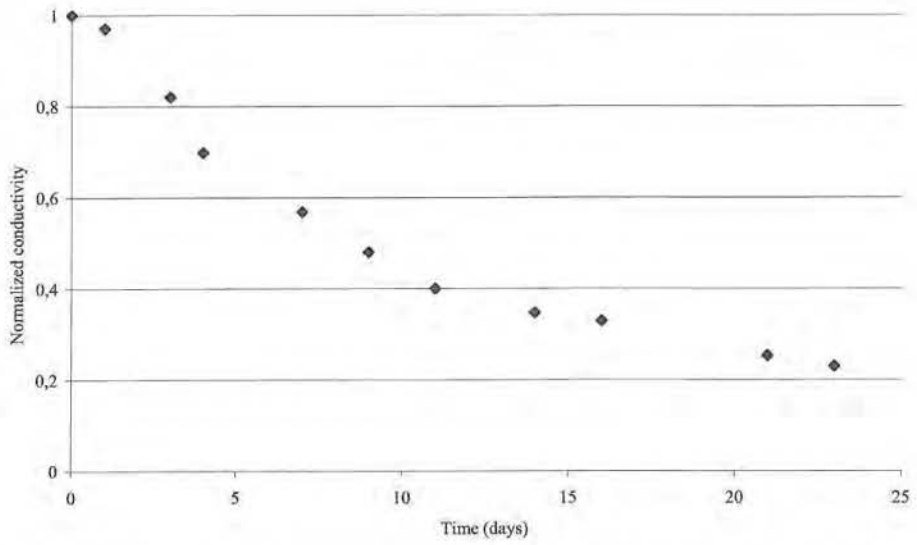

Figure 3-7: Aging under ambient conditions of the conductivity of in situ $NOBF_4$ doped, plasma polymerized polypyrrole.

Conclusions

Plasma polymerization at atmospheric pressure of polypyrrole with simultaneous addition of iodine, didn't lead to in situ doped polypyrrole coatings. The obtained film contained a lot of structural defects and the iodine content in the coating was rather low. Because the conjugation was partially destroyed, no conductivity was measured. Better results were obtained when $NOBF_4$ was added to the plasma carrier gas. A black film was deposited, which means that light over the entire visual range is absorbed. Conductivities up to $1{,}8 \times 10^{-2}$ S/cm could be reached. These are all indications that the conjugated system was significantly extended during plasma polymerization and that doping has occurred. One issue is still a problem, however. In situ doped plasma polypyrrole coatings are quite inhomogeneous, both on the width and the length of the electrode. These problems might be solved by using a DBD system that moves over the length of the samples and by developing a new injection system.

3.3 Plasma polymerization of in situ doped polyaniline

While most conjugated polymers are doped by using oxidants or reductants, polyaniline is doped with acids. The amine groups of polyaniline are protonated by acids. This way, these amine groups are positively charged. The charges can move along the polymer backbone, because of the different resonance forms of the conjugated system. The anions of the acids are incorporated in the conjugated polymer coating as counter ions.

However, polyaniline, can not be acid doped when it is in its completely reduced leucoemeraldine form. It has to be oxidized, first. When polymerized with an oxidant, polyaniline is usually already in its semi-oxidized emeraldine base form. Plasma polymerization of polyaniline, however, did not lead to this emeraldine base form. Since plasma polymerization of pyrrole could be enhanced by the addition of an oxidant, the same approach is studied for aniline. Ammonium persulfate (APS - figure 3-8) is often used as an oxidant

for chemical synthesis of polyaniline[16-18]. Any acid could in principle be used for doping, but hydrochloric acid is chosen here.

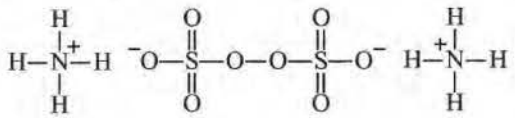

Figure 3-8: Chemical structure of ammonium persulfate (APS).

In situ doped plasma polyaniline: chemical structure

As aniline polymerization should result in blue or green coatings, the color of the deposited coatings can be used as a first evaluation method. The yellow-brown color of plasma polyaniline deposited without the presence of an oxidant or acid, indicates that no (extended) conjugated system has formed. The influence of the addition of aqueous solutions of an oxidant or an acid is studied here. The resulting coating color is presented in table 3-4. Addition of the oxidant APS still results in yellow brown coatings. Also the injection of the acid hydrogen chloride has the same effect. When both the acid and the oxidant are injected simultaneously, a green colored coating can be obtained, which is a typical color for polyaniline emeraldine salt. Consequently, besides the oxidant, it is necessary to add an acid. When polyaniline is polymerized in a solvent, an acidic environment is also used to protonate the aniline monomer, which increases its reactivity[19].

	Oxidant	Dopant	Color
A	-	-	yellow-brown
B	APS	-	yellow-brown
C	-	HCl	yellow-brown
D	APS	HCl	green

Table 3-4: The color of plasma polymerized polyaniline coatings with simultaneous addition of an oxidant and/or a dopant.

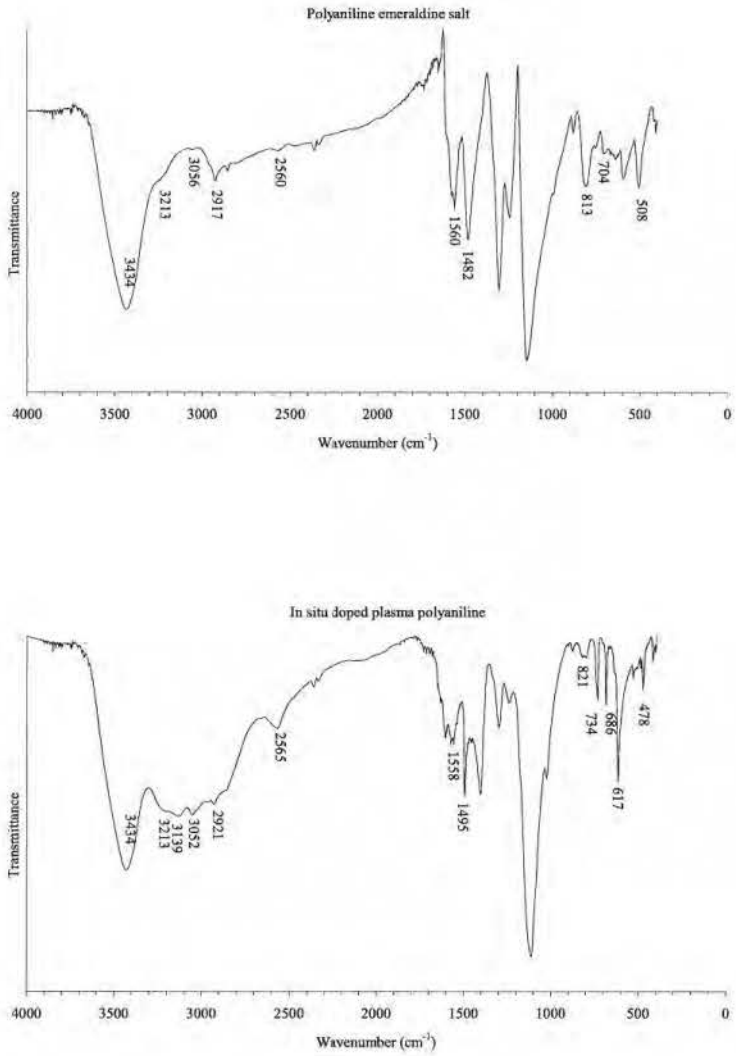

Figure 3-9: Infrared spectrum of polyaniniline emeraldine salt and of in situ HCl doped plasma polyaniline.

Vibration	Wavenumber (cm^{-1}) Polyaniline emeraldine salt	Wavenumber (cm^{-1}) Doped plasma polyaniline
N-H stretch amine	3434	3434
N-H stretch hydrogen bonded amine	3213	3213
C-H stretch on double bond	3056	3052 3139
C-H stretch on saturated bond	2847 2917	2847 2921
NH^+ stretch	2560	2556
C=C stretch benzene ring	1482 1560 1573 1604	1495 1558 1573 1606
C-N stretch aromatic amine	1304	1300
C-H in plane bends	950-1200	950-1200
C-H out of plane bend para disubstituted benzene	813	821
C-H out of plane bend mono substituted benzene	704 747	686 734
C-Cl stretch	-	617
Ring deformation	508	478

Table 3-5: Detailed peak assignment for chemically polymerized polyaniline emeraldine salt and plasma polymerized in situ doped polyaniline.

The chemical structure of in situ doped plasma polyaniline can be studied with infrared spectroscopy. As a reference, a commercial emeraldine base polyaniline was doped with an aqueous hygrogen chloride solution. The infrared spectrum of the so formed emeraldine salt, as well as the in situ doped plasma polymerized polyaniline spectrum, are shown in figure 3-9. A detailed peak assignment is presented in table 3-5.

When emeraldine base polyaniline is doped, the infrared spectrum looks somewhat different (figure 2-5). The N-H stretching band (3434 cm^{-1}) increases in intensity, because of protonation by the acid. The presence of the chlorine anion splits the benzene C=C stretching band at 1560 cm^{-1} up in several peaks.

Also, some sp^3 hybridized C-H stretches around 2917 cm^{-1} are seen, indicating that some double bonds might have got lost during addition reactions.
In situ hydrogen chloride doped plasma polymerized polyaniline shows a similar infrared spectrum. The aromatic stretching band at 1558 cm^{-1} again splits up in several peaks. Some differences might be seen, however. The peak at 2565 cm^{-1}, resulting from positively charged N-H stretches has a higher intensity, indicating a higher charge density on the polymer chains. Absorptions at 686 and 734 cm^{-1} result from monosubstituted benzene rings. Since di-substitution is expected for polyaniline, the polymers must have low molecular weight or have reacted in an unconventional way. The absorption peak around 617 cm^{-1} might come form C-Cl stretches. The presence of chlorine functions on the aromatic benzene ring increases the intensity of the C-H in plane vibrations (1117 cm^{-1}) significantly. This phenomenon is also seen in the commercial polyaniline salt. It might also influence the C-H out of plane vibrations.

Properties

Plasma deposition of polyaniline in the presence of APS and HCl, results in green coatings. The absorption of light in the visual range is responsible for the observed color. As presented in figure 3-10, this in situ doped plasma polyaniline (B) indeed has absorption maxima that are red-shifted, compared to plasma polyaniline without additives (A). The absorption close to the UV-range has broadened up to 450 nm. Furthermore, a second absorption maximum, at 850 nm is seen, which comes from charges on the polymer chain that form polarons and bipolarons. These polarons and bipolarons, decrease the bandgap of the polymer, resulting in the observed red shift[20, 21].
After immersing the in situ doped plasma polyaniline coating in water for 24 hours, the color of the coating turns blue. In PH neutral water, doped polyaniline is easily deprotonated because the chlorine counter ions are not very voluminous and diffuse out of the coating. This means that the coating is dedoped. The plasma polyaniline is now in it's emeraldine base form. In the UV/VIS spectrum, this dedoping can be seen as a blue shift of the absorption

maxima. Dedoping increases the energy gap again, shifting the absorption maximum to shorter wavelengths (C). For more stable doping, more voluminous or insoluble dopants should be used.

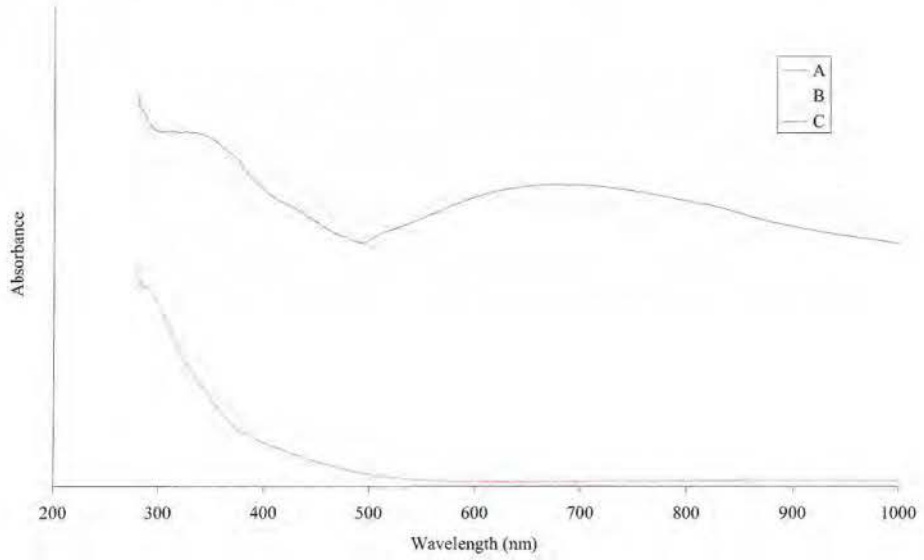

Figure 3-10: UV/VIS absorption of (A) plasma polyaniline without additives, (B) in situ HCl doped plasma polyaniline, (C) in situ doped plasma polyaniline after 24h immersion in water.

The conductivity of in situ doped plasma polyaniline coatings is presented in figure 3-11. When polymerized in a continuous power mode, a conductivity of 0,5 S/cm was measured (in dry nitrogen atmosphere) which was nearly independent of the ambient humidity.

The in situ HCl doped plasma polyaniline thus show the expected green color and a conductivity in the semiconductor range. However, the homogeneity is still a problem. As was already seen with in situ doped plasma polypyrrole, only a small part of the electrode area is really covered with the green coating. The green coating (a few square centimeter) is seen close to the gas inlet, in the centre. The area coated with green polyaniline can be slightly increased by using the pulsed power mode. The plasma is than sequentially turned on and off for 5s. This allows precursor and dopant to mix more efficiently during the

plasma off times. However, conductivity decreases 7 times and also the deposition rate is 4 times slower, as is presented in table 3-6. When precursor and dopant are better mixed, local high concentrations of dopant and oxidant are no longer present, which results in lower deposition rate and doping degree. Variation of the pulse length did not improve the performance either.

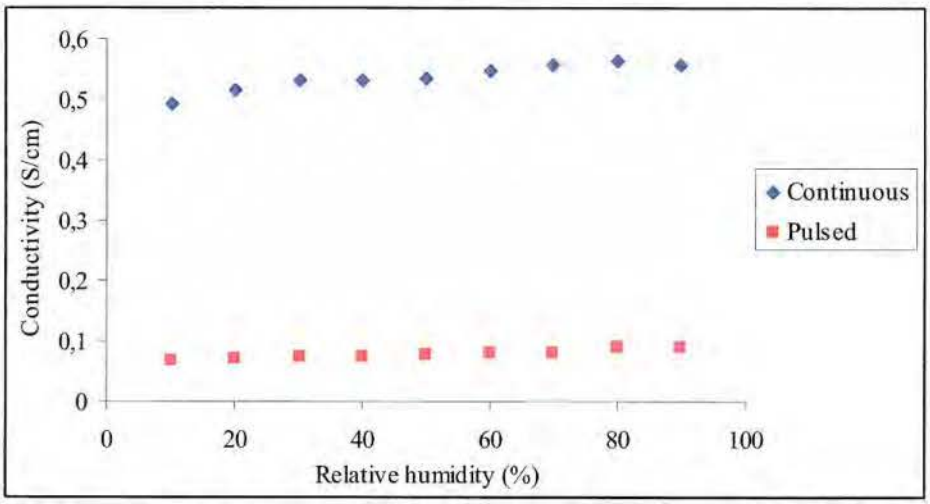

Figure 3-11: Conductivity as a function of relative humidity for in situ HCl doped polyaniline, plasma polymerized in a continuous or pulsed (5s on - 5s off) power mode.

	Power mode	Conductivity S/cm	Deposition rate nm/min
1	continuous	$4{,}9 \times 10^{-1}$	610
2	pulsed	$6{,}9 \times 10^{-2}$	143

Table 3-6: Conductivity and deposition rate for in situ HCl doped polyaniline, plasma polymerized in a continuous and pulsed (5s on, 5s off) power mode.

The stability of the conductivity of in situ HCl doped plasma polyaniline is presented in table 3-7. After 120 days, the conductivity has decreased 40%. This is a better result than the one obtained for polypyrrole, because polyaniline is not that sensitive for oxidative degradation. If plasma polymerization is done in the pulsed power mode, conductivity has decreased

49% after 120 days. The conductivity probably ages a little bit faster in this case because the coatings are thinner[22].

	Power mode	Conductivity (S/cm)		Loss
		No aging	120 days aging	
1	Continuous	$4{,}9 \times 10^{-1}$	$2{,}92 \times 10^{-1}$	40%
2	Pulsed	$6{,}9 \times 10^{-2}$	$3{,}54 \times 10^{-2}$	49%

Table 3-7: Conductivity loss for in situ HCl doped plasma polyaniline after aging for 120 days in air.

Conlcusions

Plasma polymerization of aniline at atmospheric pressure, with simultaneous addition of an oxidant (APS), did not result in polyaniline. When besides the oxidant also an acid dopant (HCl) is added to the carrier gas, a green coating is achieved which is indicative for polyaniline emeraldine salt. Conductivities up to 0,5 S/cm could be obtained this way. However, the homogeneity of the coatings is still a major issue. Green coating deposition is only seen in the front centre of the electrode. Plasma polymerization in a pulsed power mode results in slight improvement, although conductivity and deposition rate are negatively influenced. In order to use these coatings in applications, a more homogeneous injection of the dopant and oxidant is necessary.

3.4 Experimental part

Characterization methods

The thickness of the plasma deposited coatings was measured with an UBC 14 profilometer of UBM, using the diamond probe.

The composition of the plasma deposited coatings was studied with an x-ray photoelectron spectrometer (XPS) from Thermo with a theta probe. Monochromatic soft X-rays of Al Kα at 1486.6 eV were used to irradiate the coatings deposited on glass substrates. Spectra were obtained at 100 W with a spot size of 400 μm. To determine the elemental composition of each surface, survey spectra were recorded at 300 eV pass energy and 1 eV step size. To compensate for the charging of non-conductive polymers, an argon flood gun was used at 6 eV and 25 μA emission. The photoelectron spectral peak areas were scaled to deal with instrument sensitivity and ionization probabilities affording surface concentrations in atom percent.

The chemical structure of the plasma deposited coatings was studied with a Nexus Fourier transformed infrared spectrometer from Thermo. The samples were prepared by scraping off the coating from the glass substrate, mixing it with potassium bromide and pressing it into a pellet. The potassium bromide (99+, FTIR grade) was purchased from Sigma Aldrich and used after drying at 120°C.

The absorption of UV and visual light by the plasma deposited coatings was measured on coatings, deposited on glass slides with a Lambda 900 UV/VIS/NIR spectrometer from Perkin Elmer.

The conductivity of the plasma deposited coatings was calculated from their resistance. Two silver electrodes were coated onto the coating surface with silver paste. The resistance of the coating was measured under a nitrogen atmosphere with a Fluke 189 True RMS multimeter. Specific conductivity was calculated from these resistance measurements. The influence of the humidity on the conductivity was tested in a humidity chamber. The humidity is adjusted by a nitrogen flow that has passed through water.

Chemicals

All chemicals were used without further purification. The following chemicals are used in this chapter: pyrrole (98%, Sigma Aldrich), iodine (99,8%, ACS reagent, Sigma Aldrich), nitrosonium tetrafluoroborate (98%, Fluka), ethanol (PA, >99,9%, Merck), aniline (99%, Sigma Aldrich), hydrogen chloride (PA, 37%, Merck), polyaniline (Mw: 10000 g/mol, Sigma Aldrich).

Plasma reactor

The plasma is generated with a dielectric barrier discharge between two horizontally placed electrodes. The lower electrode is covered by a glass dielectric of 5 mm thickness, while the upper electrode is uncovered. A high ac voltage is used on the lower electrode, which has an area of 560 cm^2 (21,5 x 26 cm). Power is supplied by a G10 S-V AFS generator, that is carefully tuned for the used frequency and the specific electrode configuration, in order to minimize power losses. The upper electrode is grounded. The gap between the glass dielectric and the uncovered electrode is 2 mm. The gas flow rate is controlled with an MKS mass flow controller. The precursors are injected into the plasma as an aerosol, generated with a TSI constant output atomizer type 3076. Before entering the plasma the aerosol is mixed with the carrier gas, which is used to transport the aerosol towards the plasma. Additional reagents are injected by a second aerosol generator and mixed just in front of the plasma zone. The coatings where deposited onto glass substrates which were placed onto the dielectric.

Plasma parameters

All plasma parameters used, are presented in the tables below. The different parameters shown are:

- **Chemicals**: the precursors or precursor solutions that are injected into the plasma as an aerosol
- **Press**: the gas pressure used to generate the aerosols
- **Power**: the power per square cm, used on the high voltage electrode
- **Time**: the total reaction time
- **Gas**: the gasses used to create the plasma and their concentration

- **Flow**: the total gas flow rate in standard liters per minute
- **Freq**: the high voltage frequency
- **Pulse**: The on and off times of the plasma, when the power is applied in the block wave pulsed mode.

3.2 Plasma polymerization of in situ doped polypyrrole

	Chemicals	Press (bar)	Power (W/cm²)	Time (s)	Gas	Flow (sl/min)	Freq (kHz)
A	Pyrrole	2	0,13	180	N_2	20	1,5
B	Pyrrole	2	0,18	120	N_2	10	1,5
	Iodine (60°C)	2					
C	Pyrrole	2	0,18	120	N_2	10	1,5
	$NOBF_4$ (5%) in ethanol	2					

3.3 Plasma polymerization of in situ doped polyaniline

	Chemicals	Press	Power	Pulse (s)		Time	Gas	Flow	Freq
		bar	W/cm²	on	off	s		sl/min	kHz
A	Aniline	2	0,13	-	-	180	N_2	20	1,5
B	Aniline	2	0,18	-	-	180	N_2	10	1,5
	APS (aq) (5%)	3							
C	Aniline	2	0,18	-	-	180	N_2	10	1,5
	HCl (aq) (5%)	3							
D	Aniline	2	0,18	-	-	180	N_2	10	1,5
	APS (5%) + HCl (5%) (aq)	3							
E	Aniline	2	0,18	5	5	600	N_2	10	1,5
	APS (5%) + HCl (5%) (aq)	3							

3.5 References

1 M. E. Leyva, G. M. O. Barra, B. G. Soares, *Synthetic Metals* **2001**, 123, 443

2 S. Yang, R. Brown, J. Sinko, *European coatings conference* **2005**,

3 K. S. Jang, H. Lee, B. Moon, *Synthetic Metals* **2004**, 143, 289

4 J. W. Jang, K. W. Lee, C. E. Lee, *Solid State Communications* **2004**, 131, 697

5 M. G. Olayo, G. J. Cruz, E. Ordonez, J. Morales, R. Olayo, *Polymer* **2004**, 45, 3565

6 S. L. Shenoy, D. Cohen, R. A. Weiss, C. Erkey, *The Journal of Supercritical Fluids* **2004**, 28, 233

7 M. Brie, R. Turcu, A. Mihut, *Materials Chemistry and Physics* **1997**, 49, 174

8 G. S. Gohil, V. V. Binsu, V. K. Shahi, *Journal of Membrane Science* **2006**, 280, 210

9 M. Omastova, M. Trchova, J. Pionteck, J. Prokes, J. Stejskal, *Synthetic Metals* **2004**, 143, 153

10 R. Ansari, N. K. Fahim, *Reactive and Functional Polymers* **2007**, 67, 367

11 O. Czupinski, R. Jakubas, A. Pietraszko, *Journal of Molecular Structure* **2004**, 704, 177

12 Z. Kebede, S.-E. Lindquist, *Solar Energy Materials and Solar Cells* **1999**, 57, 259

13 M. C. Henry, C. C. Hsueh, B. P. Timko, M. S. Freund, *Journal of the Electrochemical Society* **2001**, 148, D155

14 H. Shigi, M. Kishimoto, H. Yakabe, B. Deore, T. Nagaoka, *Analytical Sciences* **2002**, 18, 41

15 A. Kaynak, L. Rintoul, G. A. George, *Materials Research Bulletin* **2000**, 35, 813

16 T. K. Rout, G. Jha, A. K. Singh, N. Bandyopadhyay, O. N. Mohanty, *Surface and Coatings Technology* **2003**, 167, 16

17 S. Jain, S. Chakane, A. B. Samui, V. N. Krishnamurthy, S. V. Bhoraskar, *Sensors and Actuators B-Chemical* **2003**, 96, 124

18 R. M. Torresi, S. d. Souza, J. E. P. d. Silva, S. I. C. d. Torresi, *Electrochimica Acta* **2005**, 50, 2213

19 C. Jeyaprabha, S. Sathiyanarayanan, G. Venkatachari, *Applied Surface Science* **2006**, In Press, Corrected Proof,

20 B. Wessling, *Synthetic Metals* **1998**, 93, 143

21 M. Malta, E. R. Gonzalez, R. M. Torresi, *Polymer* **2002**, 43, 5895

22 M. Trchova, I. Sedenkova, E. Tobolkova, J. Stejskal, *Polymer Degradation and Stability* **2004**, 86, 179

Chapter 4

Plasma polymerized conjugated polymers for corrosion protection of metals

4.1 Introduction

Corrosion is the destructive oxidation of a metal by chemical reactions with its environment. It is a major concern for metal parts used in manufactured products in terms of aesthetics, safety and functionality. The U.S. Federal Highway Administration, recently released a 2 year study on the direct costs associated with metallic corrosion[1]. Between 1999 and 2001, the total annual estimated direct cost of corrosion in the United states is 276 billion dollar, approximately 3.1% of the nation's Gross Domestic Product. This is approximately 970 dollar per person per year. There's no doubt, that improved corrosion protection can have an enormous economical impact.
Corrosion is influenced by a lot of factors[2]. A fundamental requirement for corrosion is the presence of a thin film of electrolyte that can form on metallic surfaces when exposed to a critical level of humidity. A first important factor is thus the relative humidity. In the presence of such thin electrolyte films, corrosion proceeds by balanced anodic an cathodic reactions (figure 4-1). The anodic oxidation reaction involves the corrosion attack of the metal, while the cathodic reaction is usually oxygen reduction.

Anode reaction: $2\ Fe \rightarrow 2\ Fe^{2+} + 4\ e^-$
Cathode reaction: $O_2 + 2\ H_2O + 4\ e^- \rightarrow 4\ OH^-$

Other factors, that accelerate corrosion are the deposition of aerosol particles (sea spray, wind blown dust,...) and the presence of pollutants (sulfur dioxide, nitrogen oxides,...).

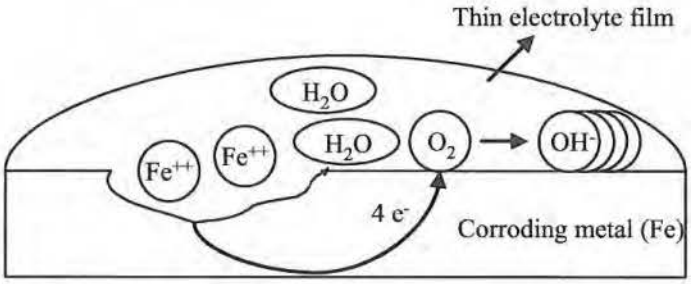

Figure 4-1: Schematic presentation of corroding iron.

The most common way to avoid corrosion is to coat the metal, so preventing contact with the hazardous environment. In order to provide adequate corrosion protection, coatings must be uniform, well adhered, pore free and self healing (for applications where physical damage to the coating may occur). There are a large number of technologies available for corrosion resistant coating on metals as has been reviewed by Gray et al.[3] and Twite et al.[4]. Common methods are:

- Electrochemical plating (e.g. galvanization)
- Conversion coatings (e.g. chromates)
- Hydride coatings
- Anodizing
- Laser surface alloying/cladding
- Organic coatings:
  - Gas phase deposition
  - Painting
  - Powder coating
  - E-coating
  - Sol-gel coating
  - Polymer plating
  - Plasma polymerization

This thesis aims at the development of an in line process for deposition of corrosion protection layers for cold rolled flat steel. Cold rolled flat steel products are widely used as structural parts in many industries like automotive

or house ware manufacturing. Corrosion protection of such a material is achieved by means of galvanization. Nevertheless, zinc in the galvanization layer is very sensitive to corrosion and "white rust" (zinc hydroxides) is often formed during transportation and storage of the galvanized steel sheets.

Chromium conversion coatings based on hexavalent chromium are usually deposited on steel sheets to protect the galvanization layer and the underneath steel. Hexavalent chromium reacts with the galvanization layer in a process involving the oxidation of the metal substrate and the reduction of the chromate ions to form a trivalent chromium hydroxide inorganic polymer network of uncertain stoichiometry[5-7]. This inorganic network acts as a passivating barrier layer. It decreases both the rate of the anodic metal dissolution reaction as the oxygen reduction on the metal surface. Hexavalent chromium species are absorbed onto the Cr(III) inorganic polymer. Since hexavalent chromate is soluble in water, it can migrate towards scratches in the protective layer and protect the exposed metal surface. The presence of this water soluble species therefore provides a self-healing effect, which is the reason why alternatives for chromium conversion coatings are rare. Unfortunately, hexavalent chromium is being banned because of its toxicity, as described in two European directives, in the field of automotive industry[8] and electrical and electronic equipment manufacturers[9]. These directives restrict the use of certain hazardous compounds in vehicles and electrical and electronic equipment, in order to contribute to the protection of human health and the environment. This has stimulated the development of more environmentally friendly alternative treatments for corrosion protection of metals.

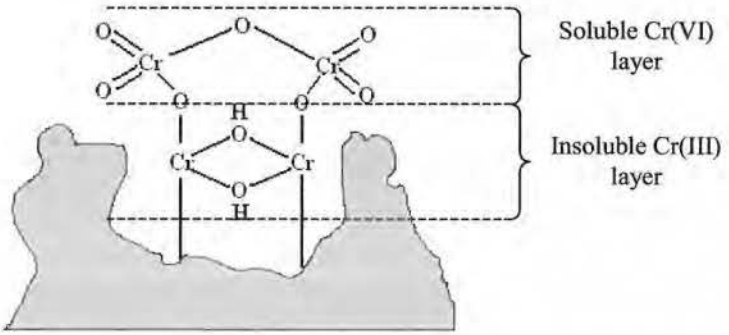

Figure 4-2: Schematic presentation of corrosion protection of metals by chromium conversion coatings. The double structure of an insoluble and soluble layer acts as a passivating self-healing coating.

It is known that conjugated polymers can also provide corrosion protection of metals with self-healing properties[10, 11]. Especially polyaniline is known for its excellent corrosion protection. Today, polyaniline is still the subject of a lot of corrosion studies. Several hypotheses have been suggested for the protection mechanism of polyaniline[12]:

- It contributes to the formation of an electric field at the metal surface, restricting the flow of electrons from metal to oxidant.
- It forms a dense, strong adherent, low porosity film similar to a barrier coating.
- It forms protective layers of metal oxides on the metal surface.

It is believed that the last mechanism proposed is responsible for the self healing properties of polyaniline. A possible mechanism for this self healing effect is presented in figure 4-3[13-15]. The emeraldine salt (ES) form of polyaniline is able to oxidize the metal substrate (iron). Therefore Fe^{2+} ions are also formed in the scratch when the polyaniline coating is damaged. By oxidizing the iron, the green emeraldine salt turns into the yellow leucoemeraldine form of polyaniline. In this process, protons are set free,

which results in a PH decrease. Oxygen from the air will oxidize the iron further towards Fe^{3+} and will also return the conjugated polymer in its oxidized state (blue emeraldine base). The scratch is filled with insoluble Fe_2O_3, after reaction with hydroxyl ions. These iron oxides form a passive layer that protects the metal against further oxidation. When the acid reaction medium is not removed from the coating, the emeraldine base will again be protonated, forming emeraldine salt.

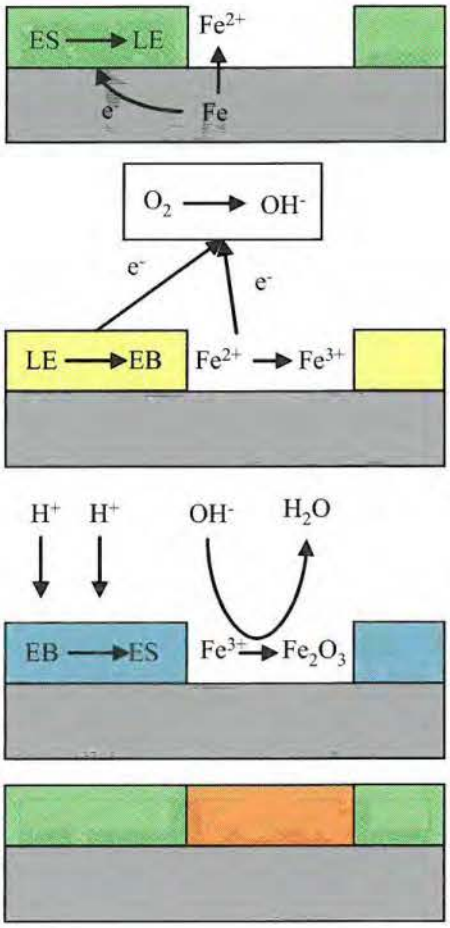

Figure 4-3: Schematic presentation of metal corrosion protection in a scratch by polyaniline.

The mechanism above implies that the reaction products produced in the different protection steps are not removed from the reaction medium. To make

this happen, polyaniline is usually combined with a barrier layer in corrosion protection paints. Another approach, which works well, is the combination of polyaniline with a polyanion such as poly(acrilic acid) or poly(styrene sulfonic acid)[16]. These poly acids form a stable double helix structure. The polyanion, that acts as the counter ion will not leach out of the coating.

While polyaniline[17-21] is mostly used for corrosion protection of metals, good results are also obtained with other conjugated polymers, such as polypyrrole[22, 23] and polythiophene[24, 25]. In this thesis, homogeneous plasma polymers with good mechanical properties were obtained with thiophene and EDOT. The corrosion protection properties of these polymers are studied in this chapter. Since it is known that conjugated polymers perform better in corrosion protection when they are combined with barrier coatings[26, 27], such combination with a plasma polymerized barrier coating is also discussed here.

The corrosion protection of the plasma deposited coatings are studied within an electrochemical cell and with salt spray tests. The electrochemical cell used, is presented in figure 4-4. In this setup, the sample under study acts as working electrode and is placed in the sample holder. The electrochemical cell is filled with a corrosive electrolyte solution (3,5% aqueous NaCl solution). On the other side of the cell a platinum counter electrode is situated. The reference electrode is placed in a tube, connected with a luggin capillary, which minimizes ohmic drops. This instrument allows to measure the open circuit potential as well as anodic and cathodic polarization curves. Although electrochemical measurements can provide a lot of information on the corrosion mechanism, it differs from a real corrosion environment. Salt spray tests can give a more realistic idea about the lifetime of metals. In salt spray tests, metals are exposed to a continuous salt spray for several days.

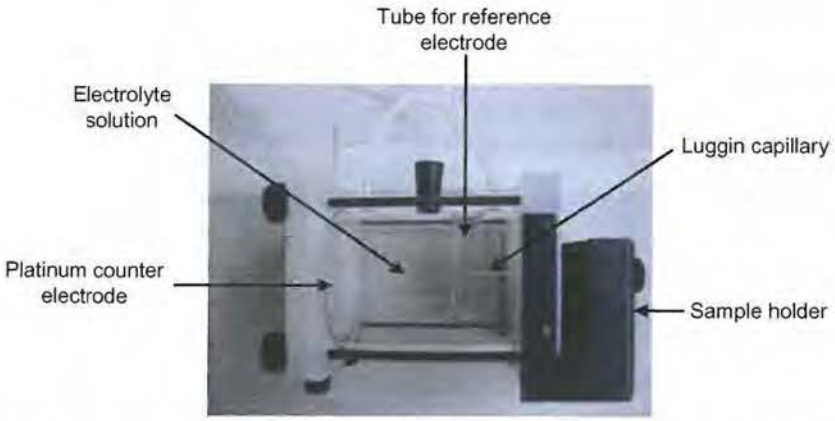

Figure 4-4: Picture of an electrochemical cell for evaluation of the corrosion behavior of metals.

4.2 Corrosion protection of steel by plasma polythiophene

Plasma deposition of polythiophene at atmospheric pressure was already discussed in section 2.4. It resulted in coatings with many structural defects and a conjugated system that had only shortly extended. However, conductivity was measured after doping. Since the coatings did not delaminate from the substrate in water, they could be suitable for corrosion protection of metals. The corrosion resistance of plasma polythiophene is studied in an electrochemical cell. As it is not clear whether the doped or undoped form of conjugated polymers have the best corrosion protection properties for galvanized steel, both were tested. The doped form of plasma polythiophene was obtained by holding the coated samples in iodine vapor.

Figure 4-5 presents the evolution of the open circuit potentials when immersed in a saline solution for 15 hours. The bare steel substrate is compared with doped and undoped plasma polythiophene. The potential of the bare steel substrate quickly decreases, pointing out the corrosion process of the metal, before to stabilize at a stable value, close to –0.7 $V_{Ag/AgCl,}$ which is the corrosion potential classically measured on steel immersed in NaCl solution.

The potential of the steel piece coated with undoped polythiophene first stabilizes after 30 minutes close to –0,61 $V_{Ag/AgCl}$ before to decrease down to -0.68 $V_{Ag/AgCl}$. The corrosion potential of undoped polythiophene is therefore higher than the one of the substrate, over the entire time interval. This shows that the coating is electrochemically active and cathodic with respect to the steel substrate. A potential of -0,61 $V_{Ag/AgCl}$ can be measured as soon as the sample is immersed, which results from a small amount of micro-defects in the coating and the establishment of an electrical pathway between the substrate and the solution through the pores of the coating. Since the roughness profile of the steel substrate reaches some micrometers and is balanced with a coating thickness of some few hundred of nanometers, it might be expected that a fraction of the steel surface is uncovered and in direct contact with the electrolyte. The measured potential therefore not corresponds to the open-circuit potential of the polymer but to a mixed potential.

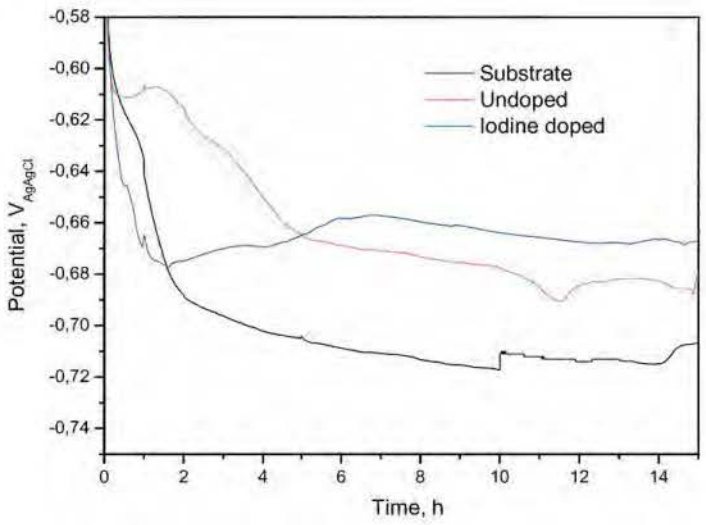

Figure 4-5: Evolution of the open circuit potential of uncovered steel and covered with undoped or iodine doped plasma polythiophene, when immersed in a saline solution.

The open circuit potential of the steel piece coated with doped plasma polythiophene quickly decreases when the piece is immersed and stabilizes to a value close to the one of the undoped sample. In contrast with the undoped sample, there is no potential plateau. This plateau, which ranges from 0.5 to 2 hours, may be related with the water uptake of the coating. When a coated sample is immersed in the NaCl solution, the electrolyte progressively penetrates the layer until the substrate is reached and the corrosion process begins. As the coating contains carbonyl functions which make the coatings more hydrophilic, this assumption could be likely. Another hypothesis would be that the sudden decrease of the potential may be correlated with the delamination of the layer. Indeed, if the coating delaminates from the substrate, the metal is exposed and a quick decrease of the potential can be expected.

More information about the corrosion mechanism, as well as the corrosion rate can be obtained from polarization curves. Figure 4-6 presents the polarization in both the cathodic and the anodic direction for the bare steel substrate. The black curve presents the measured value of the current when the potential is varied. This measured current is the sum of the net oxygen reduction current and the net iron oxidation current, which can not be measured. The red curve presents the reduction of oxygen. This is the most important reaction at the cathodic side of the curve (left side). From a certain potential (about -0,8 $V_{Ag/AgCl}$) the oxygen reduction is so fast that it is limited by diffusion of oxygen towards the electrode. The blue curve is the iron dissolution curve. This is the most important reaction at the anodic side of the graph (right side). When oxidation and reduction current are equal, no current is measured. This happens at the corrosion potential of steel.

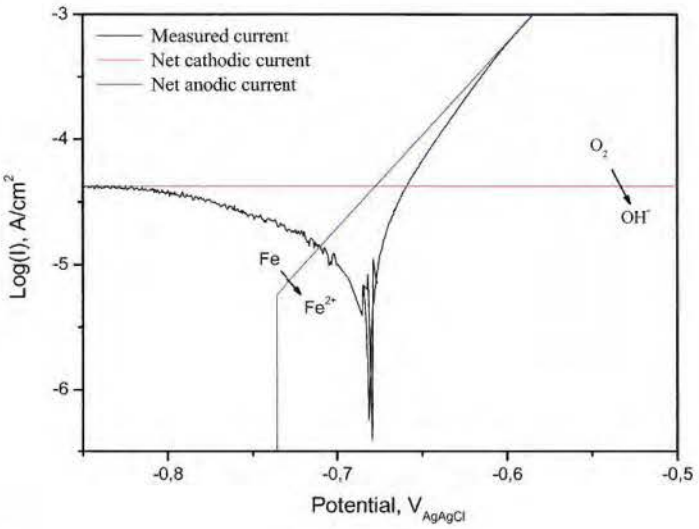

Figure 4-6: The cathodic and anodic polarization current for bare steel. The oxygen reduction and iron oxidation curves are also presented.

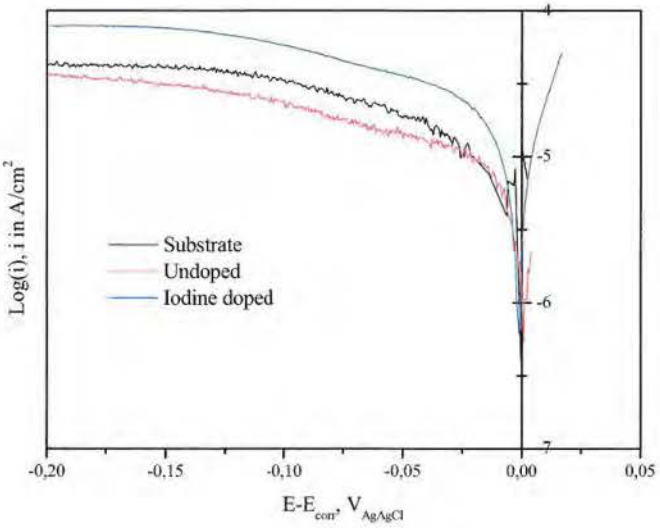

Figure 4-7: Evolution of the cathodic current, when the applied overvoltage is varied for uncovered steel and covered with doped or undoped plasma polythiophene.

Figure 4-7 presents the cathodic branch of the polarization curves for bare steel as well as for steel covered with undoped or iodine doped plasma polythiophene. In this graph the overvoltages are presented, which is the difference between the applied voltage and the corrosion voltage for a certain sample.

The polarization curve of the steel sample coated with undoped plasma polythiophene reaches the oxygen diffusion limited current density asymptotically, as was also observed for bare steel. Different is that it follows a pseudo-linear evolution first, before reaching the asymptote. The galvanic coupling between the coating and the substrate may induce this lowering of the cathodic reaction kinetic. Indeed, polythiophene has electrochemical properties as has been shown by the increased corrosion potential in comparison with the bare steel substrate. In such configuration, the corrosion mechanism leads to a separation of both anodic and cathodic reactions that do not occur at the same location on the surface. The coating supports the cathodic reaction, whereas the anodic one is iron dissolution through the pores of the layer. Since the cathodic reaction does not occur on the same material, the behavior of the system under polarization changes. Coating steel with polythiophene thus generates a cathodic corrosion inhibition.

The cathodic current of the steel sample covered with iodine doped plasma polythiophene is not limited by oxygen diffusion. The limiting current is higher than the one for bare steel. This means that there is another reduction reaction besides oxygen reduction. Indeed, the coating also contains iodine, which also has strong oxidative properties. The cathode current is now limited by the sum of oxygen and iodine reduction.

The rate of corrosion can be evaluated by means of the corrosion current. The higher the corrosion current, the faster the metal corrodes. This corrosion current is the current at the corrosion potential. Although, no net current is measured at this point, as oxidation and reduction rate are equal, the corrosion current can be calculated by extrapolating the cathodic current of each sample towards the corrosion potential. The values obtained this way are presented in table 4-1.

	Corrosion current (μA/cm²)
Substrate	37
Undoped	10
Iodine doped	32

Table 4-1: Corrosion current of bare steel and steel covered with undoped or iodine doped plasma polythiophene

The corrosion current indicates that a small decrease of the corrosion rate is achieved through polythiophene deposition. However, the effect is rather small. Doping of the polythiophene layer with iodine does not improve the corrosion protection at all. Protection is even worse after doping.

Figure 4-8 presents the anodic part of the polarization curves of bare steel and steel covered with undoped or iodine doped plasma polythiophene. The anodic reaction is iron dissolution. The three anodic branches are parallel in a large range of potential. This means that the same anodic process occurs at each sample. If the corrosion protection was active, other anodic reactions, besides iron dissolution would occur. So, both the undoped as the iodine doped plasma polythiophene are not able to provide active corrosion protection of steel.

In conclusion can be stated that doped plasma polythiophene does not provide any corrosion protection of steel at all. The undoped polymer, however is able to decrease the corrosion rate by acting as a barrier. An active corrosion protection was not achieved. Because the porous nature of the coating, the protection is not sufficient. Probably, a part of the rough steel structure is exposed due to the small thickness of the coating.

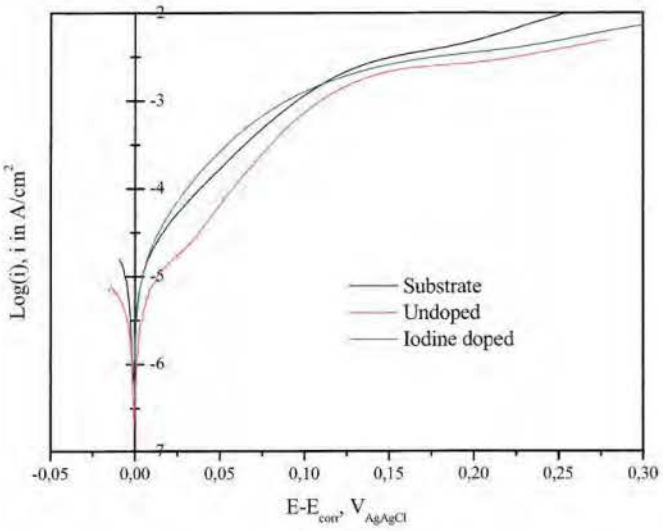

Figure 4-8: *Evolution of the anodic current, when the applied overvoltage is varied for bare steel and steel covered with iodine doped or undoped plasma polythiophene.*

4.3 Corrosion protection of galvanized steel by plasma PEDOT

Plasma polymerization of EDOT at atmospheric pressure in a translating DBD reactor, resulted in blue coatings, indicating that the conjugated system has significantly extended. The performance of these plasma PEDOT coatings as corrosion protection layers is studied by polarization curves (Tafel plots). Samples were prepared by plasma depositing PEDOT layers on galvanized steel. The polarization curves are presented in figure 4-9. The corrosion current and potential are shown in table 4-2.

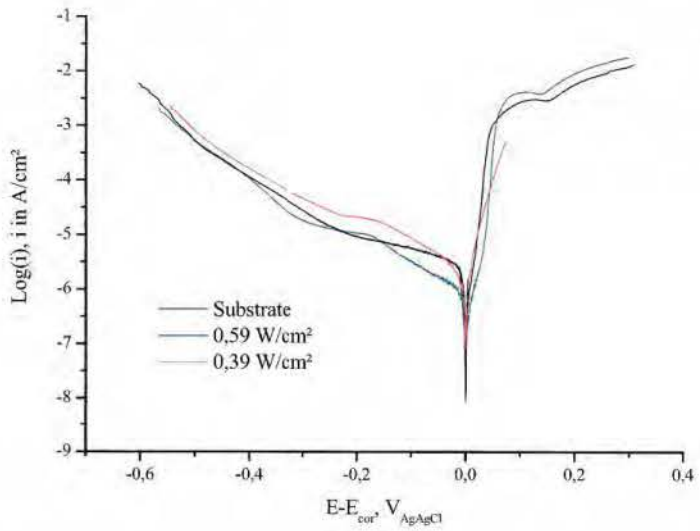

Figure 4-9: Polarization curve of bare galvanized steel and galvanized steel covered with PEDOT coatings, plasma deposited at 0,39 W/cm² and 0,59 W/cm².

When galvanized steel is covered with a PEDOT coating, plasma polymerized at 0,39 W/cm², the cathodic polarization curve (left part) has a different shape than for an uncovered substrate. This means that the coating has an influence on the corrosion behavior. The corrosion current (table 4-2), however, does not improve. The reason for this is that the PEDOT coating itself is also electrochemically active. The polarization curves are not only influenced by the redox reactions of the corroding metal, but also redox reactions with the coating itself might occur[28]. Conjugated polymers can be doped or undoped by oxidation and reduction. Since the plasma PEDOT coatings are conductive, they probably exist in a partially (plasma) doped form. The measured cathodic current then results from the reactions:

$O_2 + H_2O + 4e^- \rightarrow 4\ OH^-$

$PEDOT_{doped} + ne^- \rightarrow PEDOT_{undoped}$

The measured corrosion current is therefore overestimated. While the cathodic current of the bare substrate quickly increases towards the diffusion limit for oxygen, the current of the PEDOT coating deposited at 0,39 W/cm² exceeds this limit, which is only possible with a second oxidation mechanism, confirming the hypothesis stated before.

	Corrosion current (A/cm²)	**Corrosion potential (V)**
Substrate	3.82×10^{-6}	-1,089
PEDOT 0,39 W/cm²	$2,39 \times 10^{-6}$	-1,083
PEDOT 0,59 W/cm²	$8,39 \times 10^{-7}$	-1,074

Table 4-2: Corrosion current and potential for galvanized steel that is uncovered and covered with a PEDOT coating, plasma polymerized at 0,39 or 0,59 W/cm².

When PEDOT is deposited at 0,59 W/cm², a small decrease in corrosion current is observed. Probably, the corrosion current is again overestimated because reduction of the coating takes place, although the cathodic part of the curve does not exceed the oxygen diffusion limited current. Possibly, PEDOT is completely reduced at this point. The anodic part of the curve does exceed the current measured for the bare substrate. A second oxidation mechanism must therefore be present, which is again a redox reaction with the coating. The measured anodic current results from two reactions:

$Fe \rightarrow Fe^{2+} + 2e^-$

$PEDOT_{undoped} \rightarrow PEDOT_{doped} + ne^-$

Both plasma deposited PEDOT coatings can cause a slight shift of the corrosion potential. This shift is too small to provide sufficient corrosion protection, as is confirmed by figure 10, which shows the corrosion of a galvanized steel sample coated with plasma PEDOT, after 10 days exposure to a spray of a saline solution at 35°C. Comparison of the sample before exposure to salt spray and after treatment, shows that the metal has significantly corroded. The conditions in the salt spray tester are too severe for the deposited

PEDOT coatings. Probably, the films are too thin to be used as a corrosion protection layer.

Figure 4-10: Pictures of plasma PEDOT coated galvanized steel samples, before and after 10 days exposure to a salt spray at 35 °C.

4.4 Corrosion protection of galvanized steel with multi-layers and hybrid coatings.

Plasma deposition of PEDOT coatings onto galvanized steel can result in a decrease of the corrosion rate of the metal. However, after exposure to a salt spray for 10 days, the coatings have severely corroded. Therefore, these coatings can not be used as a replacement for chromium conversion coatings. Probably, thicker films are needed for sufficient corrosion protection. Better results are obtained with (electro)chemically deposited coatings, which are a few micrometer thick. For use in applications the conjugated polymer is usually combined with oxygen barrier layers. As conjugated polymers are not stable in contact with air and barrier properties are not that good, the combination with barrier layers significantly improves their performance. For example, the addition of only 1% polyaniline to an epoxy primer, increased the corrosion resistance of this coating significantly[18]. The combination of plasma polymerized PEDOT with barrier coatings might also perform better.

In this section, the corrosion inhibition of multi-layers and hybrid coatings of plasma PEDOT and plasma polymerized polysiloxane coatings is studied. Plasma deposition of polysiloxane layers at atmospheric pressure is extensively documented[29-36]. Before studying the performance of multi-layers and hybrid

coatings, plasma polysiloxane coatings will first be developed and tested upon corrosion protection properties.

Plasma deposition of polysiloxane coatings

A commonly used precursor for plasma deposition of polysiloxane layers is hexamethyldisiloxane (HMDSO). The advantage of this chemical is that it results in coatings that are hydrophobic. So, besides it's barrier properties, it also prevents the formation of an electrolytic water film onto the metal, which is necessary for corrosion.

Since it is the purpose to develop a corrosion resistant system that can replace chromate conversion coatings, a comparison with this system might be useful. Figure 4-11 therefore presents galvanized steel substrates that are uncovered and covered with chromates, after a 10 day salt spray standard test. While the untreated galvanized steel piece shows severe corrosion on it's entire surface after 10 days of salt spray exposure, the chromated piece only shows a few pits.

Figure 4-11: Galvanized steel before satlspray test (A) and after 10 day salt spray treatment on an uncovered (B) and a chromated sample (C).

The coating thickness is very important for barrier layers. Corrosion species have more difficulties in reaching the metal surface, when the deposited protection layers are thicker. Figure 4-12 presents the coating thickness for plasma polymerized HMDSO in different plasma gases. The addition of an oxidative gas to the plasma, clearly increases the coating thickness. Coatings deposited in a nitrogen/oxygen mixture are three times thicker. These results correlate well with the corrosion performance of the coatings, as can be

concluded from figure 4-13. While the coatings deposited in a nitrogen plasma still show a lot of corrosion pitting, inhibition is better when deposition is done in a nitrogen/oxygen mixture. The addition of dinitrogen oxide, results in coatings that perform in between.

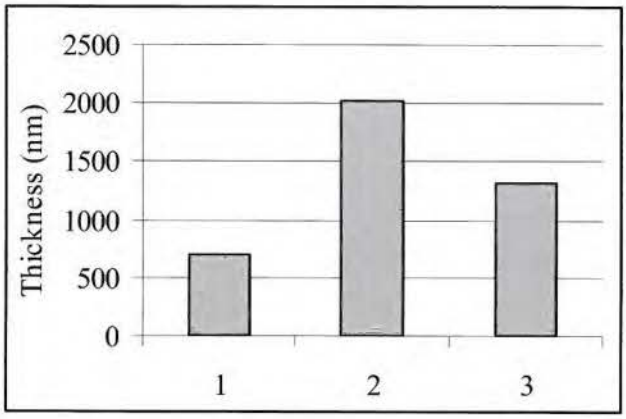

Figure 4-12: Coating thickness of polysiloxane coatings plasma polymerized in: 1) N_2, 2) N_2/O_2 (3%), 3) N_2/N_2O (5%)

Figure 4-13: Galvanized steel coated with polysiloxanes, plasma polymerized in different gases, after 10 days salt spray exposure.

Addition of an oxidative gas to the carrier gas also has an influence on the morphology of the deposited polysiloxane layers. SEM pictures (figure 4-14) show that the polysiloxane coatings deposited in a nitrogen plasma have a dense structure. This in contrast with the coatings deposited in a nitrogen/oxygen plasma, which show some porosity. This phenomenon was also studied by Grundmeier et al.[37] It is so far unclear how these holes in the

layer are formed. Despite the defects, oxygen addition results in better corrosion protection than the smooth coatings deposited in pure nitrogen. When dinitrogen oxide is added to the plasma gas, the coatings have a very rough surface with many defects.

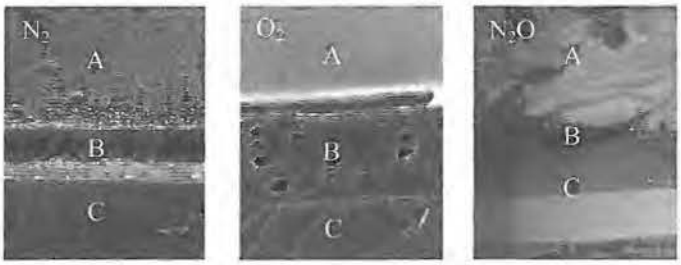

Figure 4-14: SEM pictures at 25° tilt of polysiloxane coatings plasma deposited in different carrier gases. A) coating surface, B) cross section coating C) cross section substrate.

Plasma polysiloxane depositions in the presence of oxygen, have corrosion protection properties that are close to the protection by chromate conversion coatings. However the deposition time is still very long (72 coating passes + 24 curing passes). To decrease the deposition time, the morphology of the coatings has to be improved. Indeed, the deposited coatings are quite rough, as is shown with the interferrometry picture in figure 4-15-A. This roughness is caused by the sample itself, which is an obstruction for the gas flow. The convection caused by the sample results in a rough surface topology. The obstruction in the plasma gap can be removed, by replacing the earthed electrode by a template in which the sample exactly fits (figure 4-16). This indeed results in a much smoother morphology (figure 4-15-B).

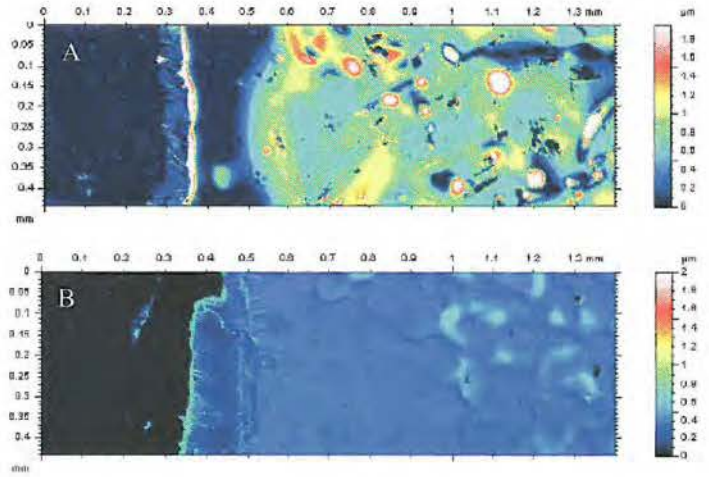

Figure 4-15: Surface roughness, measured with interferrometry for polysiloxane coatings, plasma deposited: A) without template, B) with template.

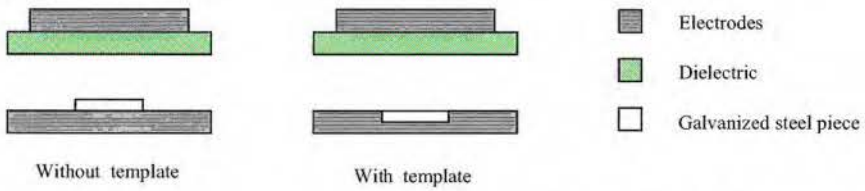

Figure 4-16: Schematic presentation of a DBD reactor with and without template.

The influence of the template and the therefrom resulting smoother morphology on the corrosion protection of galvanized steel is illustrated in figure 4-17. While the coating deposited without use of the template clearly shows pitting corrosion, the one coated under the same conditions with template shows no pitting.

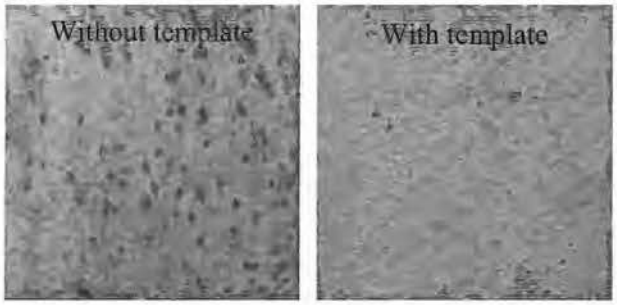

Figure 4-17: Galvanized steel covered with a polysiloxane coating, plasma deposited in a DBD reactor with and without template, after 10 days exposure to a salt spray.

When a template is used, good corrosion protection could be obtained with only 12 plasma coating steps, instead of 72. The samples presented in figure 4-18 are covered with polysiloxane layers, plasma deposited in 12 passes. The number of curing steps is varied. After the coating steps, the plasma coatings are cured with a plasma under the same conditions as in the coating steps but without further precursor addition. It is clear that these curing steps are necessary to obtain good corrosion resistance. The result is already much better when only 2 curing steps are used. 12 curing steps are needed to perform as good as chromium conversion coatings. These results are confirmed by the cathodic polarization curves and the corrosion currents extrapolated therefrom, which are presented in figure 4-19. If 12 curing steps are used, the corrosion is 3 times slower, compared to 4 curing steps. More then 12 curing steps, however doesn't lead to a further decrease of the corrosion current. The coatings, plasma deposited with 12 curing steps show no difference with the chromated galvanized steel after 10 days of salt spray and also the corrosion current is already close to chromated substrates.

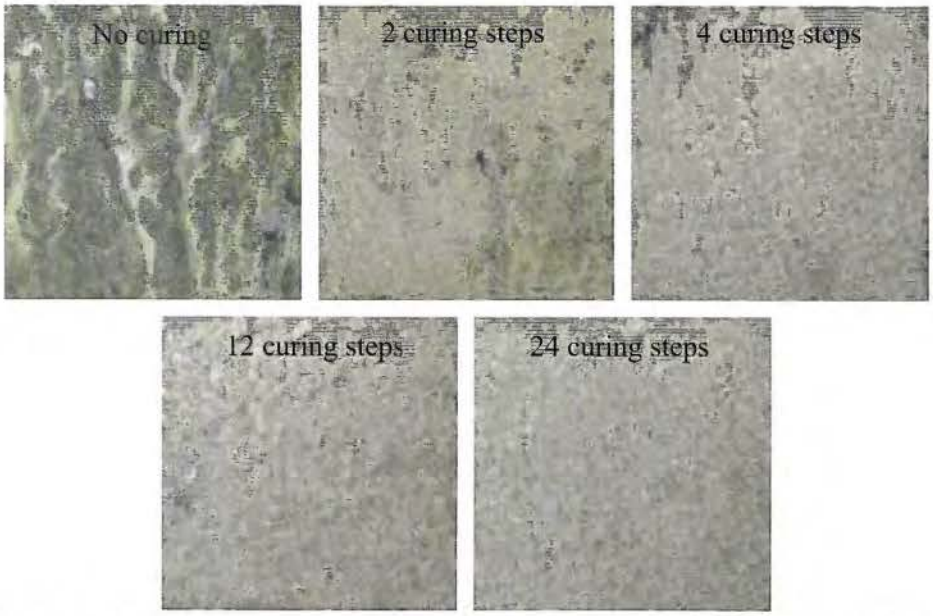

Figure 4-18: Galvanized steel covered with plasma polymerized polysiloxane coatings, plasma cured with different curing times, after 10 days of salt spray exposure.

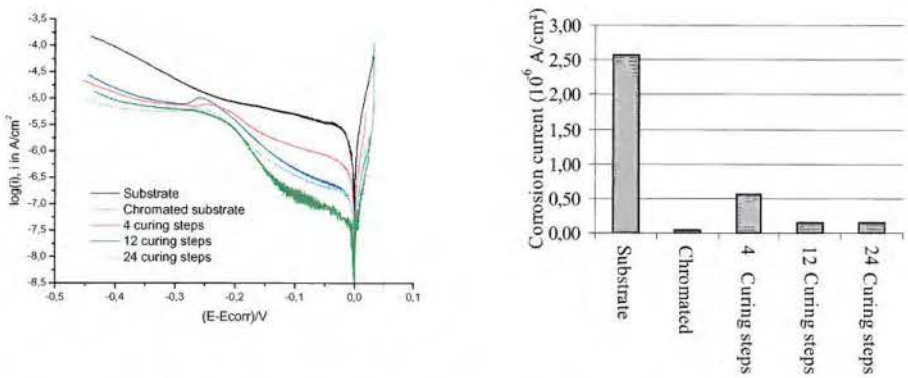

Figure 4-19: Polarization curve and corrosion current of galvanized steel, covered with plasma deposited polysiloxane and plasma cured with a different number of curing steps.

An explanation for the improved corrosion protection when curing steps are added is found in the chemical structure of the deposited layers. Figure 4-19 presents the infrared spectra of the plasma deposited polysiloxane layers.

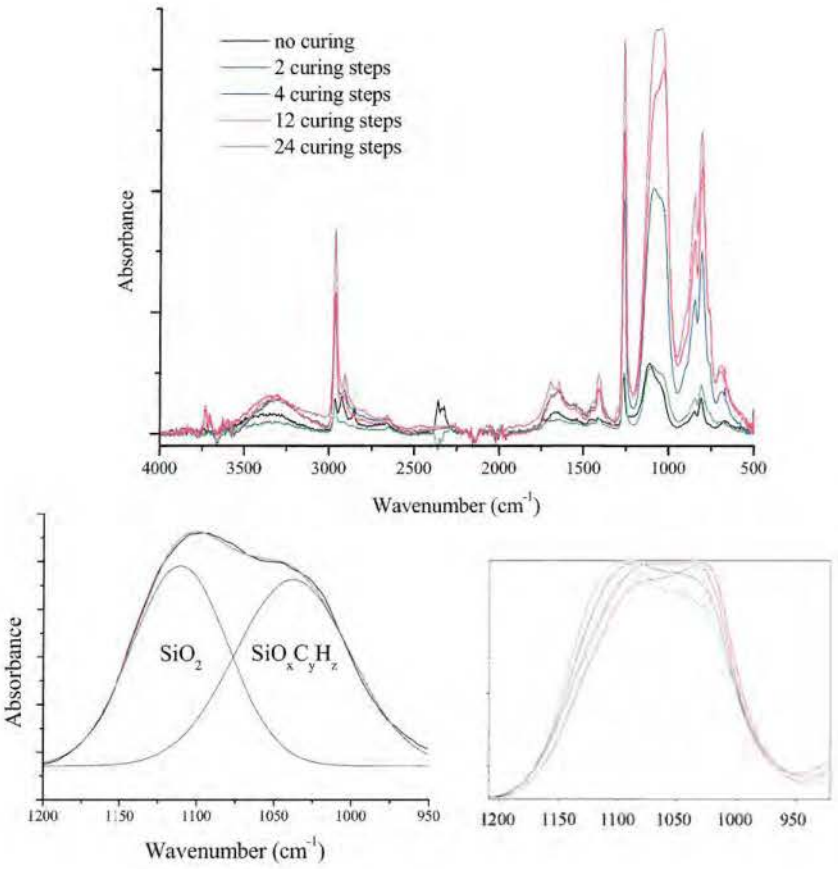

Figure 4-19: Infrared spectra of plasma deposited polysiloxanes with different number of curing steps. The SiO_2 and $SiO_xC_yH_z$ contents can be compared after peak deconvolution of the double peak around 1100 cm^{-1}.

When the curing time is short, the organic content of the layer is higher. The C-H stretching bands at 2900 cm^{-1} are then more intense than the Si-O stretching peak at 1100 cm^{-1}. This can be explained by deconvolution of the Si-O stretching peaks. The Si-O stretching vibration around 1100 cm^{-1} results from a

SiO_2 like network. The vibration at 1030 cm^{-1} results from a $SiOC_yH_z$ polysiloxane like structure[38-40]. The ratio of the peak areas of these two Si-O stretching vibration peaks is presented in figure 4-20. When the number of curing steps increases, the SiO_2 content also increases. Oxygen curing leads to etching of the Si-C bonds and cross-linking of the polymer chains by forming a SiO_2 like network[41]. The increased inorganic character of the coating improves the corrosion protection properties of the films. After 12 curing steps, no further increase of the inorganic content is observed.

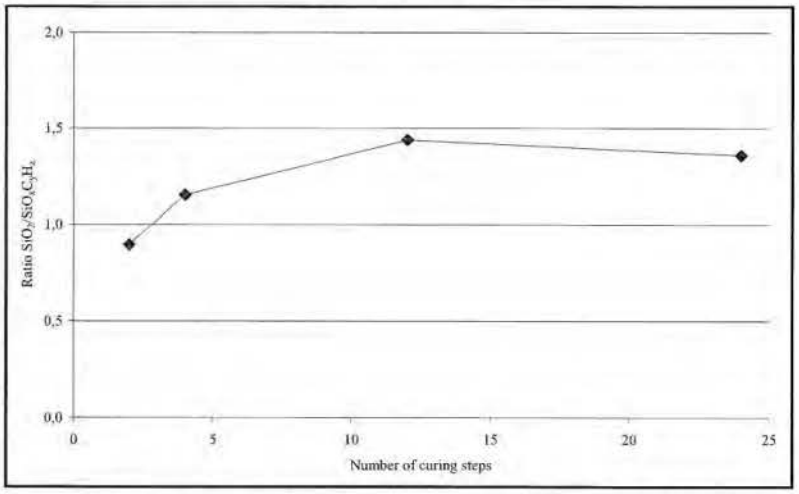

Figure 4-20: The ratio of the IR peak areas for Si-O stretching in SiO_2 (1100 cm^{-1}) and in $SiO_xC_yH_z$ (1030 cm^{-1}).

By adding oxygen to the plasma carrier gas and by using a template and curing steps, polysiloxane barrier layers could be deposited in a plasma at atmospheric pressure that have corrosion protection properties equal to chromium conversion coatings.

Plasma deposition of hybrid coatings

Plasma deposited polysiloxane layers provide good corrosion protection of galvanized steel. However, when the coatings are scratched, corrosion will

occur in the scratch. To prevent this, a second material is necessary. In this section a hybrid coating is formed by co-injecting EDOT and HMDSO. This way, a conjugated polymer is combined with a barrier layer. Figure 4-21 shows the polarization curve of such hybrid layer. The hybrid plasma deposition is compared with a pure polysiloxane layer (PHMDSO) plasma deposited under the same conditions.

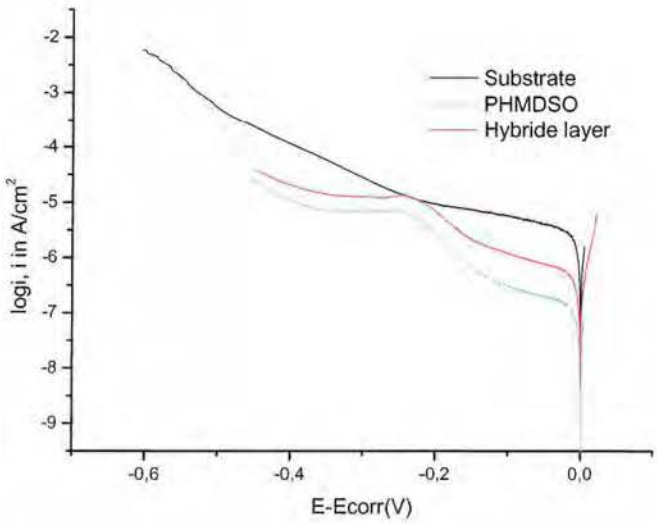

Figure 4-21: Polarization curve of uncovered galvanized steel and covered with a plasma deposited HMDSO layer or a plasma deposited HMDSO/EDOT hybrid layer.

When EDOT is incorporated in the plasma PHMDSO layer, the curve shows the same shape, but the corrosion current is higher. Possibly, the EDOT monomer will also react with HMDSO, forming a copolymer, rather than a blend. As the HMDSO units interrupt the conjugation, no extended conjugated system is formed. Furthermore, the hydrophobicity of the plasma coating is decreased by the presence of EDOT structures which will enhance the penetration of the corrosive liquid through the coating.

Plasma deposition of multi-layers

Another approach to combine conjugated polymers with barrier coatings is the use of multi-layers. Since contact with the metal substrate is desirable to provide active corrosion protection, the plasma PEDOT is deposited first, followed by plasma deposition of the PHMDSO layer (table 4-3). The corrosion protection by this double layer is evaluated by electrochemical polarization experiments, which are presented in figure 4-22. The result is compared with a PHMDSO layer, deposited under the same conditions. Although the cathodic part (left part) of the curve is parallel to the corresponding PHMDSO layer, which indicates that the corrosion process is the same (oxygen reduction), the corrosion current has increased. Possibly, the more hydrophilic PEDOT coatings swell once the corrosive solution has penetrated through the barrier layer, resulting in delamination from the substrate. This way, parts of the metal substrate are exposed to the corrosive solution.

PHMDSO layer	1x	12 steps plasma PHMDSO deposition 12 steps plasma curing
Double layer	1 x	24 steps plasma PEDOT deposition 12 steps plasma PHMDSO deposition 12 steps plasma curing
Multi layer	4 x	6 steps plasma PEDOT deposition 3 steps plasma PHMDSO deposition 3 steps plasma curing

Table 4-3: Consecutive reaction steps for the plasma deposition of pure PHMDSO, a PEDOT/PHMDSO double layer and a PEDOT/PHMDSO multi-layer.

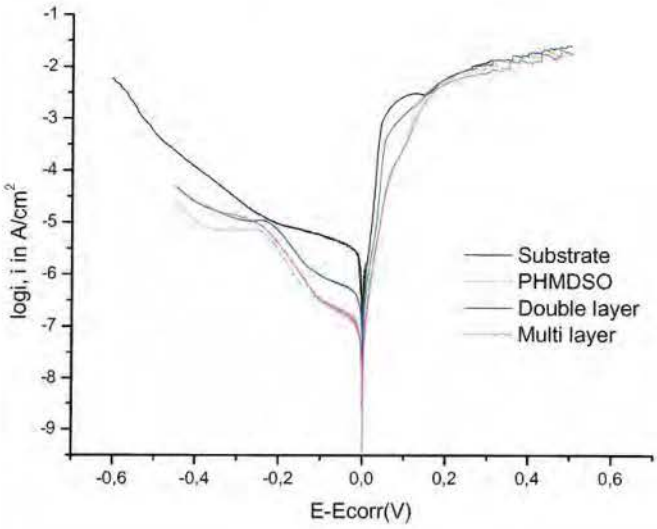

Figure 4-22: Polarization curves of uncovered galvanized steel and covered with a reference PHMDSO layer, a PEDOT/PHMDSO double layer and a PEDOT/PHMDSO multi-layer.

Finally, the corrosion protection properties of plasma deposited PEDOT/PHMDSO multi layers are studied. It is known that multi-layers often provide better corrosion protection than single layers, because properties of different layers are combined and pores in the layers are blocked at the interfaces[42-44]. Additional layers conventionally result in better corrosion protection. Figure 4-22 shows that also an 8 layered PEDOT/PHMDSO plasma coating performs better than a double layer. However, the corrosion current is not lower than the pure plasma PHMDSO layer. It is not clear whether the improvement, compared to the double layer, is due to reduced delamination or additional layers. Since the PEDOT layer directly in contact with the metal substrate is much thinner in the multi-layer, the metal area coverd with PEDOT might be smaller, resulting in a larger contact area between metal and PHMDSO and better adhesion.

Also the anodic part (right part) of the polarization curve of the mutli-layer is similar to the one of PHMDSO, indicating that the PEDOT part does not have a

significant effect on the corrosion protection of the substrate. Possibly the PEDOT coatings are too thin to passivate the metal.

4.5 Perspectives

While plasma polythiophene could be used as a barrier layer and plasma PEDOT participated in redox reactions during corrosion tests, non of these coatings provided sufficient corrosion protection for metals. Better results are expected for corrosion protection with plasma polyaniline and plasma polypyrrole. Not only because these plasma polymers resemble more the conventionally synthesized polymers, but also because they are known to perform better in corrosion protection, as has been documented extensively in literature. Unfortunately, the plasma deposited polyaniline an polypyrrole coatings at atmospheric pressure were inhomogeneous and the coated area was very small. Therefore, it was not possible to perform any corrosion tests so far.
In future work, the development of more homogeneous plasma polyaniline and plasma polypyrrole coatings should be a priority. Homogeneity might be improved by using a translating DBD reactor and by adjusting the precursor injection system for more uniform injection of monomer and oxidant. A new injection system might consist out of several injection nozzles in a chamber. It is important to adjust the geometry and the position of the nozzles in a way to minimize convection and so prevent condensation of the aerosols which would pollute the walls of the chamber. The concentration and ratio of monomer and oxidant (dopant) is also expected to be crucial. When plasma deposition of homogeneous polyaniline and polypyrrole coatings is achieved, they can be easily combined with plasma barrier coatings in multi layers and hybrid coatings.

4.6 Experimental part

Characterization methods

The chemical structure of the coatings was studied with fourier transformed infrared (FTIR) spectroscopy. The FTIR spectra were recorded on a Bruker Optics Tensor 27 spectrometer. Tests have been carried out in attenuated total reflectance (ATR) mode using a golden gate system (top plate, which includes an optical beam-condensing unit). The ATR crystal was a IIa diamond 45° (2 x 2 mm). The ATR plate was a diamond, brazed into a tungsten carbide disc. The active sampling area is 0,8 mm. A penetration depth of 2μm is reached at 1000 cm^{-1} for a material with a refractive index of 1,5.

The corrosion protection of the plasma deposited coatings is studied within a PARSTAT2273 potensiostat/galvanostat (Princeton applied research). Data was processed with Powersuite software. All experiments were carried out in a 3 electrodes electrochemical cell. The sample under study acts as working electrode and is placed in a sample holder. The electrochemical cell is filled with an aerated 3,5% aqueous NaCl electrolyte solution with a PH of 5,6. A platinum grid is used as counter electrode. A Ag/AgCl reference electrode with a potential of +197 mV referred to the normal hydrogen electrode is placed in a tube, connected with a luggin capillary, which minimizes ohmic drops. The open-circuit potential of the samples is measured versus the immersion time for a duration of 15 hours. For polarization experiments, the sample was immersed in the corrosive electrolyte solution until the free potential stabilizes. The corrosion potential is assumed to be stable if it does not evolve more than 1 mV in 5 minutes. Acquisition of the cathodic part of the curve is done by scanning the potential from +20 mV down to -600 mV versus the open circuit potential at a 0.17 mV/s scan rate. This scan rate is sufficiently low for a quasi-steady state of the system during the measurement. The anodic polarization curve is acquired according to the same protocol, but the potential is scanned from -20 mV up to +300 mV versus the open circuit potential at a 0.17 mV/s scan rate.

The corrosion protection properties of the coatings were also studied with salt spray tests. The standard DIN 50021 salt spray test was used. The temperature of the device was kept constant during the entire test at 35±2 °C. The samples

were exposed to a spray of a 50±5 g/l NaCl solution. The PH of the solution lies in between 6,5 and 7,2. The solution was sprayed under an angle of 60-75°. Condensed solution was recovered at a rate of 1,5±0,5 ml/h (funnel: diameter of 10 cm and surface of 78,5 cm^2). The concentration of the recovered liquid was controlled by conductivity measurements.

Measurement of the thickness and the coating roughness is done with a Wyko NT3300 (Veeco) white light interferometer. For thickness measurement, a part of the sample is covered with tape, to provide an uncoated part. The step height is measured. Topography data treatment is performed with Mountains Map (Digital surf). Three-dimensional topography measurements (surfometries) are adapted to have a perfectly horizontal non-coated surface. Points which are not significant for the whole topography are thresholded. The amplitude distribution function curve (height probability density curve) is then calculated for each sample.

For analysis of the coating's morphology, scanning electron microscopy (SEM) was used. Photographs of cross-sections of coated samples were taken with a JSM-6340F SEM of JEOL. To have a picture of both the coating surface and the cross section of the coatings, the samples were tilted under an angle of 25°. The cross-section of the coating also shows the coating thickness.

Chemicals

All chemicals were used without further purification. The following chemicals are used in this chapter: thiophene (99+, Sigma-Aldrich), 3,4-ethylenedioxythiophene (Sigma-Aldrich), hexamethyldisiloxane (99%, Merck), iodine (99,8%, ACS reagent, Sigma Aldrich)

Plasma reactor

The plasma is generated with a dielectric barrier discharge. The lower electrode is a stationary, grounded electrode. Two high voltage electrodes can move over the grounded electrode. These high voltage electrodes each have an area of 256 cm^2 (32 x 8 cm) and are covered with a glass dielectric of 2,2 mm thickness. Power is supplied by a G10 S-V AFS generator. The ac voltage is transformed up with a transformer that is carefully tuned to minimize power losses. The gap

between the glass dielectric and the grounded electrode is 2 mm. The gas flow rate is controlled with an MKS mass flow controller. The precursors are injected into the plasma as an aerosol, generated with a TSI constant output atomizer type 3076. Before entering the plasma, the aerosol is mixed with the carrier gas which is used to transport the aerosol towards the plasma.
When deposition was done in a stationary DBD reactor, the lower grounded electrode was an aluminium template in which the metal substrate fits. The high voltage electrode has an area of 560 cm^2.

Plasma parameters

All plasma parameters used, are presented in the tables below. The different parameters shown are:

- **Chemicals**: the precursors that are injected into the plasma as an aerosol
- **Press**: the gas pressure used to generate the aerosols
- **Power**: the power per square cm, used on the high voltage electrode
- **Time**: the total reaction time
- **Gas**: the gasses used to create the plasma and their concentration
- **Flow**: the total gas flow rate in standard liters per minute
- **Freq**: the high voltage frequency
- **Speed**: The speed at which the translating reactor moves over the samples.
- **Range**: The translation range of the moving reactor.
- **Steps**: The number of passes of the translating reactor above the samples.

4.2 Corrosion protection of steel by plasma polythiophene

Chemicals	Pressure (bar)	Power (W/cm^2)	Time (s)	Gas	Flow (sl/min)	Freq (kHz)
Thiophene	2	0,27	180	N_2	20	1,5

Doping with iodine was done in a iodine chamber. The sample was placed in the iodine vapor for 15 min.

4.3 Corrosion protection of galvanized steel by plasma PEDOT

Chemicals	Press bar	Power W/cm²	Gas	Flow sl/min	Freq kHz	Speed m/min	Range mm	steps
EDOT	2	0,39	N_2 O_2(2%)	15	1,5	2	360	24
EDOT	2	0,59	N_2 O_2(2%)	15	1,5	2	360	24

4.4 Corrosion protection of galvanized steel with multi-layers and hybrid coatings

Plasma deposition of polysiloxane coatings

Most experiments are done in two steps. The first step is a coating step, the second a plasma curing step.

* The grounded electrode was replaced by a template in which the samples fit in experiments 4 to 9.

	Chemicals	Press bar	Power W/cm²	Gas	Flow sl/min	Freq kHz	Speed m/min	Range mm	steps
1	HMDSO	2	0,84	N_2	60	6	4	360	72
	-	2	0,84	N_2	60	6	4	360	48
2	HMDSO	2	0,84	N_2 O_2(3%)	60	6	4	360	72
	-	2	0,84	N_2 O_2(3%)	60	6	4	360	48
3	HMDSO	2	0,84	N_2 N_2O(5%)	60	6	4	360	72
	-	2	0,84	N_2 N_2O(5%)	60	6	4	360	48
4*	HMDSO	2	0,84	N_2	60	6	4	360	72
		2	0,84	N_2	60	6	4	360	48
5*	HMDSO	2	0,94	N_2 O_2(3%)	30	1,5	4	360	**12**
6*	HMDSO	2	0,94	N_2 O_2(3%)	30	1,5	4	360	**12**
	-	2	0,94	N_2 O_2(3%)	30	1,5	4	360	**2**
7*	HMDSO	2	0,94	N_2 O_2(3%)	30	1,5	4	360	**12**
	-	2	0,94	N_2 O_2(3%)	30	1,5	4	360	**4**
8*	HMDSO	2	0,94	N_2 O_2(3%)	30	1,5	4	360	**12**
	-	2	0,94	N_2 O_2(3%)	30	1,5	4	360	**12**
9*	HMDSO	2	0,94	N_2 O_2(3%)	30	1,5	4	360	**12**
	-	2	0,94	N_2 O_2(3%)	30	1,5	4	360	**24**

4.4 Corrosion protection of galvanized steel with multi-layers and hybrid coatings

Plasma deposition of hybrid coatings

Plasma deposition of multi-layers

Experiment 1: reference PHMDSO

Experiment 2: hybrid layer

Experiment 3: double layer

Experiment 4: multi-layer (8 layers)

	Chemicals	Press bar	Power W/cm²	Gas	Flow sl/min	Freq kHz	Speed m/min	Range mm	steps
1	HMDSO	2	0,59	N_2 O_2(3%)	20	1,5	4	360	12
	-	2	0,59	N_2 O_2(3%)	20	1,5	4	360	12
2	HMDSO EDOT	2	0,59	N_2 O_2(3%)	20	1,5	2	360	24
	-	2	0,59	N_2 O_2(3%)	20	1,5	2	360	12
3	EDOT	2	0,39	N_2 O_2(2%)	15	1,5	2	360	24
	HMDSO	2	0,59	N_2 O_2(3%)	20	1,5	4	360	12
	-	2	0,59	N_2 O_2(3%))	20	1,5	4	360	12
4	EDOT	2	0,39	N_2 O_2(2%)	15	6	2	360	4x6
	HMDSO	2	0,59	N_2 O_2(3%)	20	1,5	4	360	4x3
	-	2	0,59	N_2 O_2(3%))	20	1,5	4	360	4x3

4.7 References

1 G. H. Koch, M. P. H. Brongers, N. G. Thompson, P. Y. Virmani, J. H. Payer, *FHWA* **2002**,

2 P. R. Roberge, R. D. Klassen, P. W. Haberecht, *Materials & Design* **2002**, 23, 321

3 J. E. Gray, B. Luan, *Journal of Alloys and Compounds* **2002**, 336, 88

4 R. L. Twite, G. P. Bierwagen, *Progress in Organic Coatings* **1998**, 33, 91

5 X. Zhang, W. G. Sloof, A. Hovestad, E. P. M. van Westing, H. Terryn, J. H. W. de Wit, *Surface and Coatings Technology* **2005**, 197, 168

6 Z. L. Long, Y. C. Zhou, L. Xiao, *Applied Surface Science* **2003**, 218, 124

7 C. Gabrielli, M. Keddam, F. Minouflet-Laurent, K. Ogle, H. Perrot, *Electrochimica Acta* **2003**, 48, 965

8 *European directive 2000/53/EC*

9 *European directive 2002/95/EC*

10 E. W. Brooman, *Metal Finishing* **2002**, 100, 104

11 P. Zarras, J. D. Stenger-Smith, *Electroactive Polymers for Corrosion Control* **2003**, 843, 2

12 P. Zarras, N. Anderson, C. Webber, D. J. Irvin, J. A. Irvin, A. Guenthner, J. D. Stenger-Smith, *Radiation Physics and Chemistry* **2003**, 68, 387

13 B. Wessling, *Electroactive Polymers for Corrosion Control* **2003**, 843, 34

14 P. J. Kinlen, D. C. Silverman, C. R. Jeffreys, *Synthetic Metals* **1997**, 85, 1327

15 T. D. Nguyen, T. A. Nguyen, M. C. Pham, B. Piro, B. Normand, H. Takenouti, *Journal of Electroanalytical Chemistry* **2004**, 572, 225

16 S. Yang, R. Brown, J. Sinko, *European coatings conference* **2005**,

17 B. C. Berry, A. U. Shaikh, T. Viswanathan, *Electroactive Polymers for Corrosion Control* **2003**, 843, 182

18 S. C. Yang, R. Brown, R. Racicot, Y. Lin, F. McClarnon, *Electroactive Polymers for Corrosion Control* **2003**, 843, 196

19 X. H. Wang, J. L. Lu, J. Li, X. B. Jing, F. S. Wang, *Electroactive Polymers for Corrosion Control* **2003**, 843, 254

20 A. T. Ozyilmaz, M. Erbil, B. Yazici, *Thin Solid Films* **2006**, 496, 431

21 T. Wang, Y. J. Tan, *Materials Science and Engineering: B Science and Technologies of Advanced Materials and Polymers for Defence and Aerospace Applications* **2006**, 132, 48

22 J. I. Martins, T. C. Reis, M. Bazzaoui, E. A. Bazzaoui, L. Martins, *Corrosion Science* **2004**, 46, 2361

23 M. A. L. Garcia, M. A. Smit, *Journal of Power Sources* **2006**, 158, 397

24 T. Tuken, B. Yazici, M. Erbil, *Progress in Organic Coatings* **2004**, 51, 205

25 C. Ocampo, E. Armelin, F. Liesa, C. Aleman, X. Ramis, J. I. Iribarren, *Progress in Organic Coatings* **2005**, 53, 217

26 R. M. Torresi, S. d. Souza, J. E. P. d. Silva, S. I. C. d. Torresi, *Electrochimica Acta* **2005**, 50, 2213

27 G. Williams, R. J. Holness, D. A. Worsley, H. N. McMurray, *Electrochemistry Communications* **2004**, 6, 549

28 P. Ocon, A. B. Cristobal, P. Herrasti, E. Fatas, *Corrosion Science* **2005**, 47, 649

29 O. Goossens, E. Dekempeneer, D. Vangeneugden, R. Van de Leest, C. Leys, *Surface & Coatings Technology* **2001**, 142, 474

30 Y. Sawada, S. Ogawa, M. Kogoma, *Journal of Physics D: Applied Physics* **1995**, 28, 1661

31 H. R. Lee, D. J. Kim, K. H. Lee, *Surface & Coatings Technology* **2001**, 142, 468

32 G. R. Prasad, S. Daniels, D. C. Cameron, B. P. McNamara, E. Tully, R. O'Kennedy, *Surface and Coatings Technology PSE 2004* **2005**, 200, 1031

33 F. Massines, N. Gherardi, A. Fornelli, S. Martin, *Surface and Coatings Technology ICMCTF 2005* **2005**, 200, 1855

34 O. Goossens, S. Paulussen, D. Vangeneugden, H. Vrielinck, F. Callens, C. Leys, J. Meneve, *New Diamond and Frontier Carbon Technology* **2003**, 13, 221

35 A. Sonnenfeld, T. M. Tun, L. Zajíčková, K. V. Kozlov, H.-E. Wagner, J. F. Behnke, R. Hippler, *Plasmas and Polymers* **2001**, 6, 237

36 C. P. Klages, M. Eichler, R. Thyen, *New Diamond and Frontier Carbon Technology* **2003**, 13, 175

37 G. Grundmeier, P. Thiemann, J. Carpentier, V. Barranco, *Surface & Coatings Technology* **2003**, 174, 996

38 N. Viart, D. Niznansky, J. L. Rehspringer, *Journal of Sol-Gel Science and Technology* **1997**, 8, 183

39 G. Borvon, A. Goullet, A. Granier, G. Turban, *Plasmas and Polymers* **2002**, 7, 341

40 B. C. Trasferetti, R. V. Gelamo, F. P. Rouxinol, M. A. B. de Moraes, C. U. Davanzo, *Chemistry of Materials* **2005**, 17, 4685

41 R. Clergereaux, M. Calafat, F. Benitez, D. Escaich, I. Savin de Larclause, P. Raynaud, J. Esteve, *Thin Solid Films* **2007**, 515, 3452

42 S. Kaciulis, A. Mezzi, G. Montesperelli, F. Lamastra, M. Rapone, F. Casadei, T. Valente, G. Gusmano, *Surface and Coatings Technology* **2006**, 201, 313

43 T. Liu, C. Dong, S. Wu, K. Tang, J. Wang, J. Jia, *Surface and Coatings Technology*
The Eighth International Workshop on Plasma-Based Ion Implantation and Deposition, The Eighth International Workshop on Plasma-Based Ion Implantation and Deposition **2007**, 201, 6737

44 W. V. K. Grips, H. C. Barshilia, V. E. Selvi, Kalavati, K. S. Rajam, *Thin Solid Films* **2006**, 514, 204

Summary

An introduction into plasma chemistry is presented in **chapter one**. Plasma is often called the forth state of matter. When enough energy is added to a gas, it no longer contains only neutral molecules, but also ions, electrons and excited molecules. Typical for this condition is the emission of light. Natural plasma's only exist at very high temperatures (>10000 K). While these temperatures are too high for industrial application, cold plasmas can be created by using electric fields. Electrons are accelerated in the electric field and collide with the gas molecules, which results in ionization of the gas. This opens up a lot of possibilities for industrial application of such plasmas. In this work, it will be used for chemical vapor deposition of polymers at atmospheric pressure.

Plasma deposition of polymers at vacuum pressure is already known for quite a long time. Recently it is also done at atmospheric pressure. The advantage of plasma polymerization is that it is a dry technique. Because no solvents are needed, plasmas are interesting from an ecological point of view. Furthermore, the very reactive plasma often leads to cross-linking and reactions with the substrate, which results in better mechanical properties. While plasma deposition at low pressure is a batch technique, depositions at atmospheric pressure can be easily implemented in an industrial production line (reel to reel).

In this work, plasma processes will be used for the deposition of conjugated polymers. These polymers are special because they are (semi-)conductive after doping. Therefore they can be used for a lot of applications. However, their rigid structure makes them insoluble and difficult to process. Today, (electro)chemically produced conjugated polymers can be synthesized in batch processes for applications with high added value. In-line processing is still difficult. Therefore, plasma technology at atmospheric pressure is presented as an alternative synthesis method.

In **chapter two**, the influence of the different plasma parameters onto the deposited conjugated polymer coatings is studied. Monomers and low molecular weight polymers were used as precursor.

To deposit plasma polyaniline coatings, a low molecular weight polyaniline was injected in the plasma to be cross-linked. However, solubility of the injected polyaniline was to low to form a coating. Better results were obtained with the monomer aniline. Plasma polymerization of aniline was influenced by the different plasma parameters which affected both the thickness and the chemical structure of the films. Higher power, resulted in a higher deposition rate, but the monomer was more fragmented. Deposition rate was also increased by the addition of oxygen to the carrier gas. However, this introduced unwanted carbonyl functions in the polyaniline layer. Better structure retention could be obtained when deposition was done in pure nitrogen or helium. The plasma coatings were thicker when a high frequency was used. However, higher frequencies again resulted in more fragmentation. Above 25 kHz, macroscopic patterns were seen in the coating morphology, while the coatings had a smooth surface at low frequency. The gas flow had no large influence on the chemical structure of the deposition, but lower gas flow did result in thicker coatings.

Variation of all these parameters resulted in many different plasma coatings. However, non of the experiments that were done, resulted in the expected blue polyaniline coatings. All depositions had a yellow-brown outlook and absorbed light close to the UV range. Furthermore, no conductivity was measured after doping. When the coatings were immersed in water or other liquids they delaminated from the substrate or dissolved. The desired polyaniline coating was thus not obtained by a plasma deposition at atmospheric pressure, yet. Best structure retention was realized at low power, low frequency and in an oxygen free environment.

Plasma polymerization of pyrrole at atmospheric pressure resulted in coatings which showed the chemical functionalities of polypyrrole. However, some other functionalities such as saturated bonds, triple bonds and carbonyl functions were formed. These structural defects resulted in yellow-brown coatings instead of the expected green polypyrrole. Increased power or addition

of a small oxygen concentration to the carrier gas, increased the deposition rate significantly. However, it also increased the number of defects in the plasma coatings. Because of these defects, non of the plasma polypyrrole coatings showed conductivity after doping. Furthermore, the films dissolved or delaminated from the substrate after immersion in water or other liquids.

Plasma deposition of polythiophene at atmospheric pressure also resulted in yellow coatings. Although, the reactive plasma induced many structural defects, which damaged the conjugated system, conductivity could be measured after iodine doping. The measured conductivity was probably due to ionic conductivity and was dependent on the humidity of the surrounding air. Deposition rate could be increased by raising the power or by the addition of a small oxygen concentration. However, this also increased the number of structural defects. Furthermore, the polythiophene coatings deposited in a nitrogen/oxygen plasma swelled and delaminated after being immersed in water, which makes them less interesting for most applications. When plasma deposition occurred in pure nitrogen or helium, the coatings were mechanically more stable when immersed in liquids.

Since plasma deposition at low pressure of aromatic heterocycles showed better structure retention when the aromatic ring contained certain substitutes, plasma deposition at atmospheric pressure of some thiophene derivatives was also studied. Although electron donating substitutes on the thiophene ring increased structure retention in coatings plasma deposited at low pressure, this trend was not observed for 3-methylthiophene, polymerized at atmospheric pressure. Infrared spectra showed the same defects as were seen in plasma polythiophene. The plasma poly(3-methylthiophene) even showed less conductivity after doping.

Plasma polymerization at atmospheric pressure of another thiophene derivative, EDOT, resulted in colored coatings when a small oxygen concentration was added to the plasma gas. When an on-off block wave pulsed plasma was used, structural defects could be decreased, resulting in a blue coating, which is a typical color for PEDOT. Probably, the blue coating is formed during the off-times of the plasma. Conductivities up to 1×10^{-2} S/cm were obtained without

doping. It is so far unclear why doping causes a decrease in conductivity. Possibly, remaining radicals cause a degradation of the conjugated system.
While the coatings deposited in a stationary DBD reactor were inhomogeneous across the length of the electrode, the application of a translating DBD reactor resulted in homogeneous films. Reaction rate could be increased by applying a higher oxygen concentration. However, at a concentration of 3%, a second absorption maximum in the visible range was seen, indicating side reactions or low molecular weight fractions. While an increased power did not have any effect on the coating thickness nor on the absorption behaviour, an increased gas flow did decrease the reaction rate. Finally, the coating rate could also be increased by increasing the pressure on the aerosol generator (higher aerosol concentrations). At a pressure of 3 bar, a second absorption maximum was seen, probably due to the formation of an oligomeric fraction.

In **chapter three**, it is studied whether plasma polymerization of conjugated polymers can be improved by the co-injection of oxidants. Since oxidants are also able to dope these conjugated polymers, an in situ doping effect is expected.
Plasma polymerization of pyrrole at atmospheric pressure with simultaneous addition of iodine, didn't result in in situ doped polypyrrole coatings. The obtained film still contained a lot of structural defects and the iodine content in the coating was rather low. Because the conjugation was partially destroyed, no conductivity was measured. Better results were obtained when $NOBF_4$ was added to the plasma carrier gas. A black film was deposited, which means that light over the entire visible range is absorbed. Conductivities up to $1{,}8 \times 10^{-2}$ S/cm could be reached. These are all indications that the conjugated system had significantly extended during plasma polymerization and that the coatings were doped. One issue is still a problem, however. In situ doped plasma polypyrrole coatings are quite inhomogeneous, both in the width and the length of the electrode.
A similar approach has been used for the plasma polymerization of polyaniline at atmospheric pressure. Plasma depositions with aniline and with simultaneous addition of an oxidant (APS), did not result in polyaniline. When besides the

oxidant, also an acid dopant (HCl) is added to the carrier gas, a green coating is achieved which is the typical color for polyaniline emeraldine salt. Conductivities up to 0,5 S/cm could be obtained this way. The homogeneity of the coatings, however was again a major issue. Green deposition is only observed at the front of the electrode. Plasma polymerization in a pulsed power mode slightly increased the coated area, although conductivity and deposition rate were negatively influenced. These problems might be solved by using a DBD system that moves over the length of the samples and by developing a new more homogeneous injection system.

The corrosion protection properties of plasma deposited conjugated polymers at atmospheric pressure are studied in **chapter four**. Electrochemical corrosion tests indicated that iodine doped plasma polythiophene did not provide any corrosion protection of steel at all. Undoped plasma polythiophene however, was able to decrease the corrosion rate by acting as a physical barrier. Because the porous nature of the coating, the protection was not sufficient. Probably, part of the rough steel structure is exposed due to the small thickness of the coating. An active corrosion protection could not be achieved with plasma polythiophene.

Plasma PEDOT coatings deposited on galvanized steel also participated in redox reactions after polarization in an electrochemical cell by switching between it's doped and undoped state (electrochemical doping). Although, a small decrease in corrosion current could be realized, corrosion protection with these layers was not sufficient, as is demonstrated with salt spray tests. Since conjugated polymers usually perform best in combination with barrier layers, this approach was also studied for plasma PEDOT. Therefore a plasma deposited polysiloxane layer was developed. Corrosion protection of galvanized steel equal to chromate conversion coatings could be reached when HMDSO was plasma deposited in a nitrogen/oxygen mixture and by applying a plasma curing step after polymerization. Addition of oxygen to the discharge gas increased the coating thickness, while the curing step increased the inorganic content of the coatings. In order to obtain smooth coatings with better corrosion protection, the galvanized steel substrate was placed in a template.

Combination of the plasma PEDOT coatings with these plasma polysiloxane coatings in hybrid coatings and multi-layers did not result in better corrosion protection than the barrier layer alone. Possibly, the plasma PEDOT coatings are too thin to assist in corrosion protection of galvanized steel or plasma PEDOT does not have this intrinsic corrosion protecting property.

Samenvatting

Een inleiding in de wereld van de plasma chemie is weergegeven in **hoofdstuk één**. Plasma wordt vaak de vierde aggregatietoestand genoemd. Wanneer genoeg energie wordt toegevoegd aan een gas, bestaat het niet langer enkel uit neutrale moleculen, maar ook uit ionen, elektronen en geëxciteerde moleculen. Typisch voor plasma's is de uitstraling van licht. Natuurlijke plasma's komen enkel voor bij zeer hoge temperaturen (>10000K). Deze temperaturen zijn veel te hoog voor industriële toepassing. Door gebruik te maken van een elektrisch veld kunnen deze plasma's echter ook opgewekt worden bij lagere temperatuur. Versnelling van de elektronen in het elektrisch veld leidt tot botsingen met de gas moleculen en ionisatie van dit gas. Deze koude plasma's kunnen gebruikt worden in een hele waaier aan industriële toepassingen. Eén daarvan is chemical vapor deposition van polymeren bij atmosfeerdruk, het onderwerp van deze thesis.

Afzetten van polymeren met plasma's in vacuüm is reeds geruime tijd gekend. Later werd dit ook mogelijk bij atmosfeerdruk. Het grote voordeel van plasma polymerisatie is dat het een droge techniek is. Er zijn geen solventen nodig, wat zeer interessant is vanuit een ecologisch oogpunt. Deze reactieve plasma's kunnen ook leiden tot de vorming van polymeer netwerken en reactie met het substraat, wat de mechanische eigenschappen van de deklagen verbetert. Plasma afzetting bij lage druk is echter een batch proces. Werken bij atmosfeerdruk is interessanter, daar het gemakkelijker kan geïmplementeerd worden in industriële productie processen (reel-to-reel).

In deze thesis zullen plasma processen gebruikt worden voor de afzetting van geconjugeerde polymeren. Wat deze polymeren speciaal maakt is dat ze halfgeleiding vertonen na doperen, wat ze interessant maakt voor een heleboel toepassingen. Hun starre structuur maakt hen echter onoplosbaar en moeilijk te verwerken. Vandaag worden geconjugeerde polymeren vaak (electro)chemisch gesynthetiseerd in batch processen voor toepassingen met een hoge toegevoegde waarde. Het is nog steeds moeilijk om ze te verwerken in een

continue proces. Daarom wordt plasma polymerisatie bij atmosfeerdruk hier voorgesteld als een alternatieve synthesemethode.

In **hoofdstuk twee** wordt de invloed van de verschillende plasma parameters op de afgezette lagen bestudeerd. Als precursor worden monomeren en laag moleculair gewicht polymeren gebruikt.
Eerst werd getracht polyaniline coatings af te zetten door laag moleculair gewicht polyaniline te injecteren in het plasma en het daarin te vernetten. De oplosbaarheid van het polyaniline was echter te laag om een voldoende hoge concentratie te injecteren die tot afzetting van een deklaag zou leiden. Betere resultaten werden bekomen wanneer het monomeer aniline werd geïnjecteerd. Variatie van de plasmaparameters leidde tot afzettingen met verschillende diktes en chemische structuren. Een hoger vermogen resulteerde in een hogere depositiesnelheid maar het monomeer was ook meer gefragmenteerd. De reactiesnelheid kon ook worden verhoogd door een kleine zuurstofconcentratie toe te voegen aan het dragergas. Hierdoor werden echter ongewenste carbonylfuncties ingebouwd in de coating. Beter behoud van de chemische structuur was mogelijk door de plasmareactie uit te voeren in zuiver stikstof of helium. De deklagen waren dikker wanneer de plasmafrequentie werd verhoogd maar ook een hogere frequentie resulteerde in een hogere afbraak van de monomeerstructuur. Bij een frequentie van 25 kHz of hoger vertoonde de deklaag een patronenstructuur, terwijl het coatingoppervlak glad was bij lagere frequenties. De snelheid van het dragergas had weinig invloed op de chemische structuur van de coatings al leidde een lagere gassnelheid wel tot dikkere deklagen.
Hoewel de variatie van de verschillende plasmaparameters leidde tot verschillen in de deklagen, werd geen enkele keer de verwachte blauwe kleur van polyaniline bekomen. Alle afzettingen hadden een geel-bruine kleur en absorbeerde licht bij een golflengte dicht bij het UV gebied. Er werd ook geen geleiding gemeten na doperen. Na onderdompelen in vloeistoffen loste de deposities op of kwamen ze los van het substraat. Plasmadeposities met aniline leidde dus nog niet tot de gewenste polyaniline coatings. De structuur werd het

best behouden wanneer gewerkt werd bij laag vermogen, lage frequentie en in een zuurstofvrije omgeving.

Plasmapolymerisatie van pyrrool bij atmosfeerdruk resulteerde in afzettingen die enkele typische functionaliteiten van polypyrrool bezaten. Enkele andere functionaliteiten, zoals verzadigde koolstofverbindingen, driedubbele bindingen en carbonylfuncties werden echter ook gevormd. Deze structurele defecten gaven de afzettingen een geel-bruine kleur en niet het verwachte groene polypyrrool. Een verhoogd vermogen of de toevoeging van een kleine zuurstofconcentratie aan het dragergas leidde tot een significante verhoging van de depositiesnelheid. Het aantal structurele defecten in de coating werd echter ook verhoogd. Deze defecten zorgden er ook hier voor dat er geen geleiding werd gemeten na doperen. De deklagen loste op of ze kwamen los van het substraat, wanneer ze werden ondergedompeld in vloeistoffen.

Plasmadepositie met thiofeen bij atmosfeerdruk leidde opnieuw tot gele coatings. Hoewel het reactieve plasma ook hier dezelfde defecten introduceerde die leidden tot een beschadiging van het geconjugeerd systeem, werd er geleiding gemeten na doperen met jodium. Deze geleiding is waarschijnlijk afkomstig van ionische geleiding en is afhankelijk van de luchtvochtigheid. Depositiesnelheid kon ook hier verhoogd worden door het vermogen te verhogen of door zuurstof toe te voegen aan het dragergas, al leidde dit steeds tot een verhoogd aantal structurele defecten. De polythiofeen lagen afgezet in een plasma dat zuurstof bevat, zwollen en kwamen los van het substraat na onderdompelen in water, wat hen minder interessant maakt voor industriële applicaties. Wanneer ze afgezet werden in zuiver stikstof of helium waren de deklagen stabieler bij onderdompelen in vloeistoffen.

De literatuur toont aan dat bij plasmadepositie van aromatische heterocyclische verbindingen bij lage druk, de structuur beter behouden blijft wanneer er zich substituenten op de aromatische ring bevinden. Daarom werden ook enkele thiofeenderivaten met zulke substituenten geïnjecteerd in het plasma. Plasmadepositie met 3-methylthiofeen bij atmosfeerdruk leidde echter niet tot een vermindering van het aantal defecten. Dezelfde defecten als bij plasma gepolymeriseerd polythiofeen waren aanwezig. Er werd zelfs minder geleiding gemeten na doperen.

Plasmapolymerisatie met een ander thiofeen derivaat, nl. EDOT, leidde tot gekleurde deklagen wanneer een kleine zuurstofconcentratie werd toegevoegd aan het plasma. Door gebruik te maken van een on-off gepulseerd plasma konden de structurele defecten nog verminderd worden, wat resulteerde in blauwe afzettingen, de typische kleur van PEDOT. Waarschijnlijk werd de blauwe coating gevormd tijdens de off-tijden van het plasma. Een geleiding tot 1×10^{-2} S/cm werd gemeten voor niet gedopeerde coatings. Het is nog wel onduidelijk waarom doperen zorgt voor een lagere geleiding. Mogelijk zorgen achterblijvende radicalen voor de degradatie van het geconjugeerde systeem.
Deposities van PEDOT met een stationaire DBD reactor leverde deklagen op die niet homogeen waren over de lengte van de elektrode. Door gebruik te maken van een bewegende reactor werd dit probleem opgelost. De reactiesnelheid kon worden verhoogd door een hogere zuurstofconcentratie te gebruiken. Wanneer het dragergas 3% zuurstof bevatte, werd echter een tweede absorptiemaximum vastgesteld in het zichtbaar licht gebied, hetgeen aantoont dat er zijreacties waren of dat er een laagmoleculaire fractie gevormd werd. Terwijl een verhoging van het vermogen geen effect had op de dikte of het absorptiegedrag van de coatings, leidde een verhoging van de gassnelheid tot dunnere coatings. De depositiesnelheid kon wel verhoogd worden door de druk op de aerosolgenerator te verhogen. Bij een druk van 3 bar werd opnieuw een tweede absorptiemaximum vastgesteld, waarschijnlijk te wijten aan de vorming van een oligomere fractie.

In **hoofdstuk drie** is nagegaan of de co-injectie van een oxidans in het plasma, de eigenschappen van de geconjugeerde plasma polymeren kan verbeteren. Gezien geconjugeerde polymeren ook gedopeerd kunnen worden met een oxidans, wordt ook verwacht dat ze in situ zullen gedopeerd worden.
Plasmapolymerisatie van pyrrool bij atmosfeerdruk, met gelijktijdige injectie van jodium, leidde niet tot de vorming van in situ gedopeerd polypyrrool. De bekomen films bevatten nog steeds veel structurele defecten en de hoeveelheid jodium opgenomen in de coating was eerder laag. Omdat de conjugatie gedeeltelijk vernietigd werd in het plasma, werd geen geleiding gemeten. Betere resultaten werden gemeten wanneer $NOBF_4$ toegevoegd werd aan het

plasma dragergas. Een zwarte film werd afgezet, wat betekent dat licht over het ganse zichtbaar gebied geabsorbeerd wordt. Een geleiding van 1,8 x 10^{-2} S/cm werd gemeten. Dit zijn indicaties dat het geconjugeerd systeem significant verlengd is tijdens de plasma polymerisatie en dat het bekomen polymeer gedopeerd is. Het probleem is echter dat deze in situ gedopeerde plasma-polypyrrool deklagen niet homogeen zijn in de breedte noch in de lengte van de elektrode.

Een gelijkaardige aanpak werd gebruikt voor de plasmapolymerisatie van aniline bij atmosfeerdruk. Co-injectie van het oxidans APS leidde echter niet tot polyaniline. Wanneer er naast het oxidans ook een zuur (HCl) als dopant werd toegevoegd werd er wel een groene coating bekomen, wat de typische kleur is voor het polyaniline emeraldine zout. Een geleiding tot 0,5 S/cm kon zo bereikt worden. De homogeniteit van de coatings was echter opnieuw het probleem. De groene coating bevindt zich enkel in het begin en in het midden van de elektrode. Pulseren van het plasma zorgde voor een kleine verbetering, al daalde de geleiding en de reactiesnelheid hiermee wel. In de toekomst kunnen deze problemen mogelijk opgelost worden door gebruik te maken van een bewegende DBD reactor en door de ontwikkeling van een nieuw injectie systeem, waarmee dopant en monomeer homogener gemengd worden.

De corrosiewerende eigenschappen van geconjugeerde polymeren, gepolymeriseerd met een plasma bij atmosfeerdruk, werden bestudeerd in **hoofdstuk vier**. Uit elektrochemische corrosietesten bleek dat plasma-polythiofeen, gedopeerd met jodium geen corrosie bescherming biedt voor staal. De corrosie snelheid kon wel vertraagd worden met niet gedopeerd plasma-polythiofeen door op te treden als een barrière tegen corroderende chemicaliën. De bescherming was echter onvoldoende omwille van de poreuze natuur van de coating. Waarschijnlijk is een gedeelte van het staal blootgesteld aan corrosieve chemicaliën omdat de dunne coatings niet het ganse metaaloppervlak bedekken. Er kon ook geen actieve bescherming worden vastgesteld met deze coatings.

Plasma PEDOT coatings, afgezet op gegalvaniseerd staal namen zelf deel aan redoxreacties wanneer ze gepolariseerd werden in een elektrochemische cel

door te veranderen van doperingstoestand. Hoewel een kleine daling van de corrosiesnelheid werd vastgesteld, toonde blootstelling aan een nevel van zoutoplossing dat de corrosiebescherming ook hier onvoldoende is. Aangezien corrosie bescherming kan verbeterd worden wanneer een geconjugeerd polymeer wordt gecombineerd met een barrière laag werd dit ook toegepast voor plasma-PEDOT coatings. Hiervoor werd eerst een plasma-polysiloxaan coating ontwikkeld. Een corrosie bescherming van gegalvaniseerd staal, gelijkaardig aan chromium conversie coatings werd behaald door HMDSO te polymeriseren in een stikstof/zuurstof plasma, gevolgd door een plasma nabehandeling zonder precursor. De toevoeging van zuurstof aan het ontladingsgas leverde dikkere coatings op en de plasma nabehandeling verhoogde het anorganisch gehalte van de coatings. Door het gegalvaniseerd staalsubstraat in een patroon te plaatsen, waardoor terug een laminaire gas flow werd bekomen, werden vlakkere coatings bekomen, wat ook resulteerde in betere corrosiebescherming. Plasma hybridecoatings en Multi-layers gevormd uit PEDOT en polysiloxaan beschermde het gegalvaniseerd staal niet beter tegen corrosie dan de barrièrelaag alleen. Waarschijnlijk zijn de plasma-PEDOT coatings te dun om een rol van betekenis te spelen of bezit het plasma-PEDOT intrinsiek geen corrosiewerende eigenschappen.